7-22-2016

CD13 Regulation of Albuminuria in Response to Renal Injury

Claire Gerber
University of Connecticut, claire.gerber89@gmail.com

CD13 Regulation of Albuminuria in Response to Renal Injury

Claire Gerber, Ph.D.

University of Connecticut, 2016

Abstract

Diabetes is a serious public health threat that leads to a variety of complications including diabetic nephropathy. Initiated by elevated blood glucose levels, glomerular and proximal tubule damage promotes progressive nephron deterioration leading to end stage renal failure. A common indicator of impending kidney failure is an increase in urinary albumin levels. Urinary proteins are efficiently reabsorbed via receptor-mediated endocytosis in the epithelial cells of the renal proximal tubules by endocytic proteins megalin and cubilin. CD13 has been previously identified as a negative regulator of receptor-mediated endocytosis of numerous cell types. Urinary albumin levels were significantly decreased in $CD13^{KO}$ animals compared to wild type animals in models of diabetic nephropathy and albumin overload. CD13 negatively regulates receptor-mediated endocytosis of albumin in proximal tubules. Currently, there are limited reliable biomarkers that accurately detect renal injury and its progression. Single-pass, apically expressed proximal tubule brush border proteins (CD10, CD13 and CD26) were easily shed into the urine predicting renal obstruction in patients with ureteropelvic junction obstruction. Targeting reliable noninvasive biomarkers of renal injury is critical to diagnosing patients at risk.

CD13 Regulation of Albuminuria in Response to Renal Injury

Claire Gerber

B.S. Purdue University, 2011

M.P.H. University of Connecticut, 2016

A Dissertation

Submitted in Partial Fulfillment of the

Requirements of the Degree of

Doctor of Philosophy

at the

University of Connecticut

2016

Approval Page

Doctor of Philosophy Dissertation

CD13 Regulation of Albuminuria in Response to Renal Injury

Presented by

Claire Gerber, M.P.H., B.S.

Major Advisor _____
Linda H. Shapiro

Associate Advisor _____
Kevin P. Claffey

Associate Advisor _____
Guo-Hua Fong

University of Connecticut

2016

Acknowledgements

These past five years have been some of the most challenging, yet memorable years of my life in which I would not have made it through without the support, reassurance and encouragement of incredible individuals. To begin, I would like to thank my mentor Dr. Linda Shapiro who shaped me into the scientist that I am today. Her passion and love for science is contagious. I always appreciated the time that she took for me to discuss my experimental plans or any major life decisions. Even when I doubted myself, Linda always believed I had the potential to do great things in the field of science and beyond. From her I have learned more than just how to think like a researcher, but also the importance of perseverance and never giving up on my dreams. She has truly inspired me in more ways than she could ever know and has made me a better person.

I would also like to thank all the past and current lab members from the Shapiro and Ferrer labs that helped me along the way in my journey. I feel so lucky and privileged to work with a great group of people. I especially would like to thank Dr. Mallika Ghosh who not only helped me out in lab, but also became a dear and close friend. I would like to thank the Center for Vascular Biology. My committee members have also been integral to my success over the past five years. Dr. Kevin Claffey, Dr. Guo-Hua Fong, Dr. Hector Aguila and Dr. Fernando Ferrer have been an amazing additional support system that guided me through the many challenges of obtaining my doctoral degree. Additionally, I would like to thank Dr. Cynthia Silva for her clinical insight and contributions to my project.

Further, I would like to thank my first mentor Dr. Nancy Pelaez at Purdue University for igniting my interest in science. I remember in my second semester of college that she believed in me and all of my aspirations. She is truly a remarkable and inspirational woman who taught me the importance of passion, community and integrity. I hope that some day I can inspire the next generation the same way that she inspired me. I would also like to thank my former boss Dr. Robert McEnroe at Roche Diagnostics who taught me the importance of work-life balance and how to always have a positive attitude and a good time.

I also want to thank everyone in the Community Medicine and Health Care Program. All my friends getting their degrees in public health always inspired me. It was amazing to see the passion in this remarkable group of people and I know that each and everyone of them will go on to do great things to make our world a better place. I would also like to thank my public health advisor, Dr. Amanda Durante, for her guidance and support along the way.

I knew obtaining my doctoral degree would be challenging, but thanks to the support of my amazing friends I can say that I became a better person. First, I want to thank everyone in the West Hartford Wolves hockey club. Coaching was the absolute best part of my day and I would never have made it through these last few years without these amazing girls and their families. I also want to thank all the friends I made along the way including Veneta, Miriam, Kia, Mitch, Lauren, Juan Pablo, Lorena,

Emily and so many more who have made Connecticut that much more meaningful and enjoyable.

Of utmost importance, I would like to thank my family who has continuously supported me in all my endeavors throughout my life. I am forever grateful for my parents. They have been my pillars, keeping me upright even when my world seemed like it was too much to bear. The two of you have been my biggest inspiration. I want to also thank Manuel who has stood by my side, been my number one fan and biggest believer. Finally, I have been blessed with the best siblings in the world. Thank you for always encouraging me and picking me up when I needed it most. Thank you Mom, Dad, Jonny, Sophie, Lena and Manuel. I love you all.

Table of Contents

Table of Figures

Table of Tables

Abbreviations

AO	albumin overload
BCA	bicinchoninic acid
BSA	bovine serum albumin
CD13^{KO}	global CD13 null transgenic mice
CKD	chronic kidney disease
DAMPs	danger-associated molecular patterns
DCs	dendritic cells
DMEM	Dulbecco's Modified Eagle Medium
ELISA	enzyme linked immunosorbent assay
EMT	epithelial to mesenchymal transition
ESRD	end-stage renal disease
EV	empty vector
FcRn	neonatal Fc receptor
GAPDH	glyceraldehyde 3-phosphate dehydrogenase
GFR	glomerular filtration rate
HCl	hydrochloric acid
HRP	horseradish peroxidase
H/M	human/mouse
IL	interleukin
IRF3	interferon regulator factor 3
KIM-1	kidney injury molecule 1
LPS	lipopolysaccharide
M/H	mouse/human
MAG3	mercato-acetyl-triglycine
MCP-1	monocyte chemotactic protein 1
MyD88	myeloid differentiation primary response gene 88
NaCl	sodium chloride
NaF	sodium fluoride
NEAA	non-essential amino acids
NF-κB	nuclear factor kappa B
NGAL	neutrophil gelatinase-associated lipocalin
PAMPs	pathogen-associated molecular patterns
PAS	Periodic acid-Schiff
PVDF	polyvinyl difluoride
RANTES	regulated on activation, normal T cell expressed and secreted
RBC	red blood cell
RFU	relative fluorescence unit
RPMI	Roswell Park Memorial Institute medium
RU	relative unit
SEM	standard error of the mean
SL13	Shapiro Lab 13
STZ	streptozotocin
t ½	rate of kidney drainage
TBST	tis-Buffered Saline Tween

TGF-β	transforming growth factor
TLR4	toll-like receptor 4
TRIF	TIR-domain-containing adapter-inducing interferon-β
TRAM	TLR4 adaptor protein
UPJO	ureteropelvic junction obstruction
UUO	unilateral ureteral obstruction
WT	wild type

Chapter 1

Introduction

1.1 – Kidney Disease

Chronic kidney disease

Chronic kidney disease (CKD) affects millions of Americans yearly leading to increased medical expenditures, continuous patient monitoring, a decreased quality of life and an increase in morbidity and mortality. Of the 26 million affected yearly in the United States, approximately 1.8 million of these patients are treated for end-stage renal disease (ESRD) by renal replacement therapy involving kidney transplant, hemodialysis or peritoneal dialysis[1]. Due to the increasing prevalence of disease, developing and developed countries face significant financial burden on health care systems for cost of care for these patients ranging around $12 billion annually[2]. Patients experience severe morbidity and mortality from this debilitating disease that is irreversible and constantly progressive. Over time the kidney slowly deteriorates due to etiologies from hypertension, trauma, sepsis, toxicity, congenital abnormalities caused by obstructions within the renal tract, diabetes mellitus and many more[3,4]. Characteristics of CKD include weakening of renal excretory, homeostatic and endocrine functions[1]. Currently, there is minimal advancement in limiting the progression of renal deterioration despite implementing aggressive treatment options, which provide only some protection to the nephron.

Marcello Malpighi was the first to investigate the microanatomy of the kidney in 1666 after the introduction of a newly developed microscope. His findings determined that that the kidneys had a filtration mechanism for the blood and was also important for the production of urine. In 1837, Gabriel Valentin identified that patients who died

from proteinuria had extensive renal injury as noticed by histology[5]. Pioneers in the field of renal pathology, Franz Volhard and Theodor Fahr further identified that kidney damage often coincided with excessive protein excretion in the urine in 1914. By 1954, Jean Oliver identified the formation of protein droplets in the cytoplasm of tubular cells that had already excessive protein degradation[1,5]. Since those early days of scientific discovery and the development of new technologies, the pathogenesis of renal injury has been vastly studied in patients as well as various animal models. With the introduction of renal biopsies patient's tissue is analyzed by light, electron and immunofluorescence microscopy to diagnose various inflammatory and non-inflammatory, acute and chronic, proteinuric and hematuric, hypertensive and non-hypertensive and all other renal diseases[5].

Pathology of CKD is irreversible and includes renal fibrosis and progressive nephron loss especially altering structures of the glomerulus and the proximal tubules, important components in urine filtration[1,4]. Cellular crescent formation around the glomerulus and atrophy of tubules leads to proteinuria, an increase of protein in the urine. Indicative of renal failure, proteinuria occurs once the glomerular filtration barrier becomes overloaded requiring extensive increases in resorption capabilities by the renal proximal tubules; a burdensome task for these epithelial cells[6]. In patients, most renal dysfunction is associated with tubulointerstitial injury. Patients with diabetes and hypertension are at high risk for albuminuria, a form of proteinuria in which albumin levels are abnormally high in the urine[7]. Albumin, the most abundant circulating plasma protein, is important as it carries metabolites, hormones,

vitamins and drugs, acts as an acid/base buffer and aids in regulating blood pressure and volume[6,8,9]. Proximal tubules mediate endocytosis of over 80% of plasma proteins, including albumin[10]. Mutiligand receptors, megalin and cubilin, found on the apical side of renal proximal tubules are important in facilitation of receptor-mediated endocytosis of plasma proteins like albumin. Once absorbed these proteins are subsequently delivered to the lysosomes for degradation[6,8,10,11]. If endocytic uptake of albumin in the proximal tubules is impaired, excess albumin in the lumen increases inflammation, which may lead to epithelial to mesenchymal transition (EMT). This results in fibrosis and even more damage to the kidneys, causing a vicious cycle of continuous stress on the renal proximal tubules[9].

Diabetic nephropathy

According to the American Diabetes Association, there are over 25 million individuals who have diabetes (type 1 and type 2) and approximately 80 million who have prediabetes are at high risk of developing diabetes mellitus. About 20% of patients with diabetes (type 1 or type 2) develop diabetic nephropathy approximately 10 to 20 years after the onset of the disease; making diabetes the primary cause of ESRD with about 50% of these patients having complications from diabetes[4,12-14]. This trend has only increased over the past decade, but it seems that only a minority of diabetic individuals are exposed to certain environmental and genetic factors that determine the fate of patients' likelihood of developing diabetic nephropathy. Increased glucose levels expose tubular structures to damage at the basolateral membrane. Increased glucose filtration at the glomerulus leads to overload, resulting

in increased filtrate exposure at the proximal tubules[14]. However, the exact pathophysiology and molecular pathways that lead to renal failure caused by hyperglycemia remains unknown, albeit growing insight into studying disease progression.

Diabetes threatens renal microvasculature leading to injury of various kidney cells. It is known that patients with diabetic nephropathy experience renal hyperfiltration and microalbuminuria followed by glomerulosclerosis and tubulointerstitial fibrosis[15]. Hyperglycemia impairs the regulation of local glomerular microcirculation and manipulates the transcription and translation of genes regulating cell growth and survival, angiogenesis and the extracellular matrix. Uptake of glucose by the proximal tubule triggers hyperplasia and hypertrophy leading to increases in tubulointerstitial fibrosis, damage, hypoxia, apoptosis and renal failure.

Ureteropelvic Junction Obstruction

Ureteropelvic junction obstruction (UPJO) is a congenital anomaly that frequently leads to renal injury and renal dysfunction in infants and children. With an estimated incidence of 1 in 500 births, UPJO is the major cause of hydronephrosis and the most common cause of kidney disease in children[16]. Blockage or complete obstruction of one or both of the ureters prevents or impedes the flow of urine into the bladder from the kidney. Affected children develop long-term morbidities such as CKD and cardiovascular disease. Furthermore, obstruction underlies the majority of children with ESRD. In its most severe form, urinary tract obstruction can lead to

prenatal or early infant death[16-18]. Other children may progress to develop CKD and kidney failure requiring lifelong monitoring and renal replacement therapy (dialysis and transplantation). Moreover, all of these patients with renal dysfunction are at a greater risk of cardiovascular disease early in life[17].

An early symptom of ureteral obstruction is an increase in pressure in the proximal tubules causing distention, damage and shedding of proteins expressed on the apical surface of the proximal tubular brush border epithelium into the urine[19]. While painless, hydronephrosis can lead to progressive cellular damage due to hypoxia, ischemia, stretching, reactive oxygen species and fibrosis. This ultimately results in tubule cell death, tubular atrophy, interstitial inflammation and collagen deposition, impairing growth and development of the obstructed kidney and causing compensatory enlargement of the unaffected kidney[20-22]. Current therapeutic goals focus on halting progressive renal injury and enhancing healing which is dictated by the severity and location of the obstruction. Progress in these areas is severely hindered by the scarcity of dependable biomarkers to assess the effects of obstruction[20,23].

1.2 – Kidney Background

Structure and function of kidney

The kidneys, an excretory organ, are located in the abdominal cavity posterior to the wall of the abdomen on either side of the vertebral column[24]. As regulatory organs, the kidneys are responsible for maintaining homeostasis of bodily fluids by

regulating constant volume of fluids by varying excretion of solutes and water[24,25]. Furthermore, the kidneys maintain blood pressure, blood pH and electrolytes in the blood. Remarkably, the kidneys filter about 20% of total cardiac output daily, generating on average one liter of urine per day[26].

The kidney is a highly vascularized organ consisting of two distinct regions, an outer region referred to as the cortex and an inner region referred to as the medulla. These two regions compose the functional unit of the kidney called the nephron; the nephron's main responsibility is to produce and concentrate urine. Further structures found in the kidney include blood vessels, lymphatics and nerves. The renal artery is the major blood supply for the organ that branches progressively ultimately leading to the glomerular capillaries. A human kidney contains approximately 1.2 million nephrons. Nephrons are hollowed tubes composed of a single cell layer of uniquely specialized cells consisting of the renal corpuscle, proximal tubule, loop of Henle, distal tubule and collecting duct. Each component of the nephron is responsible for specific functions. The renal corpuscle contains the glomerulus and Bowman's capsule and is responsible for the filtration of the blood[24]. In this portion of the nephron, smaller molecules are selectively sieved in the first step of urine formation[26]. The next segment of the nephron, the proximal tubules, contains a brush border responsible for the reabsorption of metabolized proteins and other substances from the glomerular filtrate through endocytic mechanisms[27]. The loop of Henle recovers water and sodium chloride from the urine. Water is then reabsorbed in the late distal tubule and urine is then collected in the collecting ducts[25].

Glomerulus

The initial step of urine formation begins in glomerular capillaries where plasma filtrate passes through sieves into the Bowman's space. The glomerular filtration barrier is composed of capillary endothelium, glomerular basement membrane, specialized epithelial cells and podocytes[28]. The tufts of capillaries comprise the glomerulus that supplies blood via the afferent arteriole and is drained by the efferent arteriole. Epithelial cells thin out in the Bowman's space where these epithelial cells are in contact with podocytes. Each podocyte is equipped with foot processes to form the filtration barrier, which is fenestrated and allows for the movement of small molecules across the membrane like sodium, urea and glucose. The two major components of the slit diaphragm include nephrin and podocin to allow for selective filtration of molecules[24,29].

Proximal tubule

The proximal tubule begins at the urinary pole of the glomerulus and is composed of three segments (S1, S2 and S3)[30]. Structurally, the proximal tubules are highly polarized cells containing a brush border responsible for the filtration of water, sodium, chloride, potassium and other solutes. The S1 segment has important machinery that allows for efficient reabsorption, transcytosis and processing of filtered substances found in the lumen coming from the glomerular filtrate[31]. Filtered proteins are endocytosed by apical membrane receptors megalin and cubilin via receptor-mediated clathrin-dependent endocytosis[24,31,32]. Internalized substances

are degraded by lysosomes or exit the cell across the basolateral membrane mediated by the transport protein neonatal Fc receptor (FcRn) and returned to the blood[24]. The physiological processes performed by renal proximal tubules are important for maintaining the integrity and function of the kidney.

1.3 – Renal Processes

Albumin

Albumin (~65 kDa) is the most abundant circulating plasma protein in the bloodstream important in regulating acid/base balances and blood pressure as well as acting as a carrier for metabolites, hormones, vitamins, inorganic ions and medications[9,33-35]. The production and excretion of albumin, a 585 amino acid, negatively charged globular protein found in the plasma of all mammals, occurs in the liver[31]. Although not essential to life, the diverseness of various functions of albumin makes it an extremely important protein. Hypoalbuminemia, due to malnutrition or inflammation, is associated with increased mortality. Further the total level of albumin in the urine also correlates with the progression of renal injury and disease[9]. Albumin is filtered in the glomerulus; albumin filtrate is resorbed in the renal proximal tubules. In healthy humans the glomerulus filters up to 9 g of albumin daily[9] and only 10-15 mg is excreted into the urine[34].

Increased urinary albumin levels characterize albuminuria, which typically occurs after renal diseases progress. Albumin remains to be one of the strongest

biomarkers for most kidney diseases[35]. The definition of albuminuria in clinical settings is when daily urinary albumin levels exceed 30 mg[34]. With rising levels of albuminuria there is a decline in glomerular filtration rate (GFR) accelerating the risk of ESRD. Further, albuminuria represents an irreversible stage of kidney disease[36]. Albumin resorption is a vital process regulated by the epithelial cells of renal proximal tubules via clathrin-dependent and receptor-mediated endocytosis after albumin is filtered by the glomeruli[37]. Initial events leading to albuminuria reflects contributions from both processes in the glomerulus and proximal tubule[9,35]. In diabetic nephropathy there is an overload on the glomerulus, which leads to more albumin filtrate leaking into the proximal tubules. Epithelial cells of the proximal tubules are overwhelmed and experience impairment in endocytic processes of albumin and other filtrates[27]. The inability to properly endocytose excess albumin filtrates leads to the accumulation of albumin in the nephron ultimately leading to the increases seen in the urine.

The exact effect of albuminuria on renal damage is one of the biggest controversies in the field of renal injury. Many theories contemplate reasons for albuminuria being such a strong indicator of renal damage. The main hypothesis in the field states that as the disease progresses, there is an increase in proteinuria and that high concentrations of albumin and other proteins induce inflammatory responses and fibrosis[9]. *In vivo* studies in rats and mice have shown that albuminuria leads to inflammation and fibrosis[38,39]. After an 11-day model of albumin overload (AO) glomerular ultrastructure of the podocyte and glomerular basement membrane was

destroyed as visualized by electron microscopy[40]. Excess albumin uptake by proximal tubules activates inflammatory and fibrogenic mediators like RANTES (regulated on activation, normal T cell expressed and secreted), monocyte chemotactic protein-1 (MCP-1), transforming growth factor-β (TGF-β) and nuclear factor kappa B (NF-κB). Activation of these mediators leads to inflammation, fibrosis, mesangial expansion and hypertension ultimately leading to progressive renal dysfunction[1,9,34,41-44].

High albumin levels leads to atrophy and apoptosis of proximal tubule cells. Apoptosis, an active, programmed cell process occurs to avoid effects of inflammation, whereas necrosis is a passive mechanism in which a cell accidently dies due to environmental perturbations[45]. Renal tubule cell apoptosis is the common final pathway that results in a variety of different kidney injuries[46]. Most studies utilize proximal tubule cell lines to study the effects of high levels of albumin on apoptosis and necrosis. Cells are exposed to high levels of albumin or serum fragments and apoptosis levels have been assessed using various methods. *In vitro* analysis of high albumin treatment leads to increases in apoptosis[46,47]. Additionally, several *in vivo* models indicate that high levels of albumin induces apoptosis in both the glomerulus and proximal tubules[48-50]. This evidence elucidates that albumin leads to apoptotic damage, however it does not distinguish whether apoptosis occurs in response to increased uptake or excess circulating fragments of albumin present in the lumen of the nephron.

Renal endocytosis

A fundamental cellular process that affects every cell function is endocytosis; classically defined as the process in which cells internalize anything from small extracellular particles to entire cells that are incapable of passing through the plasma membrane[51-53]. A key controller of cellular homeostasis, endocytosis is convoluted as it has multiple interconnected entry routes that are regulated by cargo specificity, receptor sorting signals, endocytic adaptors and lipids[51]. It is an extensively studied process as it has shown to be involved in antigen presentation, nutrient acquisition, elimination of apoptotic cells, pathogen entry, receptor regulation, hypertension and synaptic transmission[52]. Endocytosis occurs though several distinct biochemical mechanisms, but the best understood is through clathrin-mediated endocytosis[54]. Clathrin-mediated endocytosis recruits clathrin-binding proteins to induce clathrin polymerization to drive membrane invagination and vesicle scission[51,55]. Succeeding internalization, molecules from the plasma membrane are recycled back to the surface in recycling endosomal compartments, routed to degradation pathways towards the lysosomes or returned into circulation by transcytosis[31,51,55].

In renal proximal tubules, receptor-mediated endocytosis is crucial for resorption and metabolism of substances found in the lumen coming from the glomerular filtrate. Low molecular weight proteins are readily resorbed by a mechanism heavily relying on megalin and cubilin. Healthy proximal tubules in adults take up as much as 600 mg of protein daily, however in renal injury, proximal tubules uptake machinery becomes saturated leading to cytotoxicity within the nephron[56]. All segments of the

proximal tubule express endocytic apparatus, but there is notably fewer clathrin-coated vesicles present in the S3 segment[31]. Megalin and cubilin have been identified as the two major contributors involved in receptor- and clathrin-dependent endocytosis occurring in the epithelial cells of the proximal tubules[6,27,57,58]. Megalin and cubilin are co-expressed in absorptive epithelium of small intestines, renal proximal tubules, the visceral yolk sac and the placental cytotrophoblast[32].

Megalin

Megalin, a 600 kDa transmembrane protein with a large extracellular portion, was first discovered in 1982 by Kerjaschki and Farquhar[6]. Part of the low-density lipoprotein family, megalin is the crucial driving component to aid in uptake of filtered plasma proteins[58]. Megalin is a highly conserved protein expressed on the apical surface of renal proximal tubules that contains a large extracellular domain (4,398 amino acids) built up with three different types of domains[57]. One of these domains is responsible for the pH dependent release of ligands in the endosomal compartments. Megalin has a single hydrophobic transmembrane segment (23 amino acids) and a smaller intracellular domain (209 amino acids). The N-terminal domain of megalin recruits clathrin components to the plasma membrane to initiate the early phases of endocytosis[27]. Many ligands have been identified for megalin including vitamin D-binding protein, vitamin A/retional-binding protein, β2-microglobin, α1-microglobulin and albumin[57]. Fanconi syndrome has been associated with megalin deficiency in the renal proximal tubule of patients leading to increased albuminuria[57]. Conditional knockout of megalin in the proximal tubules led

to increased levels of albuminuria when compared to control mice in an unchallenged state[11].

Cubilin

Cubilin, a smaller 460 kDa protein residing on cell surfaces, co-expresses with megalin on the apical surface of epithelial cells to recognize and bind glomerular filtrates like albumin found in the lumen of the proximal tubule[6]. Cubilin is tethered to the plasma membrane containing many different domains that binds a variety of ligands. Cubilin expression patterns mimic megalin in coated pit endocytic vesicles and the membrane-recycling pathway. It has also been visualized in lysosomes. Significant proteinuria has been identified in patients suffering from Imerslund-Gräsbech syndrome. Two Finnish families in which the disease is prevalent present with mutations in the cubilin gene[57]. Like megalin deficient mice, cubilin deficient mice display high levels of albuminuria. Mice lacking both cubilin and megalin display even higher levels of albuminuria[11].

Renal transcytosis

Uptake of excess albumin by renal proximal tubules has been well documented for over 30 years, but more recent data reveals that albumin travels across the basolateral membrane of proximal tubules for resorption back into the blood stream. Thus, albumin no longer only has the fate of being internalized and degraded by the lysosome as initially suspected. The blood reclaims albumin in a process known as transcytosis. Albumin is internalized via the megalin-cubilin complex by receptor-

mediated endocytosis into clathrin-coated vesicles. Upon internalization, acidification of the endosomes occurs causing the release of albumin from the megalin-cubilin complex. Acidification is the vital step that allows albumin to bind to FcRn within the endosomal sorting compartment. The megalin-cubilin complex is recycled back to the apical membrane, while albumin binds to the FcRn receptor at low pH and is transported back into the circulation at the basolateral membrane of renal proximal tubules[31].

FcRn

Jones and Waldmann discovered FcRn in 1972. There are two distinct binding sites on FcRn for albumin and IgG with a low binding affinity at normal physiological pH, but this binding affinity increases at acidic pH (<6.5). FcRn is expressed on vascular endothelium, epithelial cells of small intestine, liver, spleen, lung, neutrophils, monocytes, dendritic cells (DCs) and the renal proximal tubules. FcRn is a heterodimer comprised of myosin heavy chain class I-like heavy chain and β2-microglobulin. This molecule preserves the half-life of albumin by transporting albumin across membranes[59]. Mutation or deletion of FcRn lowers the serum half-life of both albumin and IgG[60,61].

TLR4 and diabetic nephropathy

TLR4

Toll-like receptor 4 (TLR4), an evolutionarily conserved family of cell receptors, is part of the innate immune system which reacts to pattern recognition receptors: pathogen-associated molecular patterns (PAMPs) and danger-associated molecular patterns (DAMPs)[62]. Upon activation by PAMPs or DAMPs, TLR4 recruits adapter molecules including myeloid differentiation primary response gene 88 (MyD88)-dependent and TIR-domain-containing adapter-inducing interferon-β (TRIF) independent pathways to elicit immune responses activating downstream pro- or anti-inflammatory signaling pathways[63,64]. Transcription factors NF-κB and interferon regulator factor 3 (IRF3) are activated to release cytokines and chemokines. TLR4 is expressed in a variety of cells in the kidney including the proximal tubules, podocytes, mesangial cells, DCs, lymphocytes and macrophages[64].

TLR4 and diabetic nephropathy

Activation of TLR4 in response to the events of renal inflammation has been observed in multiple different kidney injury models including ischemia/reperfusion, obstructive uropathy, tubulointerstitial nephritis, nephrotoxicity and diabetic nephropathy[63,64]. TLR4 deficient mice had significantly less albuminuria, renal dysfunction, activation of NF-κB and infiltration of interstitial macrophages than wild type (WT) mice in response to streptozotocin (STZ) induced diabetic nephropathy[63]. Additionally, high glucose induced activation of NF-κB in proximal tubule cells. In clinic, TLR4 is highly expressed in patients with diabetic nephropathy[65-67]. Overall,

there is strong evidence that lack of TLR4 attenuates inflammatory responses and prevents the development of diabetic nephropathy[63,68].

1.4 – Introduction to CD13

Tissue structure, expression and function of CD13

CD13 (150 kDa), aminopeptidase N, is a cell surface, type II membrane bound, zinc-dependent metalloprotease shown to be involved in angiogenesis, inflammation and receptor-mediated endocytosis. This seven-membrane protein is composed of a short cytoplasmic tail, a transmembrane spanning region and a large extracellular portion where the catalytic domain resides functions in both enzyme-dependent and -independent mechanisms (Figure 1.1)[69,70].

CD13 is highly expressed on cells of the myeloid lineage and on activated endothelial cells found in the brain, liver, intestine and kidney. Further, CD13 acts as an important mediator for monocytic/endothelial cell adhesion[71]. Like megalin, cubilin, FcRn and TLR4, CD13 is highly expressed on the apical surface of epithelial cells in the proximal tubules (Figure 1.2).

CD13 is involved in various physiological processes including peptide cleavage, signal transduction, angiogenesis and cell adhesion[70]. Since CD13's enzymatic site is sterically restricted; CD13's catalytic activity is zinc-dependent and favors neutral N-terminal amino acids on oligopeptides[72]. Recent x-ray crystallographic analysis of CD13 revealed that an eight-peptide residue loop alters the conformation to regulate

various processes by providing substrate-specificity, contributing to CD13's vast distinct activities[73].

CD13 regulates various vital normal physiological functions including the processing of peptide hormones, such as angiotensin III and IV[74], neuropeptides crucial in pain response[75] and chemokines involved in inflammation and angiogenesis[73,76]. Further, CD13 influences cell adhesion, migration and endocytic processes[70,71,77,78]. CD13 is a receptor for various mammalian coronaviruses[79,80]. Within the kidney it is a well-characterized marker that cleaves neutral amino acids from peptides and is sorted to the apical membrane of epithelial cells found in the proximal tubule[81]. Interestingly, a primary isolation protocol of proximal tubules has used CD13 as a marker to identify epithelial cells of the kidney[82].

Global CD13 deficient mouse

To discover the various functions of CD13, our lab generated a global CD13 null transgenic mouse ($CD13^{KO}$). CD13 contains 20 exons that make up the seven domains ranging in size from 18 to 205 amino acids. $CD13^{KO}$ mice were generated by deleting exons 4 through 13 of the exon region of CD13, eliminating the catalytic domain in addition to extracellular subunits as confirmed by PCR[69]. Global $CD13^{KO}$ mice show no overt phenotypic differences until challenged.

CD13 and inflammation

Inflammation is an important physiological process that becomes activated in response to infection or injury. The body detects cellular changes at the site of injury and recruits circulating monocytes present in the blood stream that are home to important chemoattractants to help resolve the infection or injury by creating an inflammatory environment[83]. This infiltration of monocytes heavily relies on adhesion molecules on both patrolling monocytes and endothelium lining the injury[84,85]. Previous data from the lab demonstrated CD13 as an important regulator of inflammatory cell trafficking. Upon injury CD13 becomes activated on epithelial cells that allows for the recruitment of circulating peripheral blood monocytes. Through homotypic adhesion between CD13 expressed on monocytes and the activated endothelial cells, inflammatory cells enter the site of infection to resolve injury. This phenomenon was demonstrated in models of hindlimb ischemia, myocardial infarction and thigolycolate peritonitis[86-88].

CD13 and endocytosis

Preliminary data in the lab as well as others have shown that CD13 regulates clathrin-mediated endocytosis, suggesting it plays a role in fundamental aspects of receptor-mediated endocytosis[77,89,90]. CD13 mediates internalization of antigens in various receptor-mediated, dynamin-dependent endocytic receptors found in DCs. DCs lacking CD13 took up ovalbumin and transferrin more efficiently than WT DCs. CD13 is shown to co-internalize in DCs, but was not shown to co-immunoprecipitate with antigen receptors[77]. CD13 also mediated TLR4 endocytosis. Immunofluorescent

analysis confirmed that CD13 was internalized into dynamin^{+} and Rab5^{+} endosomes after stimulation[91]. It was hypothesize that CD13 may interact with these important endocytic components to regulate uptake of filtrates like albumin that are passing through the lumen of the proximal tubules.

CD13 and TLR4

Previous data from the lab indicated that CD13 negatively regulates TLR4 endocytic signal transduction in inflammation. After lipopolysaccharide (LPS), a PAMP, stimulation DCs become activated and CD13 co-internalizes with TLR4, CD14 and dynamin into early endosomes. TLR4 signals in two distinct pathways: (1) via MyD88 pathway after ligation of PAMPs or DAMPs to activate the NF-κB pro-inflammatory pathway[92] or (2) endosomal signaling activating TRIF/ TLR4 adaptor protein (TRAM) pathway to activate IRF3 and further downstream anti-inflammatory cytokines[93]. The MyD88 pathway is activated independent of CD13 expression. Upon internalization of TLR4 via dynamin-dependent mechanisms, there is activation of IRF3 and the upregulation of target genes. CD13^{KO} response to inflammation is skewed towards IRF3 anti-inflammatory pathway. Thus this data indicates that CD13 is crucial for balancing the innate immune response by preserving inflammatory equilibrium of both pro-inflammatory and anti-inflammatory responses after injury[91].

1.5 – Aims of the study

The multifunctionality of CD13 prompts further investigations to determine how CD13 would react in a model of kidney injury. Recent findings from the laboratory strongly suggest CD13 to be highly involved in inflammatory processes as well as acting as an important mediator of endocytosis. The first goal of the study aimed to identify the structural components required for adhesion of peripheral monocytes to activated endothelial through the use of chimeras generated by previous lab members. The second goal of the thesis was to look at a model of renal injury since data from the lab suggested CD13 and TLR4 have been shown to be intrinsically related. The investigation sought to determine how $CD13^{KO}$ mice would behave in response to diabetic nephropathy as it has previously been demonstrated that lack of TLR4 has an improved phenotype in renal injury models. Upon further evaluation of the results, the focus shifted towards understanding how CD13 regulates renal endocytosis and whether uptake of more albumin was beneficial to overall renal prognosis. Next the study strived to determine how renal proximal tubular epithelial cells would behave in a model of diabetic nephropathy to identify how CD13 performs in a renal injury model. Finally, to evaluate clinical implications for CD13, UPJO urine samples were collected to determine their efficacy and reliability as renal injury biomarkers.

1.6 – Figures and Legends

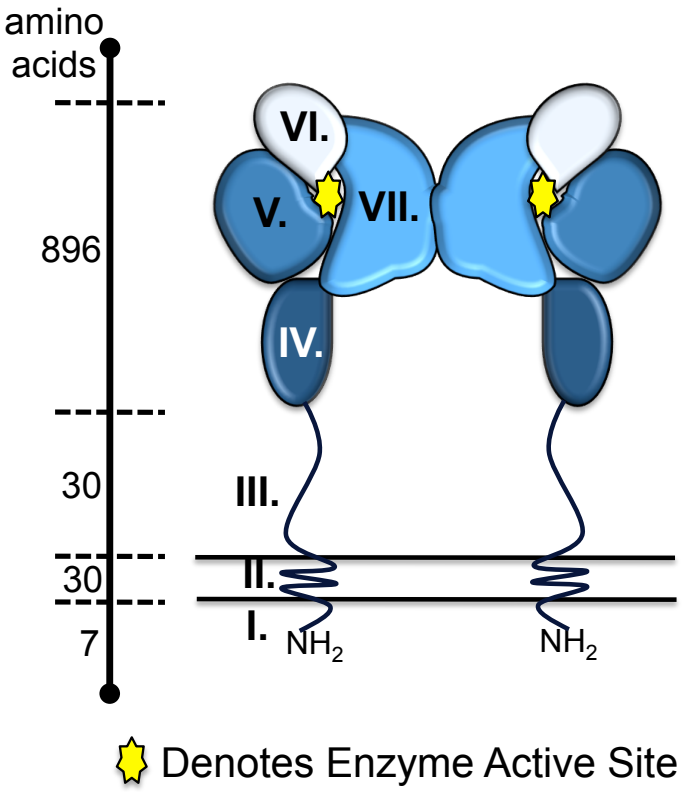

Figure 1.1 – CD13 Protein Structure.
Modified from[94].

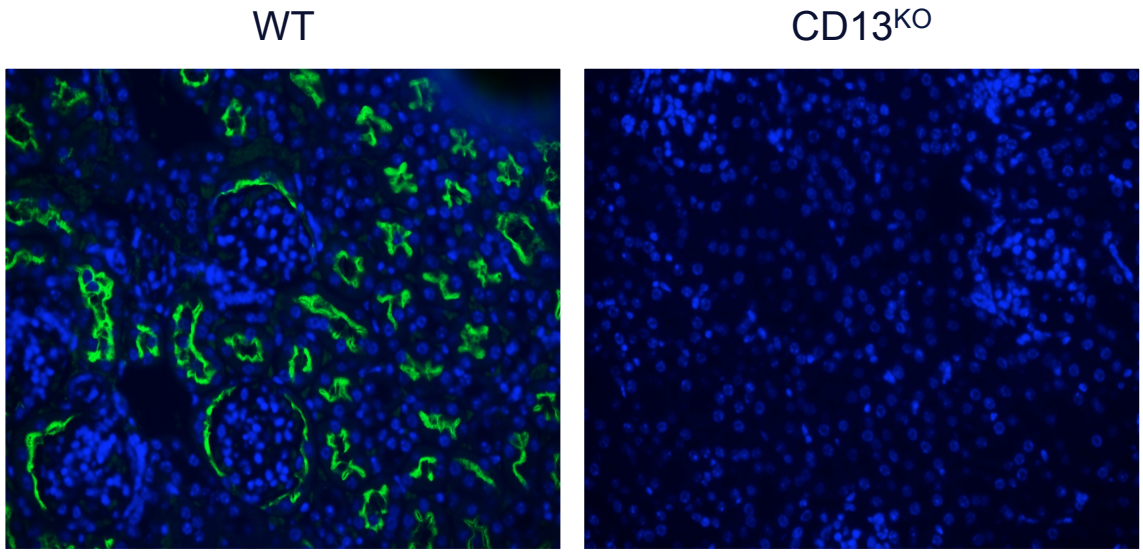

Figure 1.2 – Loss of CD13 expression in kidneys of CD13^{KO} mice.
Immunofluorescence of CD13 in the cortex of WT and CD13^{KO} kidneys. CD13 stains epithelial cells within the proximal tubules.

Chapter 2

A structure and functional analysis of CD13

*Adapted from Immunology, Published March 10, 2014 (doi: 10.1111/imm. 12279)

Molecular Mechanisms Regulating CD13-Mediated Adhesion

Mallika Ghosh[1], Claire Gerber[1], M. Mamunur Rahman[1], Kaitlyn M. Vernier[1], Flavia E. Pereira[1], Jaganathan Subramani[2], Leslie A.Caromile[1] and Linda H. Shapiro[1]

[1]Center for Vascular Biology, University of Connecticut Health Center, Farmington, CT 06030, [2]Dept of Anesthesiology, Texas Tech University Health Sciences Center, Lubbock, TX USA

The contribution to this publication included inserting the full length mouse and human CD13 constructs as well as both chimera constructs into C33a and WEHI 78/24 by infecting these cells with media containing virus expressing the constructs from amphotrophic phoenix packaging cells. Further contributions included verification of CD13 expression by western blot and flow analysis and completion of all *in vitro* adhesion assays.

2.1 – Introduction

Inflammation is a highly regulated and coordinated activity heavily relying on many different cells types to respond to infection or injury. First, the site of injury releases cytokines to signal for monocytes to insinuate injury, infection or insult within its' environment. These monocytes circulate throughout the body in the blood, bone marrow and spleen. Searching for infection or injury, monocytes bind to activated endothelium that has released vital distress signals. The inflammatory trafficking

model is well known, however the precise mechanisms that control trans-endothelial migration of the monocyte to injury site via adhesion remains poorly understood[88,95].

CD13 is highly expressed on many tissues regulating various physiological mechanisms. More recently, it has been shown that CD13 is crucial in the trafficking of immune cells, as CD13 is highly expressed on cells of myeloid lineage in addition to endothelial cells at sites of inflammation. Monocytic CD13 becomes activated by crosslinking antibodies to induce CD13 phosphorylation, leading to CD13-dependent homotypic monocyte/endothelial adhesion[71,96]. Further *in vivo* work from the lab demonstrates that at baseline $CD13^{KO}$ mice have no overt phenotypic differences, but in response to injury less infiltrating myeloid population reach the site of injury after various forms of ischemic injury[86,97]. For instance, after permanent coronary occlusion, $CD13^{KO}$ mice have fewer infiltrating myeloid population after injury affecting cardiac repair[86]. Further evidence in a different model of injury indicates that lack of CD13 affected reperfusion and muscle regeneration after hindlimb ischemia due to a reduction in infiltrating myeloid cells[97].

In this study, a thioglycollate-induced peritonitis model was utilized to confirm altered trafficking contributes to phenotypes found in other models of ischemia. Furthermore, domain specific CD13 chimeras were generated to verify that the C-terminus of CD13 regulated monocyte/endothelial cell adhesion and myeloid trafficking.

2.2 – Materials and methods

Animals

FVB CD13^{KO} mice were generated at the Gene Targeting and Transgenic Facility at the University of Connecticut Health Center[69]. All mice were housed in pathogen-free conditions with 12 h light/dark cycle and controlled temperatures at the University of Connecticut Health Center animal facilities. All procedures were performed in accordance with the Institutional and Office of Laboratory Animal Welfare guidelines.

Thioglycollate-induced sterile peritonitis

Male mice were age matched 6-8 weeks of age and were injected with 1 mL of 3% thioglycollate intraperitoneally. After 48 hours, peritoneal lavage cells were collected for flow cytometric analysis.

Flow cytometry

After collection of cells from peritoneal lavage, spleen, bone marrow and peripheral blood, cells were stained with a cocktail of antibodies at 4°C for 30 min (anti-CD45.1-PE, anti-F4/80-FITC, anti Gr-1-APCe780, anti-CD3/CD19/NK1.1/Ly6G-AF700, anti-CD11c-PECy7 and anti-CD11b-Pacific blue and UV live dead dye (to eliminate dead cells)). Flow cytometry was performed on LSRII (Becton Dickinson) and data was analyzed with FlowJo software (Tree Star). Live/dead cells were negatively gated for T-cells, B-cells, NK cells and Ly6G^{+} cells to eliminate lymphocytes, natural killer cells,

and neutrophils respectively. $CD45^+$ cells were analyzed for macrophages ($F4/80^+$ $CD11b^+$), DCs ($CD11c^+$ $CD11b^+$), inflammatory monocytes ($Gr\text{-}1^{hi}$ $CD11b^+$) and reparative monocytes ($Gr\text{-}1^{lo}$ $CD11b^+$). C33a and WEHI 78/24 cells were stained with 1:250 human CD13 monoclonal antibody 452 followed by 1:1000 goat anti-rat Alexa488 secondary and then analyzed for human CD13 by flow cytometry.

Generation of chimeras

Generation of mouse/human (M/H) chimeric molecule was previously done in the lab by using human CD13 TOPO vector that was digested stepwise with NotI and EcoRI to eliminate the N-terminal half of the construct. The NotI construct was not conserved between mouse and humans species. A mouse CD13 forward primer site was designed to add the NotI site. After the creation of forward and reverse primers for both the C-terminal and N-terminal half of the mouse cDNA, digestion was performed. EcoRI and PmeI site eliminated the C-terminal half of the human CD13 construct to generate human/mouse (H/M) CD13 chimera. Human, mouse, M/H and H/M constructs/chimeras cDNAs were cloned into the pcDNA/V5/GW/D-TOPO (Invitrogen) according to manufacturer's instruction[88].

Cell lines

U937, a human leukemic monocytic cell line; C33a, a human cervical cancer cell line; WEHI 78/24, a mouse monocytic cell line, and Phoenix amphotrophic packaging cell line (Orbigen) were used in this study. C33a and WEHI 78/24 were cultured in Dulbecco's Modified Eagle Medium (DMEM) (Life Technologies)

supplemented with 10% fetal bovine serum (HyClone) and 1% penicillin (100 units/mL)-streptomycin (100 units/mL) (Life Technologies). U937 cells were cultured in Roswell Park Memorial Institute medium (RPMI) (Life Technologies) supplemented with 10% fetal bovine serum (HyClone) and 1% penicillin (100 units/mL)-streptomycin (100 units/mL) (Life Technologies). Phoenix amphotrophic packaging cell lines were cultured with DMEM supplemented with 10% fetal bovine serum (HyClone), 1% penicillin (100 units/mL)-streptomycin (100 units/mL) (Life Technologies) and 1% non-essential amino acids (NEAA) (Life Technologies). All cell lines were cultured at 37°C with 5% CO_2.

Retroviral vector construction and infection

The V5 tagged chimeras and constructs were excised and cloned into retroviral expression vector pBM-IRES-Puro. This vector was transfected into Phoenix amphotrophic cell lines utilizing lipofectamine (Invitrogen). In one tube, 24 µg of DNA vector was added into 1.5 mL DMEM media (no other components were added to the media). In a different tube 60 µL lipofectamine was added in 1.5 mL DMEM. Both tubes were incubated at room temperature for 5 min before combining the tubes. After combination of DNA vector with lipofectamine, this was further incubated at room temperature for 2 min. This mixture was then added to 50% confluent Phoenix amphotrophic cells. After 4 h, the media was changed using DMEM containing fetal bovine serum and penicillin-streptomycin. After 48 h, the media contains viral DNA containing the vector expressing the constructs or chimeras. As a control, empty vector (EV) virus was also generated. C33a were 50% confluent prior to infection

with 10 mL virus stock containing 5 µg/mL polybrene, which neutralizes charge repulsion between virions and sialic acid on cell surface. Viral containing media was removed from C33a after 24 h and cells recovered for 48 h prior to enriching the population with 2 µg/mL puromyocin selection (as determined by a kill curve) for 48 h[88,96]. For infection of non-adherent WEHI 78/24 cells, 1 x 10^5 cells were resuspended in 5 mL virus stock in 15 mL conical tube and centrifuged at 800 g for 30 min at 32°C in the presence of 5 µg/mL polybrene. Cells were supplement in standard DMEM with fetal bovine serum, antibiotics and L-glutamine for 48 h prior to selection. Cells were enriched by puromyocin selection (1 µg/mL for 36 h).

Western blot

Cells were lysed in NP-40 lysis (1% NP-40, 150 mM sodium chloride (NaCl) and 50 mM Tris pH 8) buffer in the presence of protease inhibitors (5 mM sodium fluoride (NaF), 1 mM sodium orthovanadate and a mini protease cocktail (Roche Diagnostics)). Protein concentration was measured by bicinchoninic acid (BCA) assay (Thermo Scientific) following manufacturer's instructions. Samples were run on 10% SDS-Page gel and transferred onto polyvinylidene fluoride (PVDF) membrane. Membranes were blocked in 5% milk/tris-buffer saline tween (TBST) for 30 minutes and then incubated with primary antibody (mouse anti-human 452 1:1000 and 1:10,000 rat anti-mouse CD13) overnight at 4°C on a rocker. The next day, blots are washed thrice with TBST and incubated with secondary antibody (1:1000 goat anti-mouse horseradish peroxidase (HRP) and 1:5000 goat anti-rat HRP). Samples were visualized with chemiluminescence using SuperSignal.

Membrane was developed. Afterward the membrane was stripped for 10 minutes, it was then blocked and probed for loading control, β-actin or glyceraldehyde 3-phosphate dehydrogenase (GAPDH) (1:5000 dilution).

Quantitative adhesion assay

C33a were seeded (5 x 10^5) on 96 well tissue culture treated plates and grown to confluency overnight. Monocytes (U937 or WEHI 78/24) were labeled with calcein (0.5 µL/mL) for 30 min at room temperature in the dark. Monocytes or epithelial layer is then crosslinked with 1 µg CD13 monoclonal crosslinking antibody 452 or IgG for 30 min at 37°C. Monocytes were incubated with C33a epithelial cells to allow for adhesion. Unbound monocytes were extensively washed. Cells were lysed and fluorescence was measured at 485/530 (Biorad, Model 680) after being transferred to a black bottom plate. Each condition was assayed in triplicate.

Adoptive transfer of splenic myeloid cells and mCD13 WEHI 78/24

Differentially labeled with fluorescent dyes PKH67 (green) and PKH26 (red) (Sigma-Aldrich, St. Louis, MO), WT and $CD13^{KO}$ splenic myeloid cells or WEHI 78/24 transfectants were adoptively transferred via tail vein following thioglycollate injection. mCD13 WEHI 78/24 cells were either untreated or treated with 1 mg of Shapiro Lab 13 (SL13) monoclonal blocking antibody. After 48 h, peritoneal lavage cells were analyzed by flow cytometry.

Statistical analysis

Results are presented as mean ± standard error of mean (SEM). Statistical analysis was performed using unpaired, two-tailed *t* test on excel. Differences were considered significant at $p < 0.05$.

2.3 – Results

Previous data from the lab proved that CD13 acts as a homotypic adhesion molecule regulating monocyte/endothelial adhesion *in vitro* and that mice deficient in CD13 had different inflammatory cytokine profiles after injury, indicating that CD13 may regulate inflammatory processes through its adhesive properties. A model of thioglycollate peritonitis was used to evaluate this possibility. Inflammatory monocytes in the bone marrow, spleen, peripheral blood and peritoneal exudates in WT and $CD13^{KO}$ mice were assessed by flow cytometry. The $CD11b^{+}Gr1^{hi}$ pro-inflammatory monocyte population decreased by nearly 70% in $CD13^{KO}$ animals compared to WT, however there was no difference in the $CD11b^{+}Gr1^{lo}$ reparative monocyte. Furthermore, DCs and macrophage populations were also lowered in $CD13^{KO}$ peritoneal lavage when compared to WT lavage (Figure 2.1 A). Remarkably, inflammatory monocytes population was significantly elevated in the blood of $CD13^{KO}$ mice (Figure 2.2 B).

Next, a gain-of-function approach was used to evaluate if CD13 expression offers improved trafficking of monocytes and to confirm that infiltration of myeloid cells into the peritoneal cavity is a CD13 specific event. Adoptive transfer of CD13-expressing

monocytic WEHI 78/24 (mCD13; red) or control cells EV (EV; green) was added into the circulation of WT animals induced with thioglycollate peritonitis. More mCD13-expressing cells resided in the peritoneal cavity when compared to EV control (Figure 2.2 A). Similarly, pretreatment of mCD13-expressing WEHI 78/24 with anti-CD13 blocking monoclonal antibody (SL13; green) resulted in reduction of infiltrating cells into the peritoneal cavity (Figure 2.3 A). These cells were not cleared by the immune system, as equal numbers were present in the peripheral blood of unchallenged animals (Figure 2.2 B, Figure 2.3 B).

To investigate if binding of CD13 is species and domain specific, chimeras were generated using mouse and human constructs of CD13. CD13 is a type II protein composed of seven domains; domain I contains a short cytosolic tail, followed by domain II which is the membrane spanning domain and is highly conserved among species and finally the extracellular portion of CD13 is composed of domains III-VII (Figure 2.4 A). The extracellular domain is site to the enzymatic functions of CD13. Two different chimeras were constructed, one comprising the murine CD13 N-terminus (including domains I-V and 50% of domain VI) fused to human CD13 C-terminus (including 50% of remaining domain VI and domain VII), designated as M/H (Figure 2.4 D, F). The reciprocal chimera H/M was generated comprising the human CD13 N-terminus and C-terminus of murine CD13 (Figure 2.4 E, F). Both endothelial cells (C33a) and monocytic cells (WEHI 78/24) were infected with these clones. Flow cytometric analysis confirmed that exogenous human CD13 was expressed on human construct in addition to M/H chimera (Figure 2.5 A). Western blot analysis

confirmed that exogenous mouse CD13 was expressed on mouse construct in addition to H/M chimera (Figure 2.5 B).

Next, a functional assay was utilized to determine if the C-terminal domain was mediating homotypic monocyte/endothelial cell adhesions. Previously, reports indicated that basal adhesion of primary $CD13^{KO}$ macrophages to endothelial cells is diminished and that CD13 activation on either monocytes or macrophages induces adhesion *in vitro*[69,71,96]. *In vitro* adhesion assay utilizing the engineered cell lines were designed. Activating anti-human monoclonal antibody 452 was used to verify that the effects of trafficking obtained with the chimeric monocytic cell lines *in vivo* is due to CD13 homotypic adhesion. The various CD13-expressing monocyte cell lines were added to adherent epithelial cells C33a (expressing EV control or human CD13) activated with antibody 452 or isotype control (Figure 2.6 A). Monocytes expressing human CD13 and M/H CD13 mediated homotypic adhesion to human CD13 positive epithelial cells. Relatedly, activation of the U937 monocytes with 452 or isotype control allowed for adhesion with epithelial cells expressing human CD13 or M/H CD13 (Figure 2.6 B). Comparably, activation of WEHI 78/24 M/H CD13 with human CD13 monoclonal antibody 452 induced adhesion in epithelial cells expressing total human CD13, as well as the chimera M/H, albeit at decreased levels (Figure 2.6 C). These *in vitro* assays indicate that the C-terminal domain of CD13 mediates homotypic monocyte/endothelial cell adhesion.

Finally, the objective was to identify which domain was responsible for cellular trafficking in response to inflammation. Similar to previous experiments, differentially labeled cells with CD13-expressing monocyte lines or EV control were intravenously injected into WT mice followed by thioglycollate injection. Initial experiments by flow cytometry, confirmed that WEHI 78/24 expressing H/M chimera trafficked better to the peritoneal lavage than EV WEHI 78/24 (Figure 2.7). Flow analysis revealed that labeled peritoneal cells in the lavage were markedly higher for cells expressing H/M CD13 chimera compared to EV or M/H CD13 chimera (Figure 2.8). Importantly, the percentage of cells in circulation of other chimeras and EV control remained the same. These results indicate that the C-terminal domain is responsible for inflammatory cell trafficking.

2.4 – Discussion

Originally, CD13 was shown to be a marker of myeloid cells, where it is expressed by varying degrees on myeloid progenitors and their differentiated progeny[98]. More investigations in the lab demonstrated that CD13 is highly expressed on myeloid cell subsets expressing $CD8^+$ DCs where it mediates receptor-mediated antigen uptake leading to T cell activation[77]. Further studies identified CD13 is highly expressed on monocytes and may act as an important adhesion molecule after injury as shown in models of both myocardial infarction and hindlimb ischemia[86,97]. Intriguingly, despite the ratios of infiltrating cells being altered in both tissues types, myeloid cells were differentially affected, indicating that myeloid cell trafficking patterns might be injury- and tissue-specific[95] and that CD13 may command these trafficking phenotypes.

This study utilized an injury model of thioglycollate-induced peritonitis to validate that CD13 is an important regulator of cellular trafficking *in vivo*. Furthermore, the study also wanted to identify the specific domain responsible for mediating adhesion.

Previous studies have identified CD13 as a species specific receptor for a subtype of human coronaviruses, and this activity does not affect its enzymatic activity[80]. CD13 was first identified to have various enzyme-dependent functions like cleaving neutral amino acids from the terminus of other small molecules, as well as peptides in the renin-angiotensin system and intestinal dietary peptide[99-101]. More recent studies on CD13 have also demonstrated that CD13 has important implications beyond its enzymatic activities, identifying CD13 as a molecule that mediates homotypic adhesion between monocytic and endothelial cells[71]. This study demonstrated the importance of CD13 in monocyte-endothelial cell adhesion and trafficking by utilizing various models including thioglycollate-induced peritonitis in addition to gain-of-function adhesion assays with cells expressing mouse CD13 or treated with blocking mouse CD13 antibody.

The C-terminal domain of CD13 has been identified as an important receptor for group 1 coronaviruses each of which has a unique species-specific binding site for CD13[102,103]. Relatedly, the study found that CD13 dependent adhesion is also species specific. Through the creation of chimeric expression constructs of the N- and C-terminal domains of human and mouse CD13 in both epithelial cells and monocytes, it was shown that the C-terminal half mediates adhesion on cells

expressed on both the monocytes and the endothelial layer. *In vitro* functional assays as well as adoptive transfer studies of differentially labeled cells expressing mixed chimeras *in vivo* showed that the C-terminal region of CD13 is crucial for homotypic adhesion between endothelial cells and monocytes. Further studies will conclude whether specific regions that dictate virus host range in various coronaviruses also determines species-specific adhesion.

Subsets of various monocytes exist that are responsible for either inflammation or reparation. Depending on the microenvironment of infection, inflammatory monocytes (Gr-1^{high}/Ly6C^{high}, mouse) have two main fates after arriving at the site of infection in that they either differentiate into activating or inhibitory macrophage and DCs subsets. These inflammatory monocytes are elevated in the circulation in response to injury and infiltrate injury sites more readily than reparative monocytes[95,104]. Reparative monocytes (Gr-1^{lo} CD11b^{+}) reside in tissues and replenish tissue macrophages or DCs to aid in the healing process[104,105]. The present study found that CD13 is more highly expressed on the inflammatory monocyte subset and that migration of these inflammatory cells is skewed in CD13^{KO} mice after thioglycollate-induced peritonitis. Despite these advancements in the field, the differential trafficking to tissues after injury remains unknown and it will require more investigation to identify the precise mechanism that regulates inflammatory trafficking.

2.5 – Figures and Legends

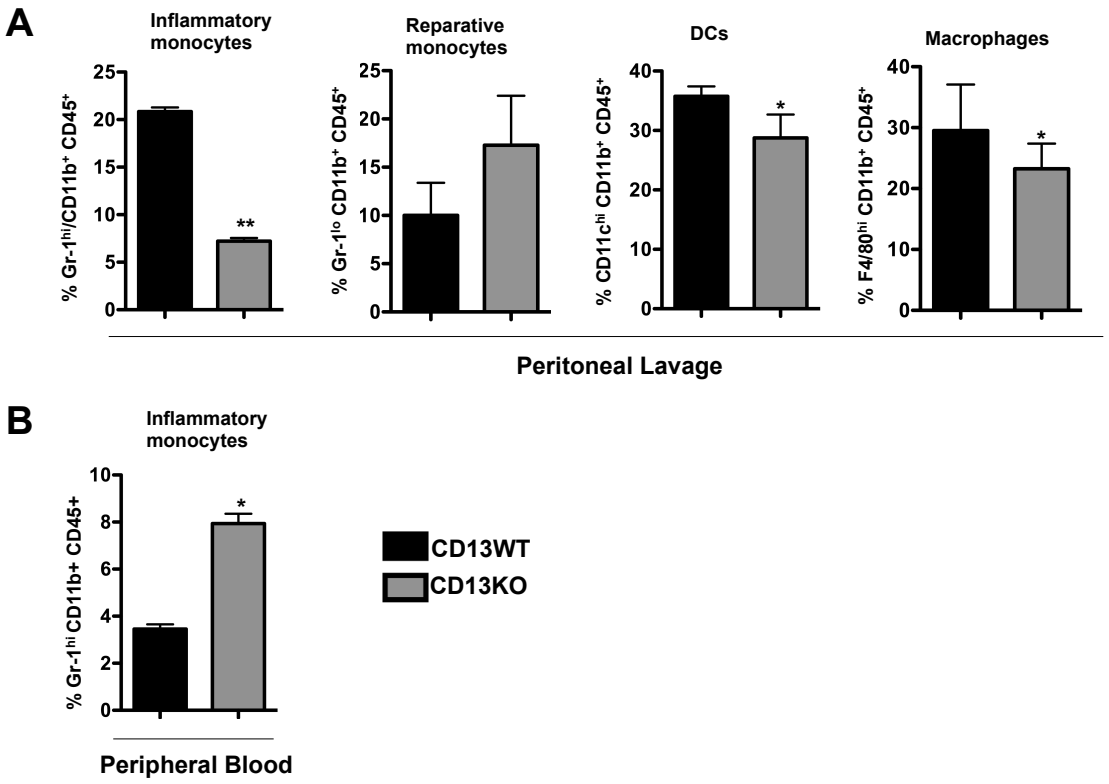

Figure 2.1 – Altered inflammatory cells in CD13^{KO} mice after thioglycollate peritonitis.

(A) Flow cytometric quantification of percent of infiltrating inflammatory monocytes (Gr-1^{hi} CD11b^{+}), reparative monocytes (Gr-1^{lo} CD11b^{+}), macrophages (F4/80^{hi} CD11b^{+}) and DCs (CD11c^{hi} CD11b^{+}) based on gated CD45^{+} cell population collected from peritoneal lavage. (B) Flow cytometric quantification of percent inflammatory monocytes (Gr-1^{hi} CD11b^{+}) in peripheral blood. Error bars represent mean ± SEM for WT (n=8) and CD13^{KO} (n=8) mice; *p<0.05.

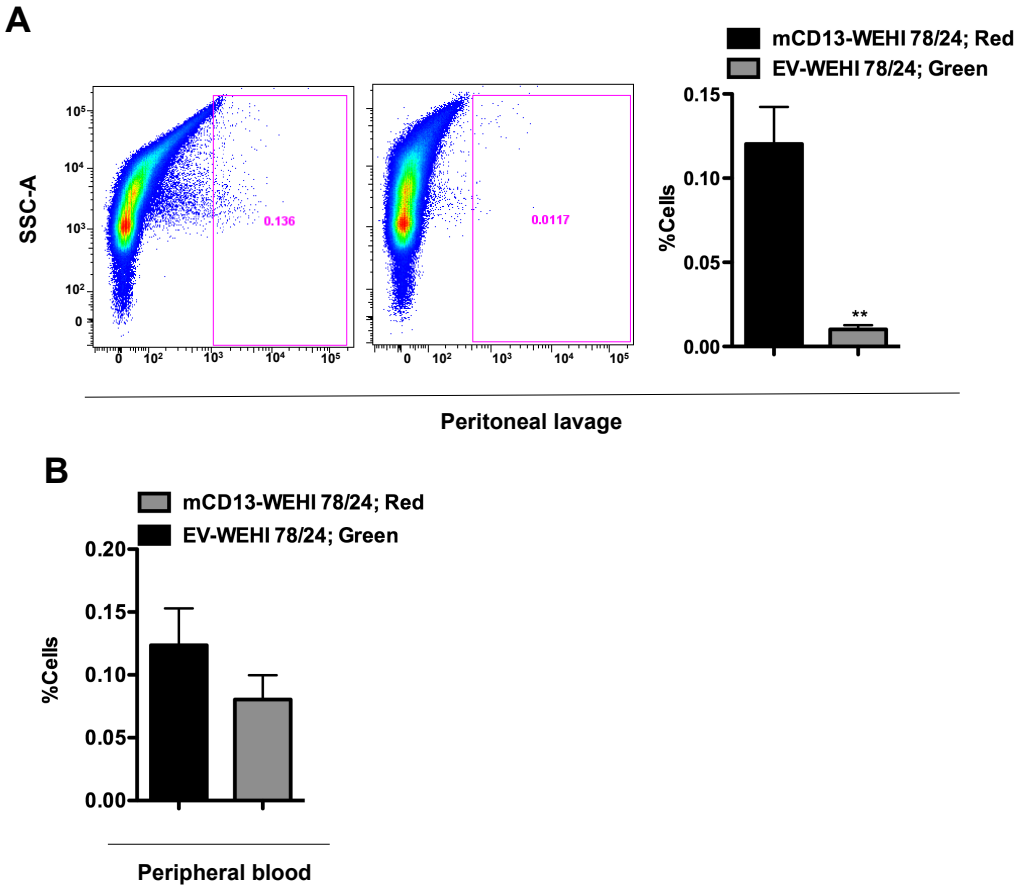

Figure 2.2 – CD13 expressing monocytes traffic to peritoneal cavity after injury. (A) Differentially labeled murine monocytic WEHI 78/24 cells with either mouse CD13 (mCD13-red) or EV control (EV-green) were adoptively transferred into thioglycollate administered WT mice. Cells expressing CD13 trafficked to peritoneal lavage as analyzed by flow cytometry. (B) Peripheral blood expressed similar percentages of labeled monocytes. Data represents average of 3 independent mice experiments. Error bars represent mean ± SEM for WT (n=5) and $CD13^{KO}$ (n=5) **p<0.01.

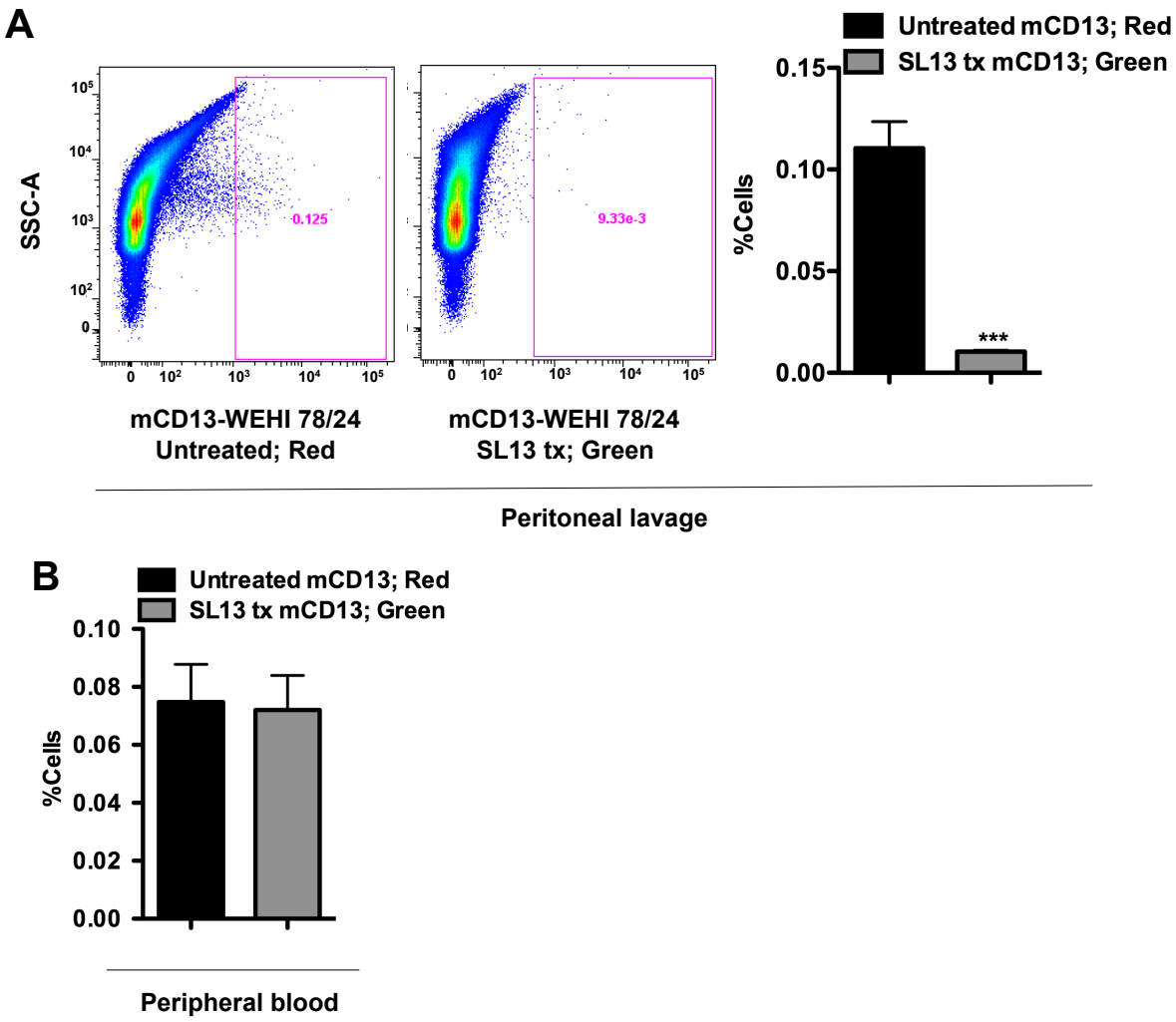

Figure 2.3 – Blocking CD13 expression inhibits monocytes trafficking to peritoneal cavity after injury.
(A) Differentially labeled murine monocytic WEHI 78/24 cells with untreated mouse CD13 (mCD13-red) or SL13 blocking antibody treated mouse CD13 (SL13 tx CD13-green) were adoptively transferred into thioglycollate administered WT mice. Cells expressing CD13 trafficked to peritoneal lavage as analyzed by flow cytometry. (B) Peripheral blood expressed similar percentages of labeled monocytes. Data represents average of 3 independent experiments. Error bars represent mean ± SEM for WT (n=5) and $CD13^{KO}$ (n=5) mice; ***p<0.001.

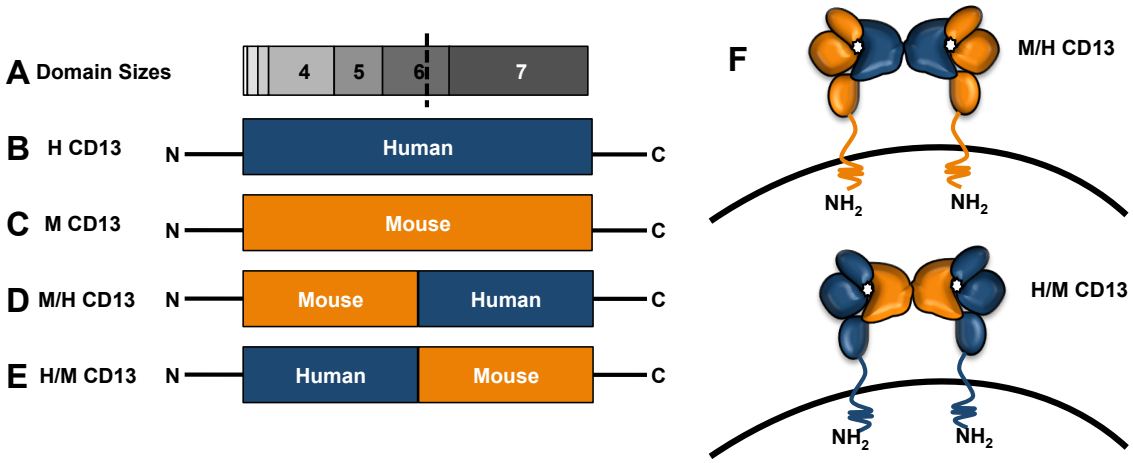

Figure 2.4 – CD13 species and domain-specific construct.
(A) Domain size represented for CD13 and dotted line represents halfway point of CD13 construct. (B) Full length human CD13 and (C) full length mouse CD13. (D, F) M/H chimera construct denotes CD13 chimera containing mouse CD13 at the N-terminal half and human CD13 at the C-terminal half and (E, F) H/M chimera construct denotes human CD13 at the N-terminal half and mouse CD13 at the C-terminal half.

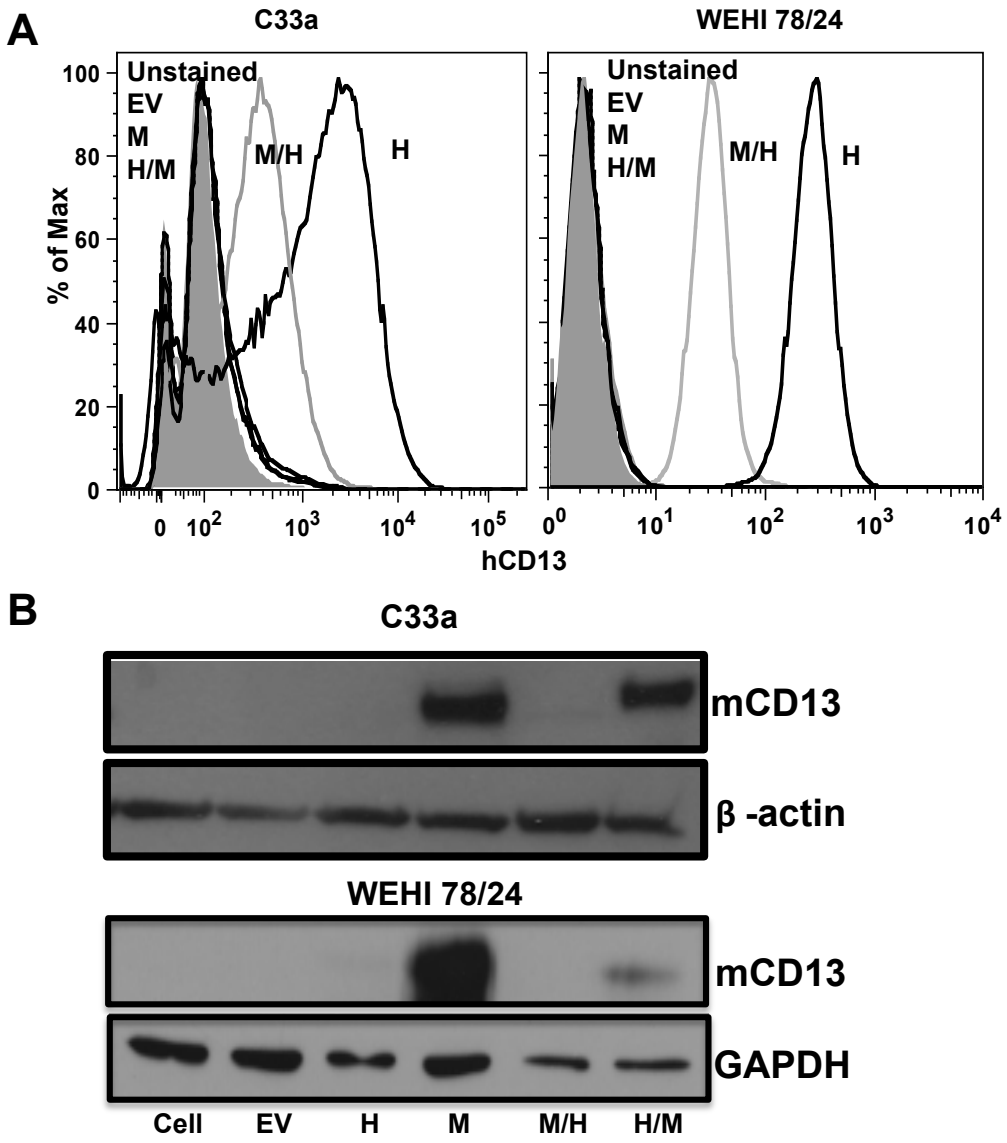

Figure 2.5 – CD13 expression in chimera constructs.
(A) Histogram of C33a and WEHI 78/24 expressing human CD13 and M/H chimera with anti human 452 CD13 monoclonal antibody as analyzed by flow cytometry. (B) Western blot analysis of C33a and WEHI 78/24 expressing mouse and H/M CD13 constructs. Data represents average of two independent experiments.

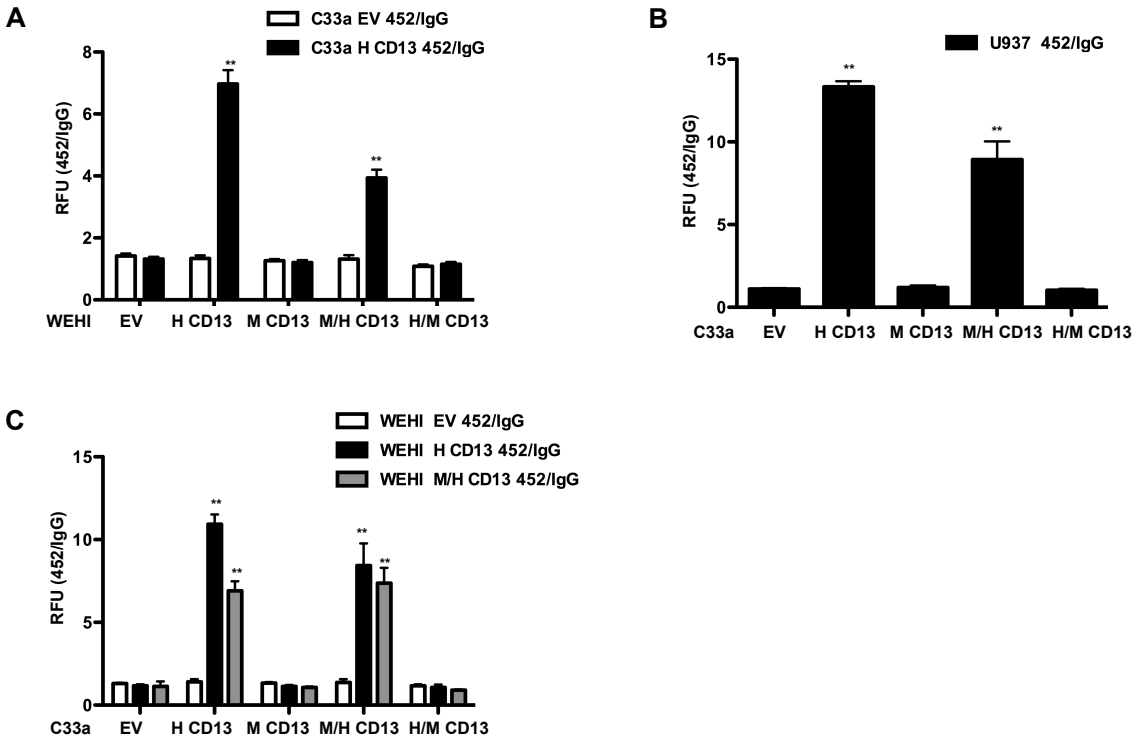

Figure 2.6 – The C-terminal domain is responsible for homotypic cell adhesion. (A) EV and human CD13 expressing C33a cells were treated with activating anti human CD13 452 monoclonal antibody or control IgG. Calcein labeled WEHI 78/24 expressing all constructs were added to the monolayer and homotypic adhesion was measured as fluorescence intensity at O.D. 485 nm and 530 nm. A significant increase in adhesion was observed in WEHI 78/24 expressing human CD13 and M/H CD13. (B) The human monocytic cell line highly expressing CD13, U937, was calcein labeled and cross-linked with 452 or IgG. U937 cells were incubated with C33a expressing all constructs and adhesion was measured. C33a expressing human CD13 and M/H CD13 showed significant adhesion with 452 activated U937 cells. (C) Comparably, WEHI 78/24 EV, human CD13 and M/H CD13 activated with 452 or IgG was added to all constructs of C33a monolayer. C33a expressing human CD13 and M/H CD13 showed significant homotypic adhesion to WEHI 78/24 expressing human CD13 and M/H CD13. Data represents ratio of relative fluorescence unit (RFU) measured upon activation with 452 to control IgG. Data represents average of 3 independent experiments ran in triplicate. Error bars represent mean ± SEM; **, $p<0.01$.

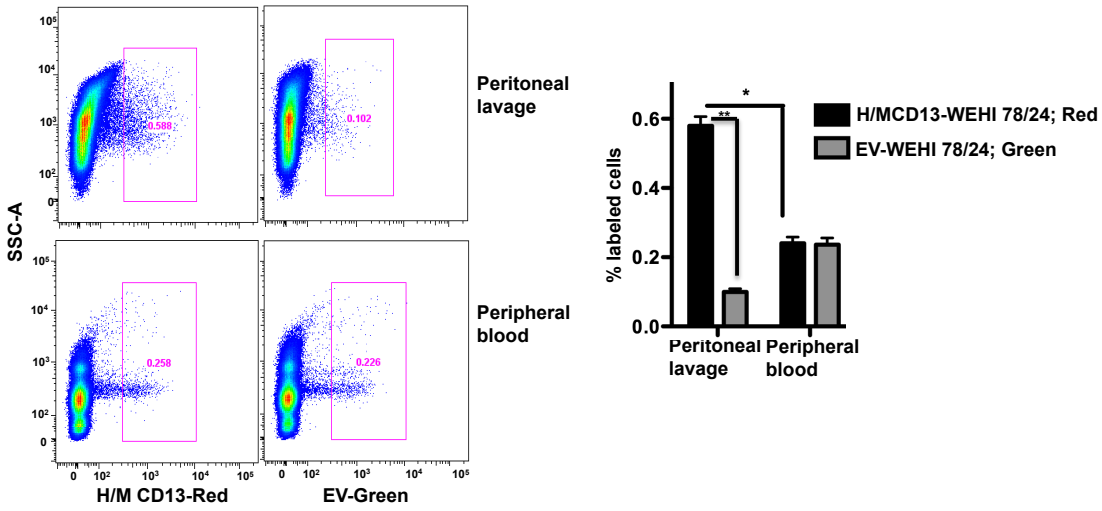

Figure 2.7 – Expression of CD13 on monocytes is vital for cell trafficking into inflamed peritoneum.

Equal number of WEHI 78/24 cells transfected with H/M (CD13; red) and EV (EV; green) were injected into WT mice after thioglycollate-induced peritonitis. Data represents average of three independent experiments. Error bars represent mean ± SEM for WT (n=5) mice; *p<0.05; **, p<0.01.

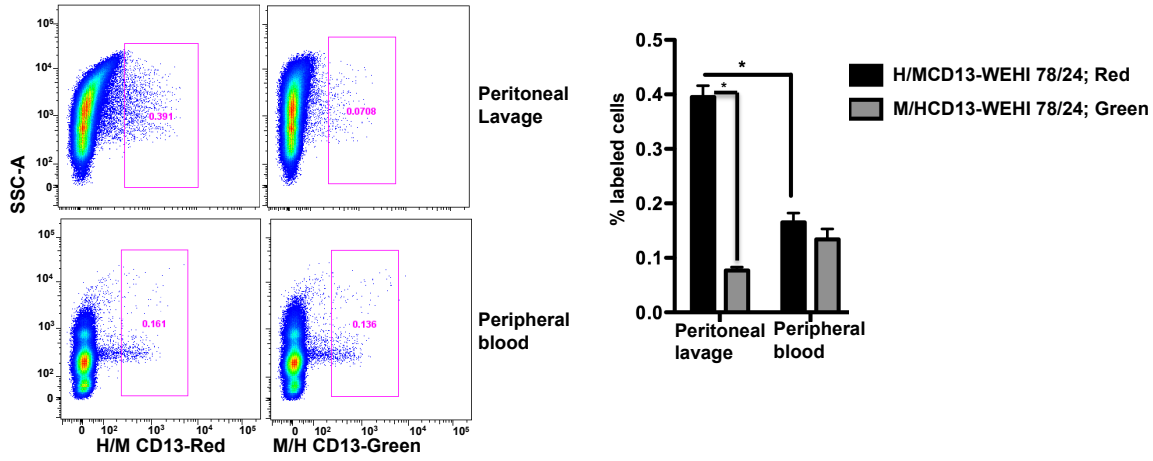

Figure 2.8 – The C-terminal half of CD13 in monocytes is vital for cell trafficking into inflamed peritoneum.
Equal number of WEHI 78/24 cells transfected with H/M (CD13; red) and M/H (CD13; green) were injected into WT mice after thioglycollate-induced peritonitis. More WEHI 78/24 expressing H/M chimera trafficked to peritoneal lavage as determined by flow cytometry. Total cells in blood were equivalent. Data represents average of three independent experiments. Error bars represent mean ± SEM for WT (n=5) mice; *p<0.05.

Chapter 3

CD13 is a novel regulator of renal tubular endocytosis

3.1 – Introduction

CKD develops in response to a variety of different insults and conditions including trauma, sepsis, toxicity, cardiovascular disease and diabetes mellitus[3,4]. Of the 26 million patients affected yearly in the United States, approximately 1.8 million of these are ultimately treated for ESRD by renal replacement therapy involving kidney transplant, hemodialysis or peritoneal dialysis. Over time the kidney slowly deteriorates due to complications from hypertension, diabetes or congenital abnormalities[1]. Currently, there has been minimal progress toward limiting the progression of renal deterioration despite implementation of the most aggressive treatment options, which provide only limited protection to the nephron.

Numerous physiological pathways are disrupted throughout disease progression that cumulatively contributes to irreversible renal injury and failure. In a healthy kidney, the glomerulus filters albumin and other low molecular weight proteins and the proximal tubules reabsorb these filtrates by endocytosis via the megalin/cubilin receptor complex[6,8-11]. Impairment of either glomerular or tubular function leads to albuminuria, promoting even further cellular dysfunction[34,41]. Urinary albumin triggers pro-inflammatory and pro-fibrotic mechanisms which further damages renal structures[35,106].

One of the major sources of CKD in the United States is diabetic nephropathy, which results from complication of diabetes mellitus. About 20% of patients with type 1 or type 2 diabetes develop diabetic nephropathy within 10 to 20 years after diabetic

onset[4,12-14]. Hyperglycemia attacks renal microvasculature leading to injury of various kidney cells found in the glomerulus and proximal tubules[12,14]. Increased glucose levels leads to damage at the basolateral membrane of proximal tubules. Increased glucose filtration at the glomerulus leads to overload, resulting in increased filtrate exposure at the proximal tubules[14]. However, the exact pathophysiology and molecular pathways that lead to renal failure caused by hyperglycemia remains unknown, albeit growing insight into studying disease progression. To induce diabetic nephropathy in this study, mice were treated with a low dose of STZ for five consecutive days. Mice develop overt diabetes within three weeks and signs of diabetic nephropathy like albuminuria within five weeks after STZ treatment[2].

Recently, it was discovered that TLR4 is activated in response to renal events observed in multiple different kidney injury models including diabetic nephropathy. TLR4 deficient mice had improved renal function, significantly less albuminuria, and decreased activation of NF-κB and infiltration of interstitial macrophages in comparison to WT mice in response to STZ induced diabetic nephropathy[63]. In humans, TLR4 is highly expressed in patients with diabetic nephropathy[65-67]. Overall, there is strong evidence that lack of TLR4 attenuates inflammatory responses and prevents the development of diabetic nephropathy[63,68].

CD13 is a cell surface, membrane-bound, metallopeptidase expressed on various myeloid cells as well as the apical surface of renal proximal tubule cells where it was

found to cleave neutral amino acids from dietary peptides[70]. Importantly, recent findings demonstrate that CD13 regulates endocytosis of immune regulator TLR4 in DCs and promotes pro-inflammatory signal transduction in response to tissue injury. PAMPs or DAMPs bind to macrophages and DCs, inducing TLR4 downstream release of cytokines. Macrophages and DCs deficient in CD13 signal towards anti-inflammatory pathways[87,91], suggesting that CD13 synchronizes the balance between pro-inflammatory and anti-inflammatory signaling.

In the proximal tubules of the kidney, receptor-mediated endocytosis is crucial for resorption and metabolism of substances found in the lumen coming from the glomerular filtrate. Megalin and cubilin have been identified as the two major contributors involved in receptor- and clathrin-dependent endocytosis occurring in the epithelial cells of the proximal tubules[6,27,57,58]. Following internalization, molecules from the plasma membrane are either recycled back to the surface in recycling endosomal compartments, sorted to the degradation pathway via late endosomes and lysosomes or returned to the circulation by transcytosis[31,51,55]. Acidification of the endosomal sorting compartment allows for the release of albumin from the megalin/cubilin receptor and the subsequent binding to the FcRn receptor. FcRn facilitates the transportation of albumin towards the basolateral membrane of the proximal tubule where it is released back into circulation[31]. Patients with mutations in the megalin or cubilin receptor, present with high urinary albumin levels[107]; indicating that alterations within the endocytic machinery of the proximal tubules affects urinary protein levels and subsequent renal injury. Importantly, like

megalin and cubilin, CD13 is highly expressed on the brush border of renal proximal tubules. Furthermore, recent data from the lab suggest that CD13 is a novel regulator of clathrin-mediated endocytosis that controls internalization of a number of receptors including transferrin, mannose and TLR4[77,89,90].

Since CD13 had been shown to intricately regulate TLR4 signaling pathways, it was hypothesized that CD13 would regulate TLR4 signaling in response to renal injury. It was also proposed that CD13 might inhibit receptor-mediated endocytosis of glomerular filtrate in proximal tubular epithelial cells.

3.2 – Materials and Methods

Mice

Global $CD13^{KO}$ mice were generated at the Gene Targeting and Transgenic facility at the University of Connecticut Health Center[69]. All mice were housed in pathogen-free conditions with 12 h light/dark cycle and controlled temperatures at the University of Connecticut Health Center animal facilities. All procedures were performed in accordance with the Institutional and Office of Laboratory Animal Welfare guidelines.

Diabetic Nephropathy

Age matched, 6 to 8 week old C57/Bl6 mice were fasted for 6 h prior to injection of 50 mg/kg of STZ in 1 M sodium citrate buffer, pH 4.5. Intraperitoneal injection was

given for 5 consecutive days to induce diabetes (n=14)[108]. Sham mice received injection of sodium citrate buffer only (n=5). Mice were housed in metabolic cages at basal time points and every 4 weeks after treatment for 24 h to collect urine.

Glucose tolerance test

Blood glucose was measured after 16 h of fasting using an Accu-Chek® glucose monitor (Roche Diagnostics) from tail vein blood. Glucose was intraperitoneally injected (20% glucose solution, 1 g/kg) and blood glucose was measured at 15, 30, 60 and 120 min after injection[109].

Electron microscopy

All processing took place at the Electron Microscopy Core at the University of Connecticut Health Center. Kidney tissue was fixed by whole body perfusion with 2.5% glutaraldehyde in 0.1 M sodium cacodylate buffer, pH 7.4. Tissues were further fixed with osmium tetroxide. Postfixation tissues were dehydrated in graded ethanol solutions. Tissues were embedded in epoxy resins and 70 mm sections were cut on the Leica ultramicrotome, mounted on 200 mesh copper grids and counterstained with uranyl acetate and lead citrate. Images were taken on Hitachi H-7650 transmission electron microscope.

Measurement of albumin and IgG clearance

Mice were given a single intravenous dose of 2 mg FITC-labeled albumin (Sigma, A9771) or 0.5 mg of FITC-labeled IgG (Sigma, F9636). Retro-orbital blood was collected 12, 24 and 48 h after injection. Samples were frozen at -80 °C and thawed at time of assay. Quantities of fluorescence were measured spectrofluorimetrically; baseline serum was used to subtract background fluorescence.

Albumin overload

WT and $CD13^{KO}$ mice 7 weeks old were given daily intraperitoneal injections of bovine serum albumin (BSA) (Sigma A-9430) dissolved in sterile saline starting at 2 mg BSA/g body weight with increasing doses of 2 mg BSA/g body weight until day 5 and a final injection was given on day 8 of 10 mg BSA/g body weight (n=9). Sham mice received injections of saline (n=3). Mice were placed in individual metabolic cages overnight on day 8 for 24 h urine collection and harvested on day 9 for further analysis[49,50].

Histology

Kidneys and pancreas were harvested and fixed in 10% formalin (Fisher Scientific) overnight at 4°C and dehydrated in 70% ethanol prior to processing and embedding. Paraffin-embedded sections were de-paraffinized in histoclear or xylene and then washed in graded ethanol prior to rehydration. For Periodic acid-Schiff (PAS) stain, slides were treated with 0.5% periodic acid (Sigma, P7875) for 15 min, rinsed in

distilled water, stained with Schiff's reagent (Rowley Biochemicals, SO-429) for 15 min. Nuclei was stained with hematoxylin for 1 min. Antigen retrieval was performed using sodium citrate buffer. Tissues were blocked for 1 h and incubated with primary antibody overnight at 4 °C (CD13 1:1000, Megalin 1:1000, FcRn 1:100). Slides were washed and the appropriate secondary antibody was added for 1 h. After the final wash, nuclei were counterstained with DAPI in mounting media (Vectashield, Vector Laboratories).

Cell culture of primary proximal tubule epithelial cells

Cortex of the kidney was removed, minced and digested in 15 mL collagenase (0.0125 g in 50 mL plain DMEM/F12 media) for 45 min at 37°C with 5% CO_2. After digestion cells were treated with red blood cell (RBC) lysis buffer for 5 minutes, followed by filtration with a 40 µm strainer before being plated onto plastic dishes ($1x10^6$ cells in a 6 cm dish or $2x10^6$ cells in a 10 cm dish). DMEM/F12 media (Corning CellGro, 10-092-CV) was supplemented with 2.5% fetal bovine serum, 1% penicillin (100 units/mL)-streptomycin (100 units/mL) (Life Technology) and 1% NEAA (Life Technology). Cells were cultured in an incubator with 5% CO_2 at 37°C. Media was changed every 3 days maintaining 1/3 of the original media.

Western blot

Cells were grown to confluency and lysed with 1% NP-40, 25 mM Tris-hydrochloric acid (HCl) (pH 7.4), 150 mM NaCl, 10 µg/mL aprotinin, 10 µg/mL leupeptin, 50 mM

β-glycerophophate, 1 mM sodium fluoride (NaF) and 100 mM NaOrhovanidate. Protein concentration was determined by BCA protein assay kit according to manufacturer's protocol (ThermoFisher Scientific). For immunoprecipitation, 500 µg of protein lysate was incubated overnight at 4°C with 2 µg antibody (IgG, CD13 or p-tyrosine). Protein G beads were added to lysate and incubated for 2 h, washed and resuspended. Lysate was denatured for 5 min at 100°C, cells were run on 10% SDS-Page gel (4% for megalin). Gels were transferred onto PVDF membranes. Blots were blocked with 5% BSA/TBST and incubated with primary antibody (1:10,000 CD13, 1:1000 E-cadherin, 1:1000 megalin, 1:5000 β-actin, 1:1000 FcRn) overnight at 4°C, washed and incubated with appropriate secondary for 1 h at room temperature. Bands were visualized with ECL and developed.

Flow cytometry

For primary cells, media was collected and cells were treated with Tryp LE (Gibco, 12605-010) for 10 min and pelleted. For kidneys, the entire kidney was minced and treated with collagenase for 1 h at 37°C. Cells were treated with RBC lysis buffer and filtered. For Annexin/PI (Life technologies, V13242) staining protocol was followed as described in manual. For albumin uptake, cells were first stained with 1:20 CD26 APC (Biolegend, 137807) and then fix/permeabilized (BD, 554741) per manufacturer's protocol. Cells were stained with 1:20 FITC albumin (R&D, IC1455G). Flow analysis was run on LSR-II and data was analyzed with FlowJo software (Tree Star).

Measurement of serum and urine

All urine was collected using metabolic cages. Mice were individually housed in metabolic cages for 24 h and urine was collected throughout this period. Diabetic mice were placed in the cage at basal, 8, 12, 16 and 20 weeks post STZ treatment. AO mice were placed in metabolic cages on day 8. Serum was collected by cardiac puncture. Albumin enzyme-linked immunosorbent assay (ELISA) (Bethyl, E90-131), urinary creatinine (R&D, KGE005) and serum creatinine (Caymen, 700460) were used to analyze albuminuria and GFR.

Statistical analysis

Results are represented as mean ± SEM. Statistical analysis was performed using unpaired, two-tailed *t* test analysis using Microsoft Excel. Differences were considered significant at $p < 0.05$.

3.3 – Results

$CD13^{KO}$ mice have decreased albuminuria 20 weeks after STZ treatment

To directly investigate the interaction of CD13 in renal injury, diabetic nephropathy was induced by injecting mice with STZ (or sham) for five consecutive days into WT and $CD13^{KO}$ mice. Mice were harvested 20 weeks after the last injection. Weight gain was assessed every four weeks. Overall weight gain was diminished in STZ treated animals compared to controls, but no overall difference was observed between WT and $CD13^{KO}$ mice (Figure 3.1). Additionally, the ratio of kidney weight

to the body weight decreased in STZ treated animals, but again there was no difference between WT and $CD13^{KO}$ animals (Figure 3.1). The pancreas is the first targeted organ during diabetic development, as the Islets of Langerhans found in the beta cells are destroyed and incapable of releasing insulin in response to STZ treatment. To rule out the pancreas as the underlying reason for identifying differences in diabetic kidneys, pancreatic histology was evaluated and glucose tolerance tests were performed. After STZ treatment, pancreatic beta cells were destroyed and surrounding architecture of the pancreas was altered as visualized by hematoxylin and eosin stain (Figure 3.2). STZ led to glucose intolerance in diabetic animals as they were incapable of returning blood glucose levels back to fasting baseline levels within two hours after intraperitoneal injection of glucose (Figure 3.3). There were no observed and functional differences between the pancreas of WT and $CD13^{KO}$ after STZ treatment. Four months after the induction of diabetes kidney function was evaluated by serum creatinine. There was a decline in kidney function in diabetic WT and $CD13^{KO}$ animals compared to sham mice (Figure 3.4) Furthermore, there was increased urinary albumin excretion in diabetic kidneys 8, 12, 16 and 20 weeks after diabetic onset compared to sham treated animals. Interestingly, total 24 h albumin excretion rate was significantly higher in WT STZ treated mice than $CD13^{KO}$ mice 20 weeks after the induction of diabetes (Figure 3.4).

$CD13^{KO}$ mice maintain normal architecture of proximal tubule brush border

Next, the integrity of cortical kidney sections was evaluated by PAS stain. Tubules were dilated, nuclei were shedding into the proximal tubules and there was overall

sclerosis of the glomerulus in both WT and $CD13^{KO}$ kidneys 20 weeks after STZ. Sham kidneys display normal characteristics and architecture with intact brush border staining (Figure 3.5). Trichrome stain of STZ treated animals reveals a slight increase in fibrosis in WT animals at 20 weeks when quantified with ImagePro Plus software (Figure 3.6). Electron microscopy was further utilized to assess morphological differences at high magnification of both the glomerulus and the proximal tubule. First, an evaluation of the glomerular structure in WT and $CD13^{KO}$ animals was performed; as it has been determined that glomerular injury is a major contributor to albuminuria. Initial glomerular anatomy revealed no stark differences between WT and $CD13^{KO}$ animals, and upon further evaluation of slit diaphragms overall structure remains mostly intact, but disruption is evident in both WT and $CD13^{KO}$ glomerulus. This ultimately leads to leaky filtration of proteins like albumin (Figure 3.7). Finally, proximal tubule integrity was assessed to determine if differences in albuminuria between WT and $CD13^{KO}$ mice was due to differences in proximal tubule structures. The integrity of the brush border revealed stark visual differences between WT and $CD13^{KO}$ proximal tubules. Brush border remained intact and normal in $CD13^{KO}$ tubules, while the brush border of WT tubules were partially destroyed and broken down (Figure 3.8). Additional evaluation of electron microscopy in the proximal tubules showed intact endocytic vesicles. Interestingly, quantification of endocytic vesicles by electron microscopy near the brush border surface revealed that $CD13^{KO}$ mice had significantly more vesicles than WT mice (Figure 3.9). Overall, there is decreased albuminuria in $CD13^{KO}$ mice. This appears to be independent of altered responses to STZ treatment specifically within the

pancreas or glomerulus, as glucose levels and glomerular histology was similar in WT and $CD13^{KO}$ animals. Instead, $CD13^{KO}$ proximal tubules had intact brush borders and increased endocytic vesicles, indicating that differences in albuminuria levels is likely due to differential response to damage in the proximal tubules.

Lack of CD13 increases uptake of albumin by proximal tubules

In an effort to uncover the mechanism of proximal tubule uptake, an *in vitro* model was utilized to identify CD13's role in albumin uptake in proximal tubules. It is known that isolated primary proximal tubular epithelial cells quickly lose expression of important proximal tubular markers after early passages including CD13 and megalin. Isolated primary proximal tubule epithelial cells expressed proximal tubule markers megalin and E-cadherin in addition to CD13 at low passage (Figure 3.10). The proximal tubule receptors megalin and cubilin are positive mediators of albumin uptake. Previously it has been shown that megalin surface expression and internalization is regulated by phosphorylation[6,27,57]. To identify the possibility of CD13 regulating albumin uptake, it was first determined if CD13 is activated in response to albumin. WT primary proximal tubule epithelial cells were treated with 1% BSA for 0, 5, 15, 30, 60 and 120 min and then lysed. Lysate was immunoprecipitated with IgG or p-Tyrosine (CD13 activation site) and then probed for CD13 to determine specific activation of CD13. A dose response with increasing length of treatment was observed indicating that BSA activates CD13 (Figure 3.11). Furthermore, uptake of leaky albumin from the glomerulus is vital and occurs at the proximal tubules. With increasing doses of FITC-albumin, $CD13^{KO}$ primary proximal

tubule epithelial cells more efficiently took up albumin than WT primary proximal tubule epithelial cells as determined by flow cytometric analysis (Figure 3.12). CD13 is a negative regulator in receptor-mediated, dynamin-dependent endocytosis of albumin in the proximal tubules.

CD13 co-localizes with FcRn in proximal tubules

Filtrates that traverse the glomerular filtration barrier are normally reabsorbed in the proximal tubules by endocytic processes. Internalized substances are either degraded by lysosomes or returned back into the bloodstream by transcytosis. Next, it was essential to determine if CD13 and megalin co-localize since megalin is a crucial mediator of albumin internalization. Immunofluorescence staining reveals that megalin and CD13 are both expressed in the brush border, but are distinctly separate. Megalin did not co-immunoprecipitate with CD13 upon further analysis (Figure 3.13). Another known regulator of albumin is FcRn, aiding in the transcytosis of albumin back into the bloodstream after uptake of albumin by the megalin-cubilin complex. FcRn binds albumin at low luminal pH after its release from the megalin-cubilin complex. Interestingly, FcRn and CD13 do co-localize at the brush border of the proximal tubule, however the two proteins do not co-immunoprecipitate. Additionally, the two proteins co-localize in vesicles inside the proximal tubules (Figure 3.14). To determine if CD13 regulated transcytosis of albumin, the half-life of albumin in WT and $CD13^{KO}$ mice was evaluated after injection of a single intravenous dose of FITC-labeled albumin. $CD13^{KO}$ mice reclaimed greater quantities of albumin than WT mice 12 and 24 h after injection, but levels equalized

after 48 h (Figure 3.15). There was no difference in the half-life of IgG between WT and $CD13^{KO}$ mice as expected as this is regulated by the glomerulus and not the proximal tubules (Figure 3.15)[60].

Primary proximal tubule epithelial cells undergo necrosis in response to high albumin doses

Reduction of urinary protein levels is known to be therapeutically beneficial, however various studies indicate that proteinuria-induced lysosomal overload underlies mechanisms leading to cell damage[31,40,49,110]. $CD13^{KO}$ proximal tubules take up albumin more efficiently than WT proximal tubules, but it was uncertain if this offered protection to the renal proximal tubules. To investigate this phenomenon, WT and $CD13^{KO}$ primary proximal tubule epithelial cells were serum starved overnight and treated with increasing doses of BSA. Upon collection of *in vitro* primary proximal tubule epithelial cells, the cells were stained with annexin and PI and then quantified by flow cytometry for total apoptosis and necrosis, respectively. No observed difference was visualized between cells positive for apoptosis or double positive for apoptosis and necrosis marker 24 or 48 h after treatment (Figure 3.16). When evaluating necrosis in primary proximal tubule epithelial cells, there was a strong time and dose dependent response for both WT and $CD13^{KO}$ cells (Figure 3.16). Despite their ability to take up more albumin, $CD13^{KO}$ primary proximal tubule epithelial cells had equivalent levels of necrosis when compared to WT cells indicating that high levels of circulating fragmented albumin might be harmful to renal proximal tubules.

AO leads to increase in albuminuria and less albumin uptake by proximal tubules in WT mice

Albuminuria is a hallmark of kidney disease and disease progression that occurs once the glomerular filtration barrier is damaged and proximal tubules endocytic machinery becomes saturated and can no longer meet the demands of filtrate uptake. Numerous studies have indicated that renal damage is exacerbated due to increasing levels of albumin at the proximal tubules, however the exact mechanism remains unknown. Thus, an *in vivo* model of AO was utilized to assess the direct effects of increased albumin on kidney injury (Figure 3.17). Serum creatinine, a measure of overall kidney function, was significantly elevated in mice treated with high levels of albumin (Figure 3.18). Albumin creatinine ratio was no different between WT and $CD13^{KO}$ shams, but was significantly higher after AO. WT mice developed significantly more albuminuria compared to $CD13^{KO}$ mice, similar to what was observed in diabetic mice (Figure 3.18). Kidneys were harvested for flow analysis to determine if $CD13^{KO}$ proximal tubules took up more albumin than WT proximal tubules. AO led to increased uptake of albumin in both WT and $CD13^{KO}$ proximal tubules compared to sham animals. Additionally, there was significant increase in the amount of albumin uptake in $CD13^{KO}$ proximal tubules in sham and AO mice (Figure 3.19).

No increase in renal necrosis or apoptosis in acute AO model

To determine if increased uptake by $CD13^{KO}$ proximal tubules leads to protection of the nephron, renal pathology was evaluated by PAS stain in addition to total apoptosis and necrosis by flow analysis. PAS stain revealed no gross damage to structural integrity after AO in either WT or $CD13^{KO}$ kidneys. Proximal tubules further displayed normal integrity of the brush border and the glomerulus displayed normal characteristics (Figure 3.20). Further analysis was done by flow cytometry to determine if overload led to more necrosis and apoptosis. Overall there was no overt difference in apoptotic cells between sham and overload as expected by lack of difference in the phenotype as observed by histological sections. Further there was a slight increase in cells that displayed characteristics of both apoptosis and necrosis after AO, albeit no significant difference (Figure 3.21). Those cells that had undergone necrosis were also no different between sham and overload. Perhaps, kidney cells can be exposed to high levels of albumin for extended periods of time before sublethal damage caused by albumin leads to overt renal injury.

3.4 – Discussion

Diabetic nephropathy is a complication that arises many years after the onset of diabetes mellitus. Chronically elevated blood glucose levels damages glomerular structures. Furthermore, advanced glycation endproducts circulating in the blood stream causes a variety of cellular damage in both the glomerulus and the proximal tubules[111]. Endocytosis of advanced glycation endproducts by the megalin receptor causes toxicity in the tubular cells[112,113]. CD13 is a multifunctional molecule that is

highly expressed on the apical surface of renal proximal tubules. Recent studies in the lab, found that CD13 controls pro-inflammatory signal transduction by regulating immune regulation of TLR4 and its subsequent signaling[91]. Deletion of TLR4 protects mice against renal injury associated with diabetes by alleviating the effects of albuminuria to reduce tubulointerstitial fibrosis and inflammation[66]. It was hypothesized that lack of CD13 would limit the progression of renal damage by altering TLR4 responses. However, the initial findings on decreased albuminuria shifted directions of the project to pursue how albuminuria contributes to and promotes further renal injury. In response to STZ induced diabetic nephropathy, albumin endocytosis via the proximal tubules is altered in the absence of CD13 leading to less albuminuria in $CD13^{KO}$ mice. However, this appeared to be independent of altered responses to STZ treatment specifically within the pancreas or glomerulus, as glucose levels and glomerular histology was similar between WT and $CD13^{KO}$ animals.

Since there was no significant differences observed in pancreatic and glomerular structures, it was speculated that decreased albuminuria in $CD13^{KO}$ mice may be due to differential proximal tubule injury. The proximal tubule has been identified as the single most important regulator of taking up albumin and other filtrates from the lumen via endocytic mechanisms by epithelial cells, the most populous cells in the kidney[30]. Many kidney disorders first manifest with injuries at the proximal tubules as these cells orchestrate the rate of attrition of renal function. Since CD13 is highly expressed on the apical surface of proximal tubules, it was postulated that absence

of CD13 at the proximal tubules increases the uptake of albumin in a STZ model of renal disease. The ultrastructure of proximal tubules in diabetic kidneys was evaluated; it was found that $CD13^{KO}$ mice had intact brush borders in comparison to WT brush borders, which were extensively damaged after 20 weeks of diabetes. Upon further evaluation of the proximal tubules by electron microscopy, more endocytic vesicles were visualized in $CD13^{KO}$ proximal tubules in comparison to WT tubules. Furthermore, CD13 was activated in a time-dependent manner in response to albumin. Importantly, *in vitro* analysis revealed that primary proximal tubule epithelial cells lacking CD13 internalized more albumin in a dose dependent manner when compared to primary proximal tubule epithelial cells expressing CD13.

Megalin and cubilin are known endocytic regulators found in the apical membrane of the proximal tubules. Previous investigations have shown that these two molecules co-localize in the brush border of renal proximal tubules and act in unison to take up glomerular ultrafiltrate proteins[114]. Increased albumin uptake in $CD13^{KO}$ cells suggested a relationship between CD13 and the megalin/cubilin receptor complex. However, immunofluorescence determined megalin and CD13 were distinctly separate on the surface of the proximal tubule. Unlike cubilin and megalin, CD13 and megalin did not co-localize. Previous investigations have examined the association of CD13 and other receptors including the mannose receptor[91]. Macrophages lacking CD13 were capable of taking up more ovalbumin compared to macrophages expressing CD13. Furthermore, CD13 was not co-localized with the mannose receptor, but did co-internalize into early endocytic vesicles[77]. Perhaps,

CD13 is acting similarly on the megalin receptor by mediating recycling of the megalin/cubilin receptor back to the membrane.

Upon internalization albumin has two main fates: being degraded by lysosomes or being returned back into the circulation by transcytosis regulated by the FcRn receptor[31]. FcRn is internalized into endocytic vesicles along with albumin bound to the megalin/cubilin complex. Acidification of these endosomal vesicles transfers the albumin molecule from the megalin/cubilin complex to FcRn where albumin is then brought to the basolateral membrane. Albumin is then returned to the circulation and megalin/cubilin is recycled back to the apical surface of proximal tubules. FcRn preserves the lifespan of albumin by mediating it's transport across the basolateral membrane of renal proximal tubules[60]. However, recent investigations have suggested that FcRn is not just responsible for the transcytosis of albumin, but may also regulate the uptake of albumin found in the lumen of renal proximal tubules as well[60,115,116]. Interestingly, others have proposed that binding of albumin to the megalin/cubilin complex results in albumin being transported only to the lysosome for degradation[57,117]. Furthermore, crystallographic evaluation of FcRn at acidic (pH 6.5) and basic pH (pH 8.2) indicates that a conformational change at pH 6.5 stabilizes the binding of albumin[115]. The lumen of the of the proximal tubule is slightly acidic with a pH around 6.8, making it very plausible that FcRn takes up albumin from the lumen of proximal tubules and brings it to the basolateral surface where albumin then undergoes transcytosis. CD13 co-localizes with FcRn in the brush border of renal proximal tubules as well as in vesicles found in the most

basolateral parts of these epithelial cells. Remarkably, $CD13^{KO}$ mice have an increased albumin half-life indicating that CD13 might be mediating transcytosis of albumin back into the bloodstream. This phenomenon possibly contributes to decreased urinary albumin levels observed in $CD13^{KO}$ mice.

It has been well established that albuminuria is an early predictor of renal injury and that origin of proteinuria is due to a combination of problems in glomerular filtration and proximal tubular reabsorption[118,119]. Increase internalization of proteins by the proximal tubules is thought to mediate inflammation and fibrosis that ultimately contributes to the death of the nephron and renal failure[120]. Previous studies have found that overloaded proximal tubules become activated and express pro-inflammatory cytokines to induce the apoptotic pathway[121]. Other studies have focused on how glomerular proteinuria injures proximal tubules[122,123]. There has been a strong emphasis in identifying the precise molecular pathway that leads to renal injury in response to protein overload.

Decreased albuminuria in $CD13^{KO}$ mice in a model of diabetic nephropathy and AO offered a suitable model to study the deleterious effects of protein accumulation in the urine. Initially, it was observed that $CD13^{KO}$ primary proximal tubule epithelial cells took up more albumin than WT tubules. Further *in vitro* evaluation determined that proximal tubules exposed to high levels of albumin were necrotic 24 and 48 h after treatment. Yet, there was no difference between WT and $CD13^{KO}$ proximal tubules as assessed by flow cytometry indicating that high levels of albumin cause

sublethal injury to proximal tubular cells. Uptake of albumin did not offer any extra protection to extremely high levels of albumin, which is toxic to proximal tubules.

To explore this concept *in vivo* an animal model of AO was utilized. Mice were treated with increasing doses of albumin for 8 days and kidneys were harvested for further analysis. Mice displayed decreased renal function as evaluated by serum creatinine. Consistent with the data from the diabetic nephropathy mice, $CD13^{KO}$ mice had decreased albuminuria which was due to increased uptake of albumin by the proximal tubules as assessed by flow analysis. Despite the change in renal function, histological analysis revealed no overt renal injury after AO in either WT or $CD13^{KO}$ animals. Finally, flow analysis of apoptotic and necrotic markers was not elevated after AO. Individuals with albuminuria inevitably develop ESRD indicating that injury related to albuminuria takes years to develop. A constant exposure of high albumin levels causes sublethal injury by activating inflammatory cytokines to promote apoptosis.

In summary, these findings identify CD13 as a novel regulator of albumin endocytosis in the proximal tubules. $CD13^{KO}$ proximal tubules more efficiently take up albumin in comparison to WT proximal tubules as observed both *in vitro* and *in vivo*. CD13 co-localizes with transcytosis receptor FcRn. $CD13^{KO}$ mice have increased albumin half-life, indicating that CD13 negatively regulates FcRn processes. Further, assessment of how albumin uptake relates to renal injury found that the process of taking up more albumin had no overall effect on the death of

proximal tubules. Finally, the use of an AO model suggests that nephron injury as a result of albuminuria is an extensive process that takes years to accumulate.

3.5 – Figures and Legends

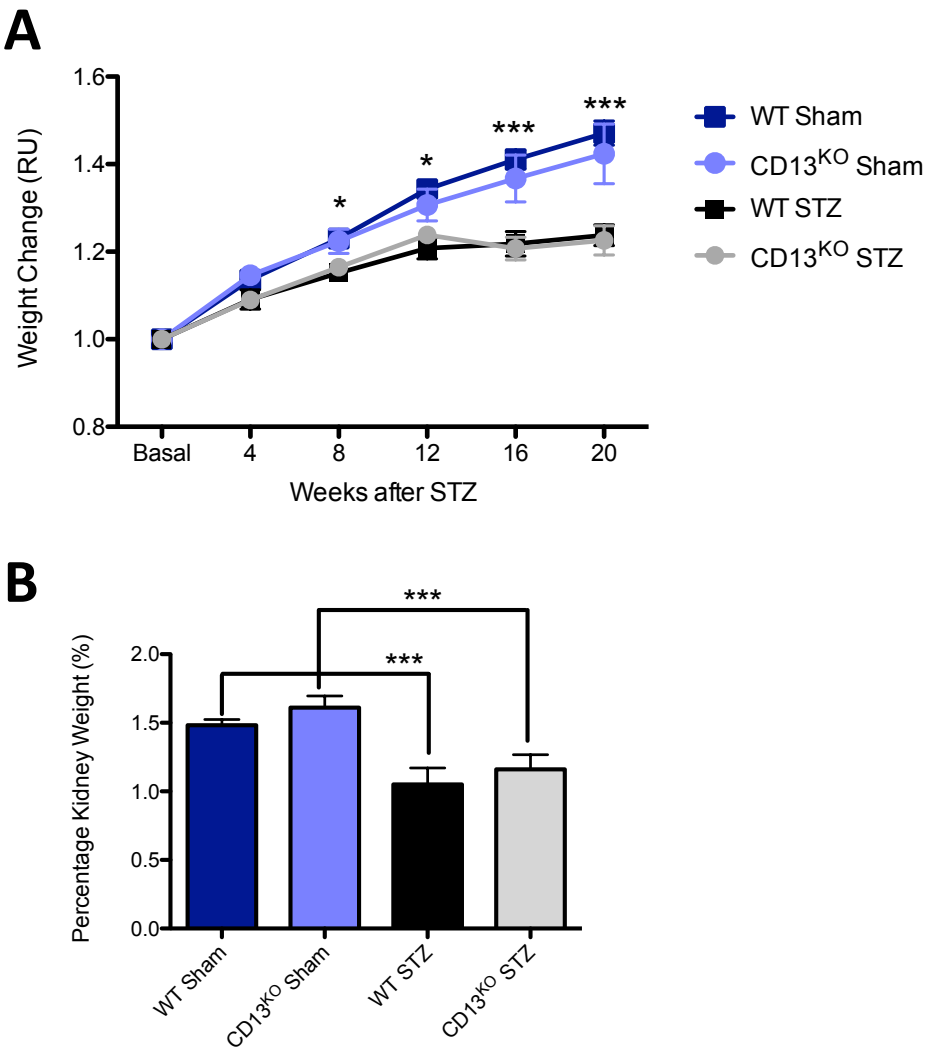

Figure 3.1 – Weight gain and kidney weight in sham and STZ treated animals. (A) Body weight normalized to basal to assess weight gain in WT and CD13^{KO} sham or STZ treated animals. (B) Ratio of kidney weight and body weight. Data represents mean ± SEM; n = 4 sham, n = 10 STZ; *, p<0.05; **, p<0.01; ***, p <0.001.

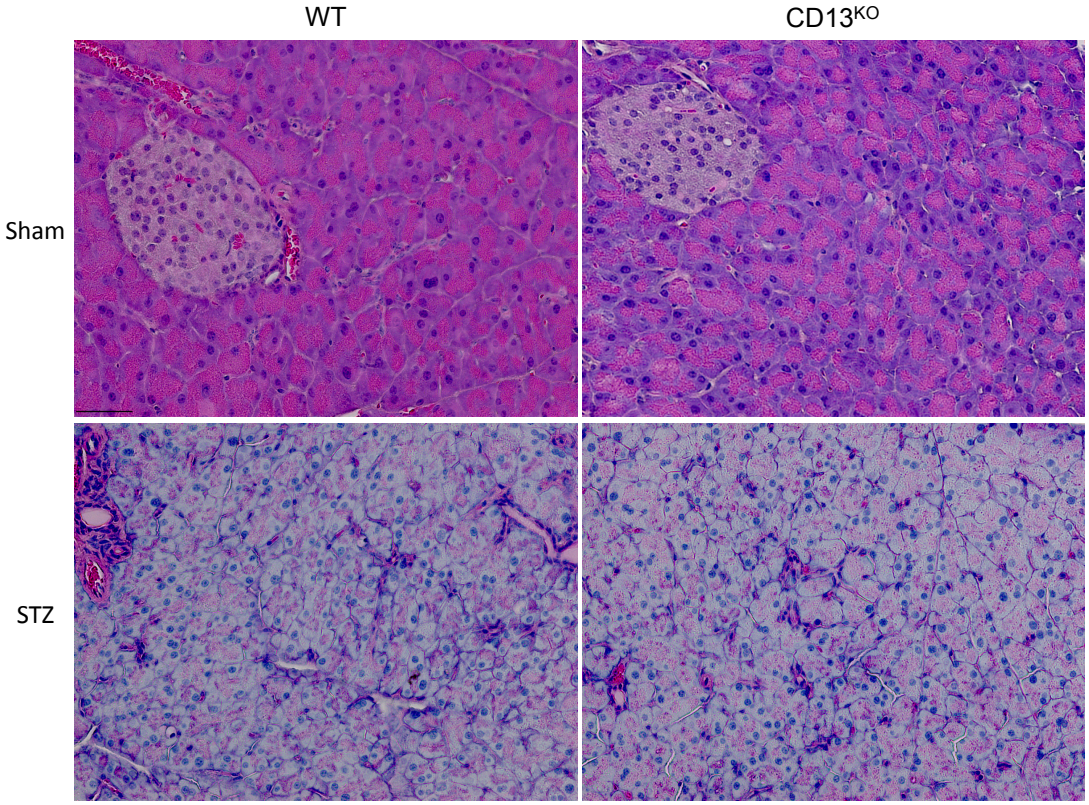

Figure 3.2 – Histology of pancreas in sham and STZ treated mice.
Hematoxylin and eosin stain of formalin-fixed paraffin embedded pancreas to assess gross architecture of pancreas. These are representative images of pancreas from WT and $CD13^{KO}$ mice after 20-week sham or STZ treatment. The scale bar represents 50 μm.

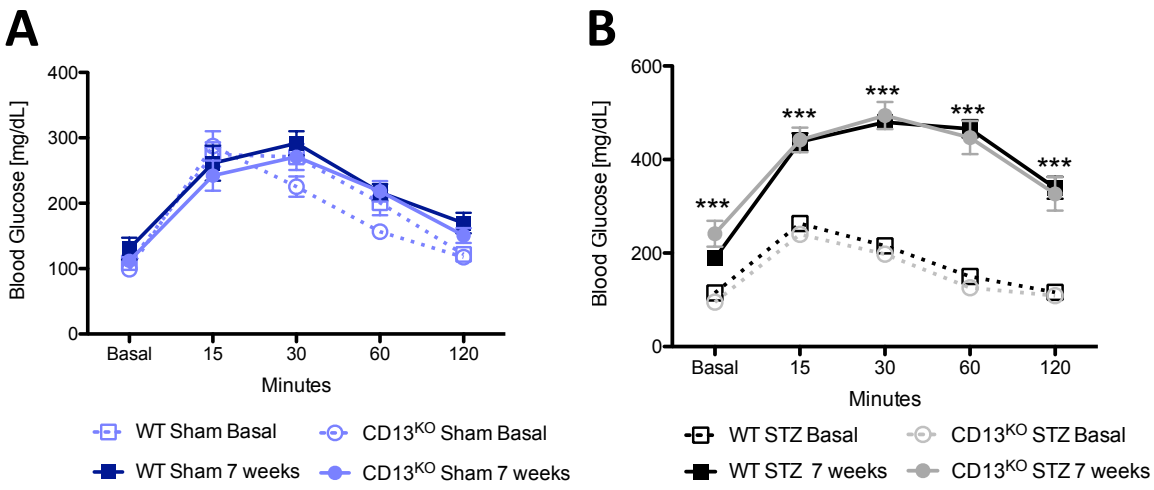

Figure 3.3 – Glucose tolerance test to assess pancreatic function in sham and STZ treated mice.
Blood glucose concentrations (mg/dL) during intraperitoneal glucose tolerance test (1 g/kg) following 16 h fast for (A) sham and (B) STZ treated animals at basal and seven weeks post injection. Data represents mean ± SEM; n = 5 sham, n = 15 STZ; ***, p <0.001.

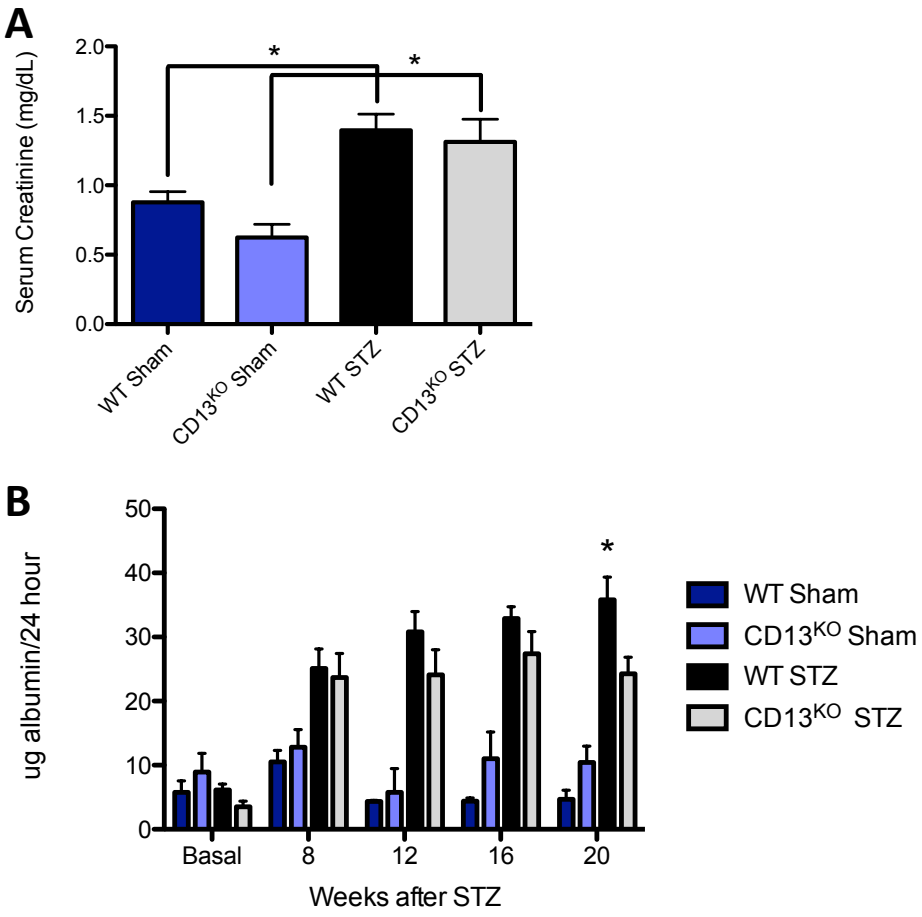

Figure 3.4 – Increased renal injury and albuminuria in mice with diabetic nephropathy.
(A) Serum creatinine was assessed in WT and CD13^{KO} mice after 20 weeks of sham or STZ treatment. (B) 24 h urinary albumin levels were measured at basal, 8, 12, 16 and 20 weeks after STZ treatment by ELISA. Data represents mean ± SEM; n = 4 sham, n = 13 STZ; *, p <0.05.

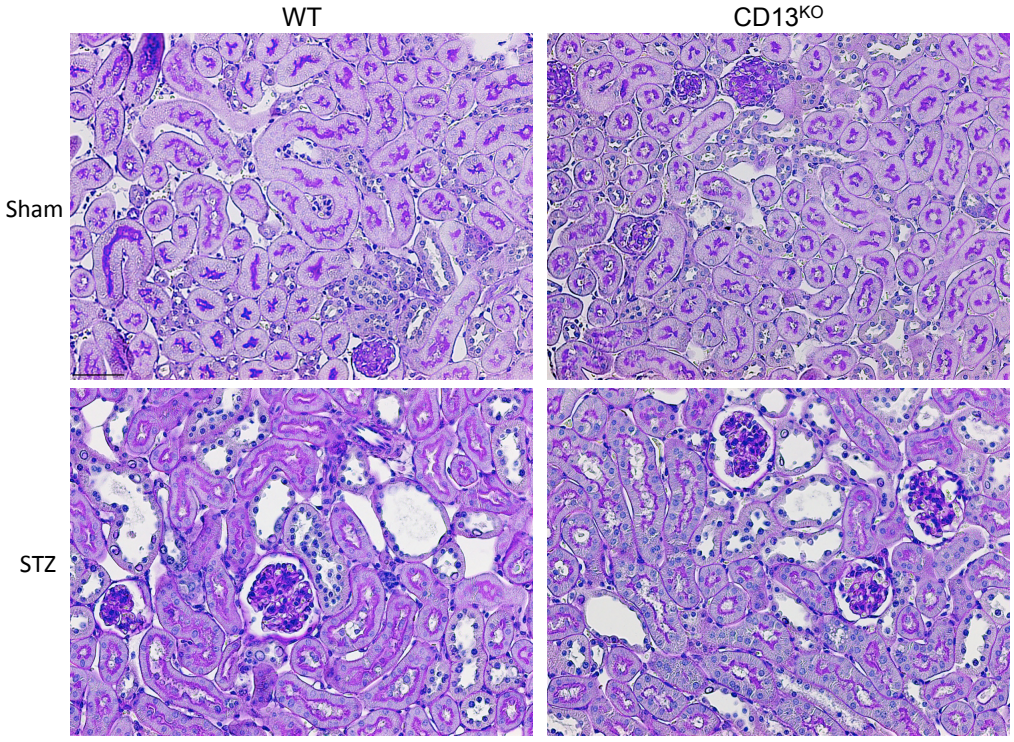

Figure 3.5 – Histology of kidney in sham and STZ treated mice.
PAS stain of formalin-fixed paraffin embedded kidneys. These are representative images of kidneys of WT and $CD13^{KO}$ mice after 20 weeks sham or STZ treatment. The scale bar represents 50 µm.

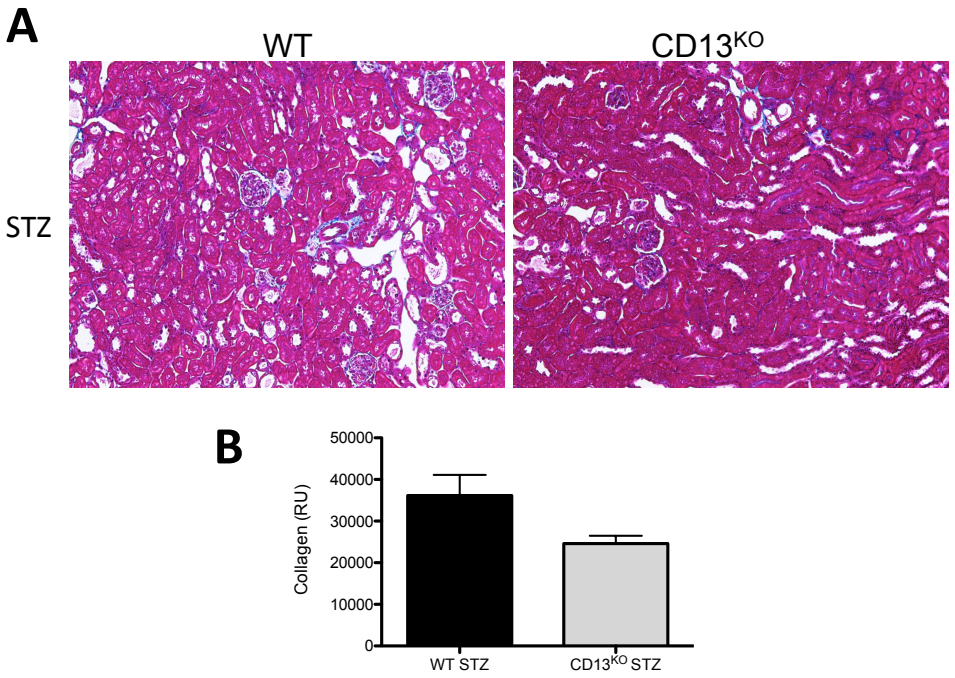

Figure 3.6 – Quantitative analysis of fibrosis by expression of collagen.
(A) Trichrome stain was used to evaluate overall fibrosis in STZ WT and CD13^{KO} kidneys 20 weeks after treatment. (B) Ten fields per kidney were analyzed and quantified with Image Pro Plus and Prism Graphpad software for total collagen (blue). Data represents mean ± SEM; n = 5.

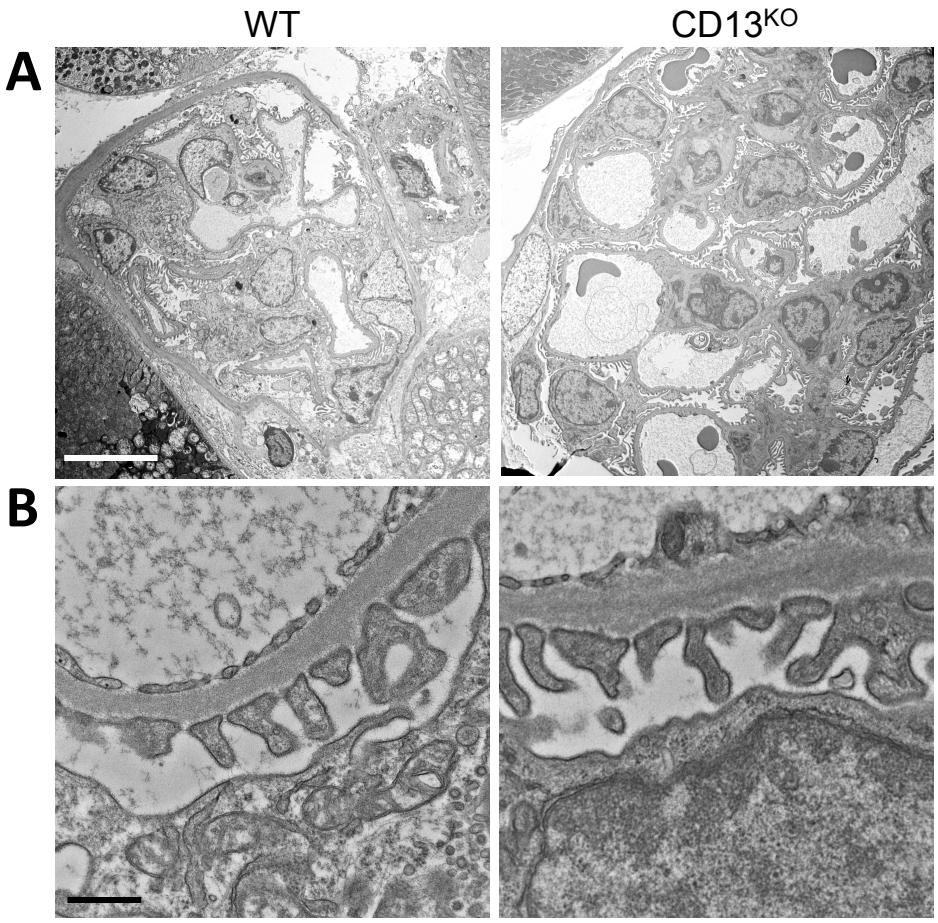

Figure 3.7 – Electron microscopy of glomerulus after 20 weeks STZ.
Glomerular morphology was evaluated by electron microscopy. (A) The upper panel depicts a representative image of an entire glomerulus (1000x). The scale bar represents 10 µm. (B) The lower panel shows the slit diaphragms of the podocytes (15,000x). The scale bar represents 500 nm.

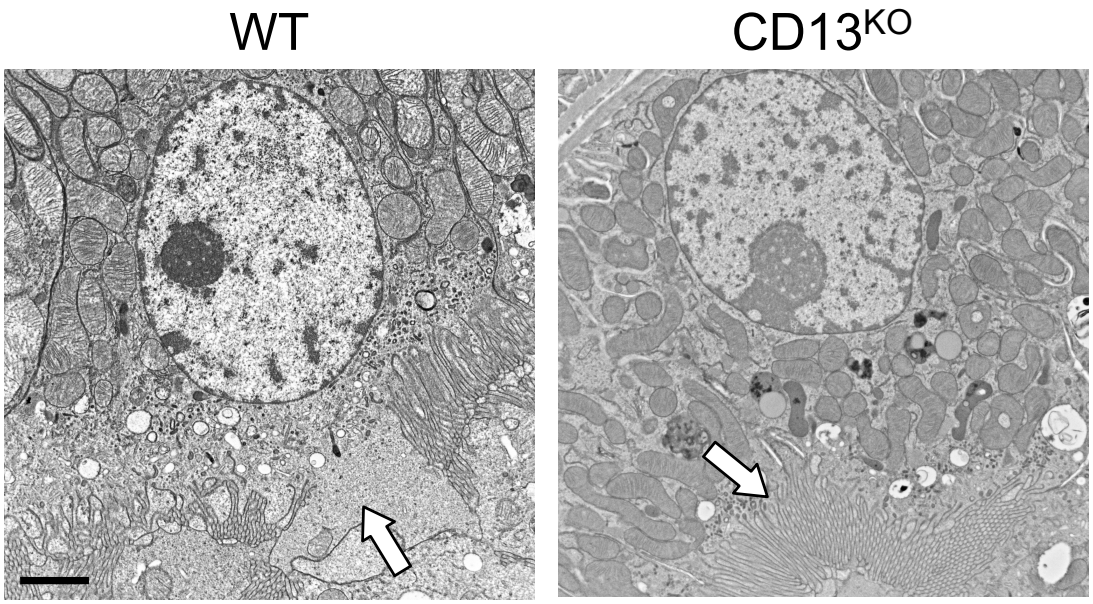

Figure 3.8 – Electron microscopy of renal proximal tubules after 20 weeks STZ. These are representative images of electron microscopy of proximal tubules 20 weeks after STZ treatment. The brush border is shown with the white arrows. Brush border is disrupted in WT proximal tubules, while $CD13^{KO}$ maintains brush border integrity. The scale bar represents 2 μm.

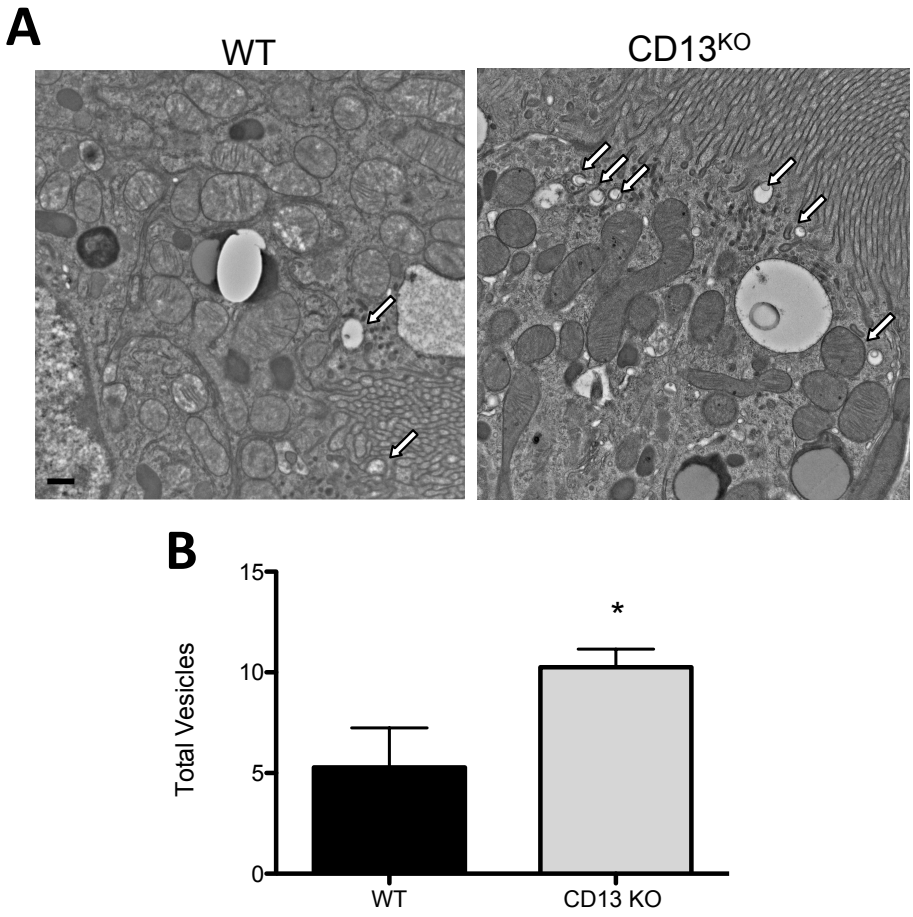

Figure 3.9 – Quantification of endocytic vesicles in proximal tubules after 20 weeks of diabetic nephropathy.
(A) Endocytic vesicles are observed by electron microscopy. Endocytic vesicles are seen below the surface of the brush border (white arrows). The scale bar represents 500 µm. (B) Quantification of total vesicles from 10 different fields. Data represents mean ± SEM; n = 1; *, p <0.05.

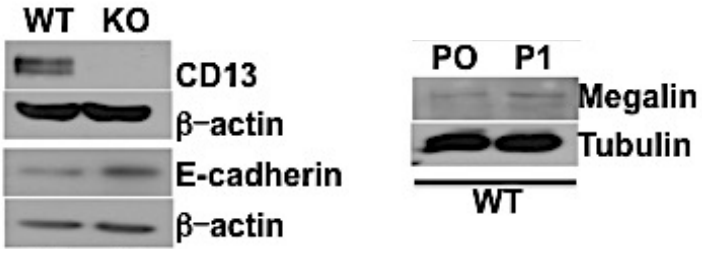

Figure 3.10 – Western blot analysis of expression of proximal tubule markers in primary proximal tubules.
CD13 expression was evaluated in WT and $CD13^{KO}$ primary proximal tubule epithelial cells by western blot analysis. CD13 is expressed only in WT primary proximal tubule epithelial cells. E-cadherin, a marker for epithelial cells, is expressed in both WT and $CD13^{KO}$ cells as confirmed by western blot analysis. Megalin expression is maintained after the first passage of primary proximal tubule epithelial cells.

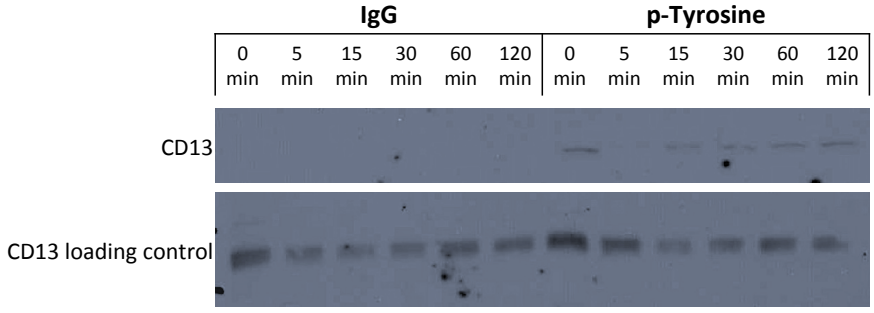

Figure 3.11– Primary proximal tubules treated with BSA activates CD13 in a temporal manner.

WT primary proximal tubule epithelial cells were serum starved overnight and treated with 1% BSA for 0, 5, 15, 30, 60 and 120 min and lysed. The lysate was immunoprecipitated with IgG or p-Tyrosine (CD13 activation site) and then probed for CD13 to determine specific activation of CD13.

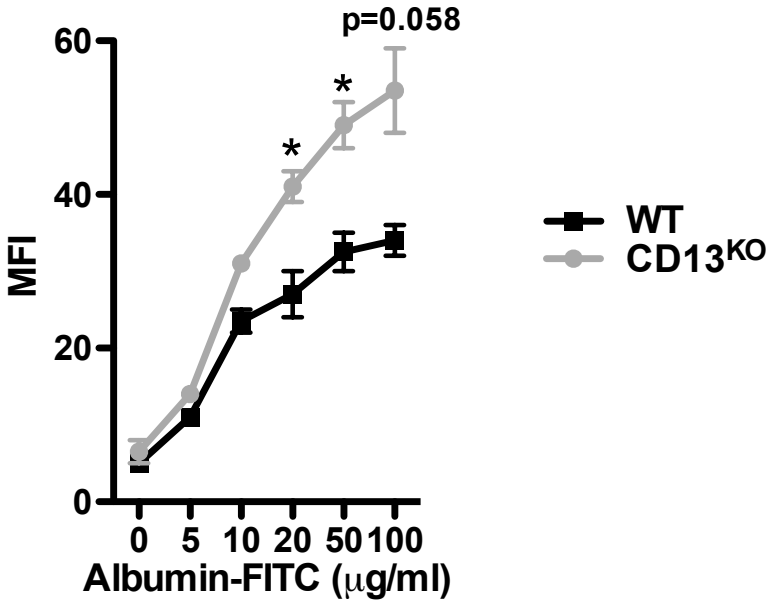

Figure 3.12 – Lack of CD13 increases uptake of albumin by primary proximal tubules.
WT and $CD13^{KO}$ primary proximal tubule epithelial cells were serum starved overnight and treated with increasing doses of Albumin-FITC for 1 h. Cells were harvested. Internalized albumin-FITC was evaluated by flow cytometry. Data represents mean ± SEM; n = 3; *, $p < 0.05$.

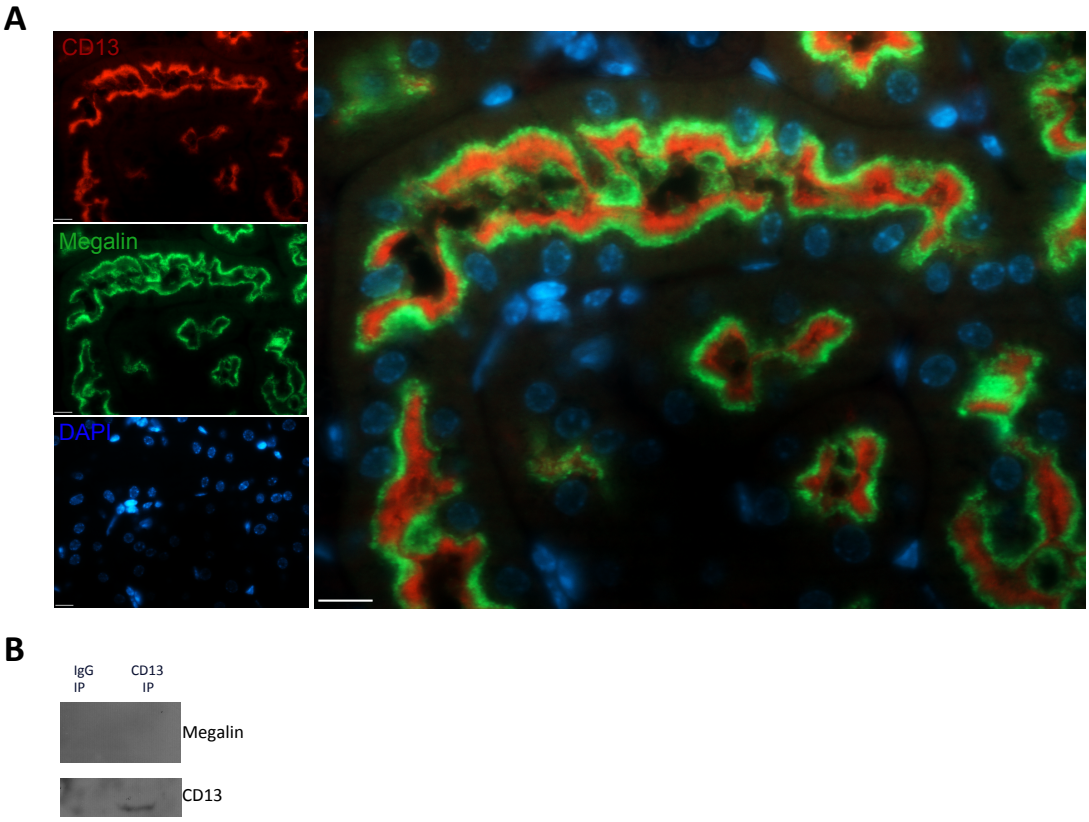

Figure 3.13 – Localization of megalin and CD13 within the kidney.
(A) WT, unchallenged kidneys were co-stained with CD13 (red), megalin (green) and DAPI (nuclear, blue). Megalin and CD13 are expressed on the apical surface of the brush borders, but do not co-localize. The scale bar represents 10 μm. (B) Confluent WT primary proximal tubule epithelial cells were lysed followed by IgG or CD13 immunoprecipitation from total protein extracts. Endogenous megalin did not co-immunoprecipitate with CD13.

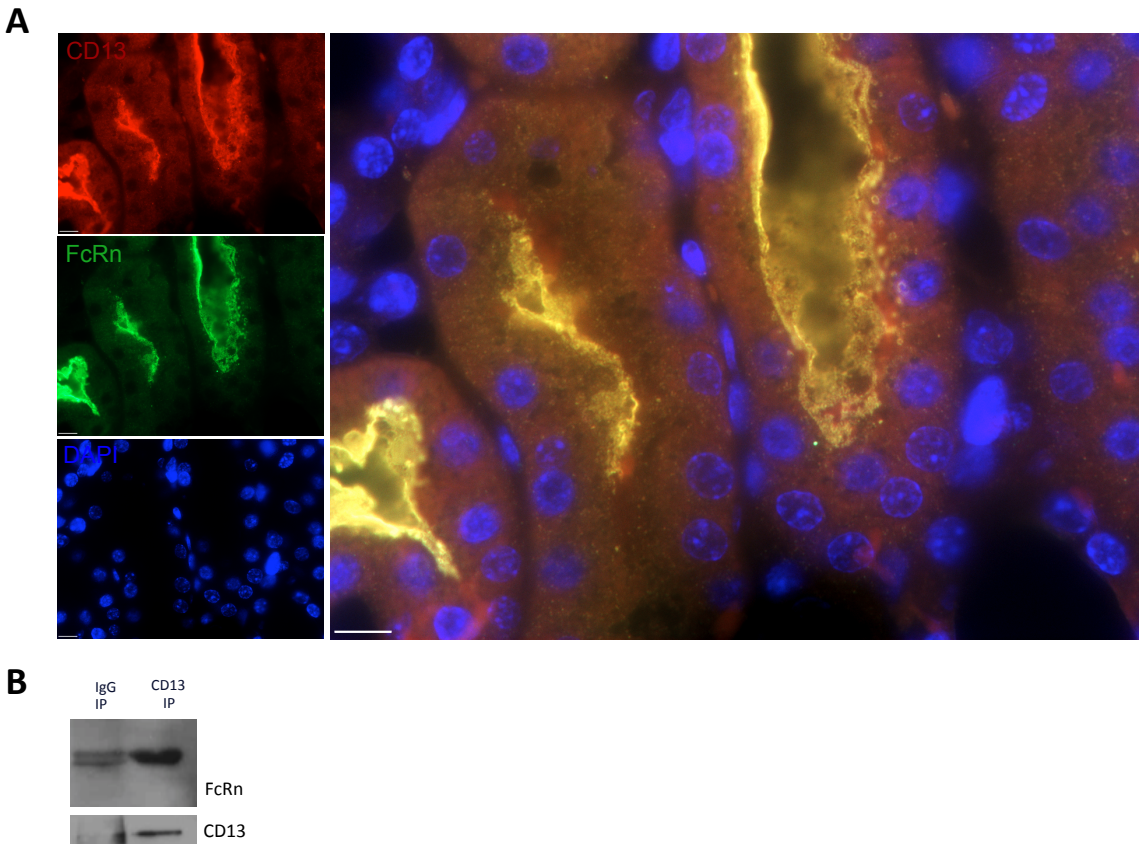

Figure 3.14 – Localization of FcRn and CD13 within the kidney.
(A) WT, unchallenged kidneys were co-stained with CD13 (red), FcRn (green) and DAPI (nuclear, blue). FcRn and CD13 are co-localized on the apical surface of the brush borders. The scale bar represents 10 μm. (B) Confluent WT primary proximal tubule epithelial cells were lysed followed by IgG or CD13 immunoprecipitation from total protein extracts. Endogenous FcRn did not co-immunoprecipitate with CD13.

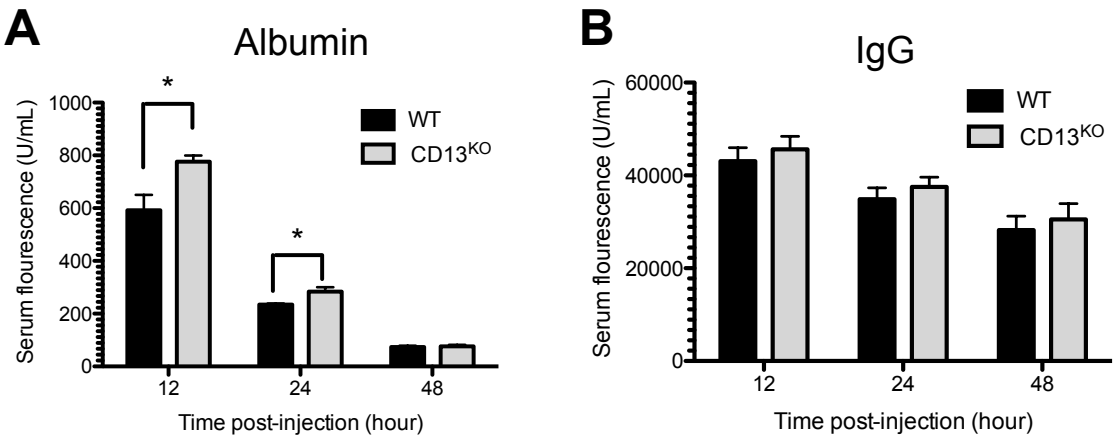

Figure 3.15 – Clearance of albumin and IgG in WT and CD13^{KO} mice.
(A) After single intravenous dose of albumin-FITC into WT and CD13^{KO} mice, clearance of albumin was measured spectrophotometrically. (B) After single intravenous dose of IgG-FITC into WT and CD13^{KO} mice, clearance of albumin was measured spectrophotometrically. For clearance data, serum fluorescence intensity of FITC was measured. Data represents mean ± SEM; n = 3; *, $p < 0.05$.

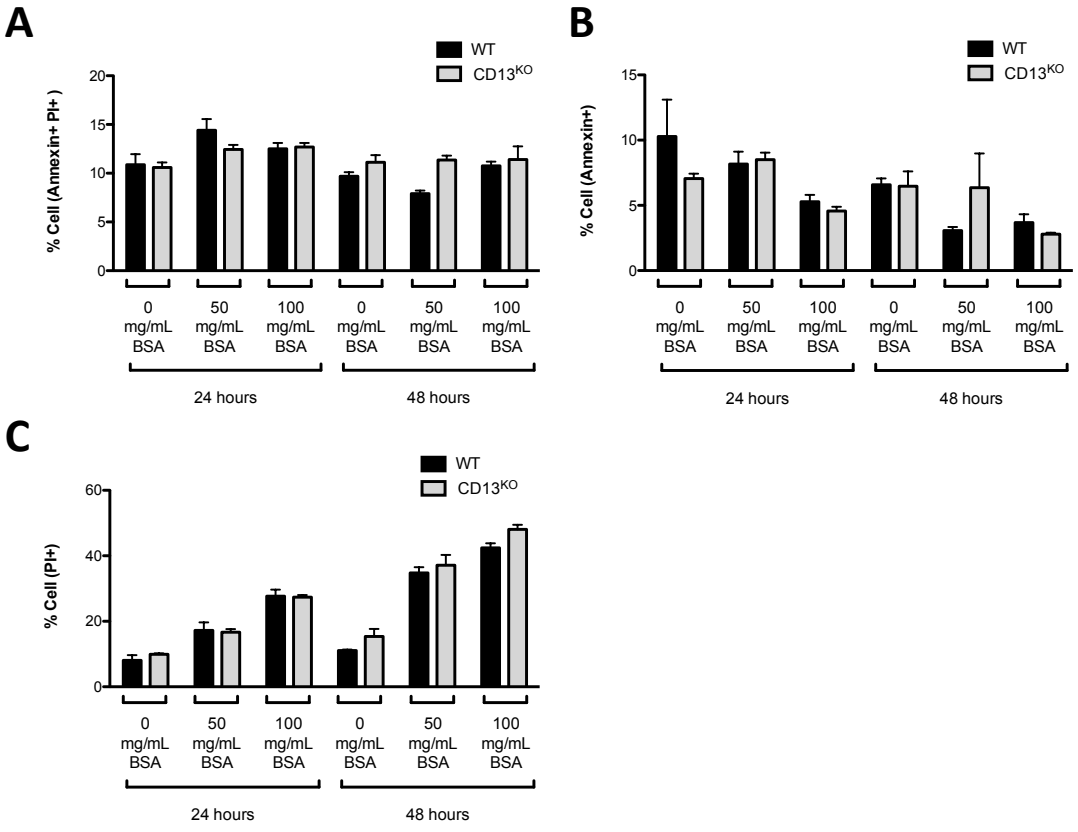

Figure 3.16 – Analysis of apoptosis and necrosis after high dose of albumin in primary proximal tubules.

WT and CD13^{KO} primary proximal tubule epithelial cells were serum starved overnight and treated with 0 mg/mL, 50 mg/mL or 100 mg/mL of BSA for 24 or 48 h. Cells were harvested and stained for annexin (apoptotic marker) and PI (necrotic marker). Total staining was measured by flow cytometry analysis for (A) annexin+ PI+ cells, (B) annexin+ cells and (C) PI+ cells. Data represents mean ± SEM; n = 3.

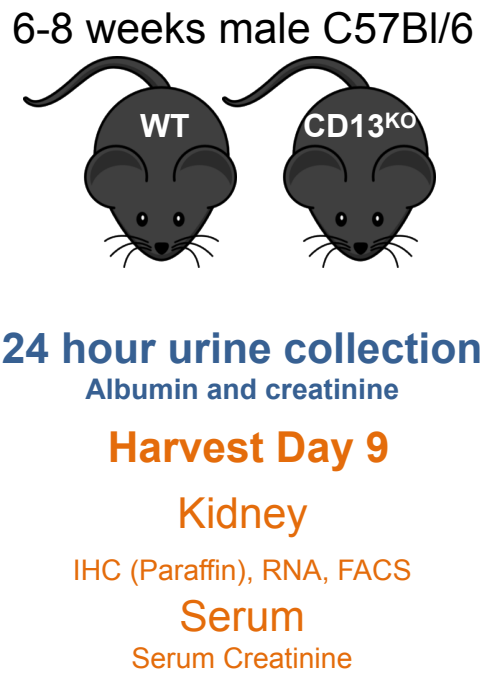

Day	Bovine Serum Albumin Dose
1	2 mg/g
2	4 mg/g
3	6 mg/g
4	8 mg/g
5	10 mg/g
6	No dose
7	No dose
8	10 mg/g
9	Harvest

Figure 3.17 – Albumin overload model.
WT and $CD13^{KO}$ mice aged 6-8 weeks were intraperitoneally injected with increasing doses of BSA. Mice were harvested on day 9. Kidneys and serum were collected for further analysis.

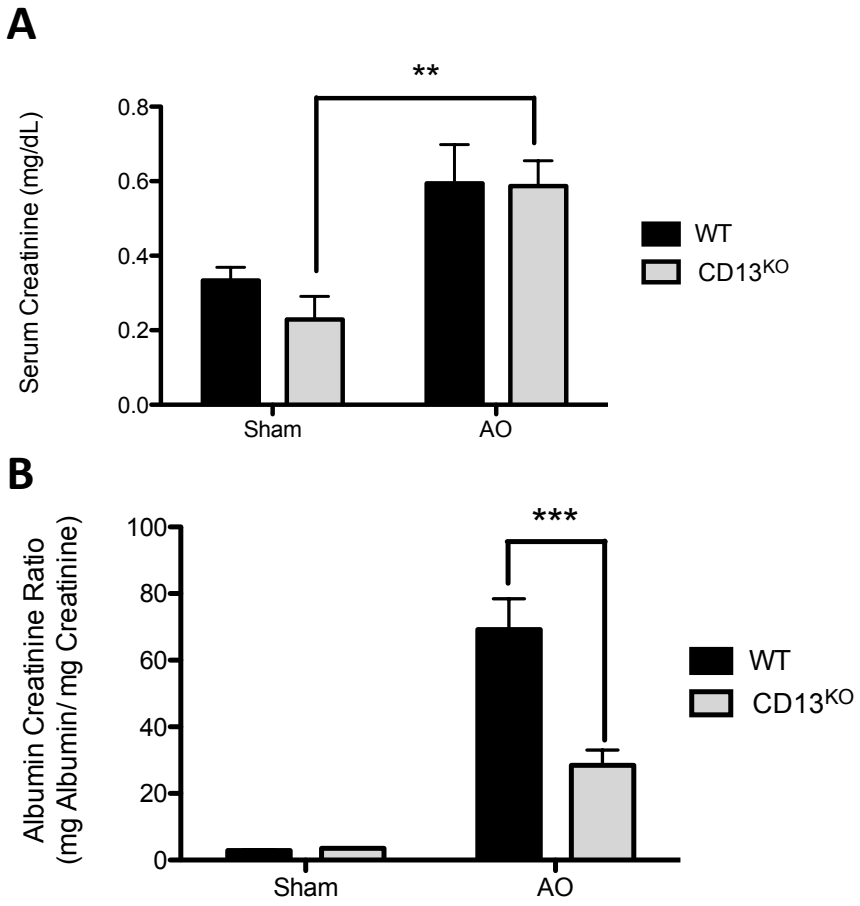

Figure 3.18 – Evaluation of renal function and albuminuria in mice after AO. (A) Serum creatinine at day 9 for sham and AO mice. (B) Albumin creatinine ratio for 24 h urine collection (Day 8 to Day 9) for sham and AO mice. Data represents mean ± SEM; n = 3 sham, n = 9 AO. **; $p<0.01$ ***; $p<0.001$.

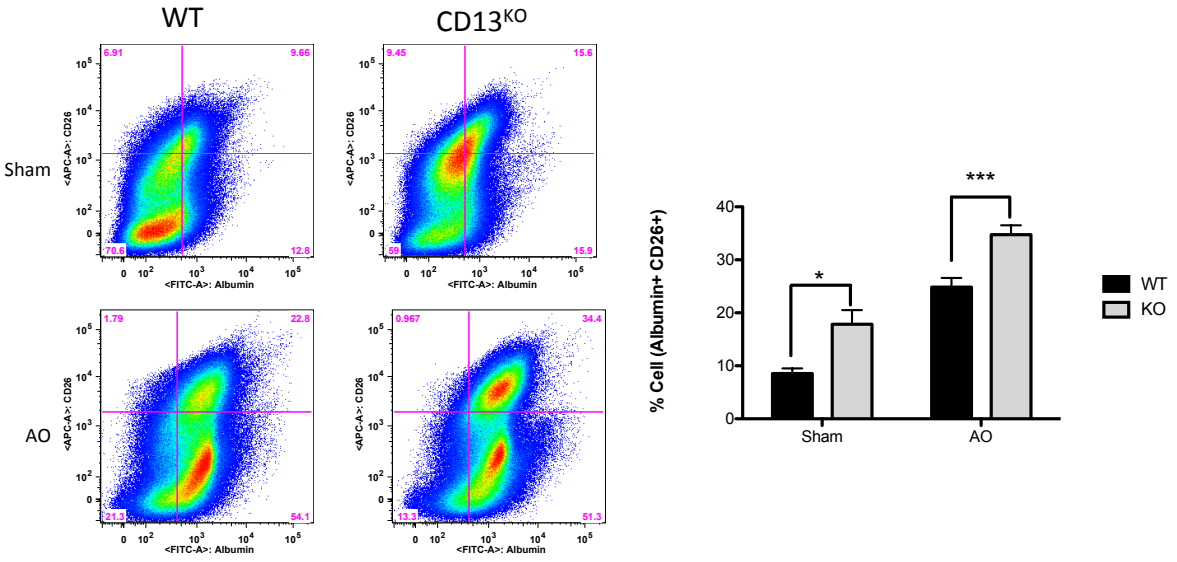

Figure 3.19 – Quantification of *in vivo* albumin uptake by renal proximal tubule cells after AO.

Flow cytometric analysis of endocytosed albumin in $CD26^{+}$ (proximal tubule) cells in sham and AO mice 9 days after AO. Data represents mean ± SEM; n = 3 sham, n = 9 AO. *; $p<0.05$ ***; $p<0.001$.

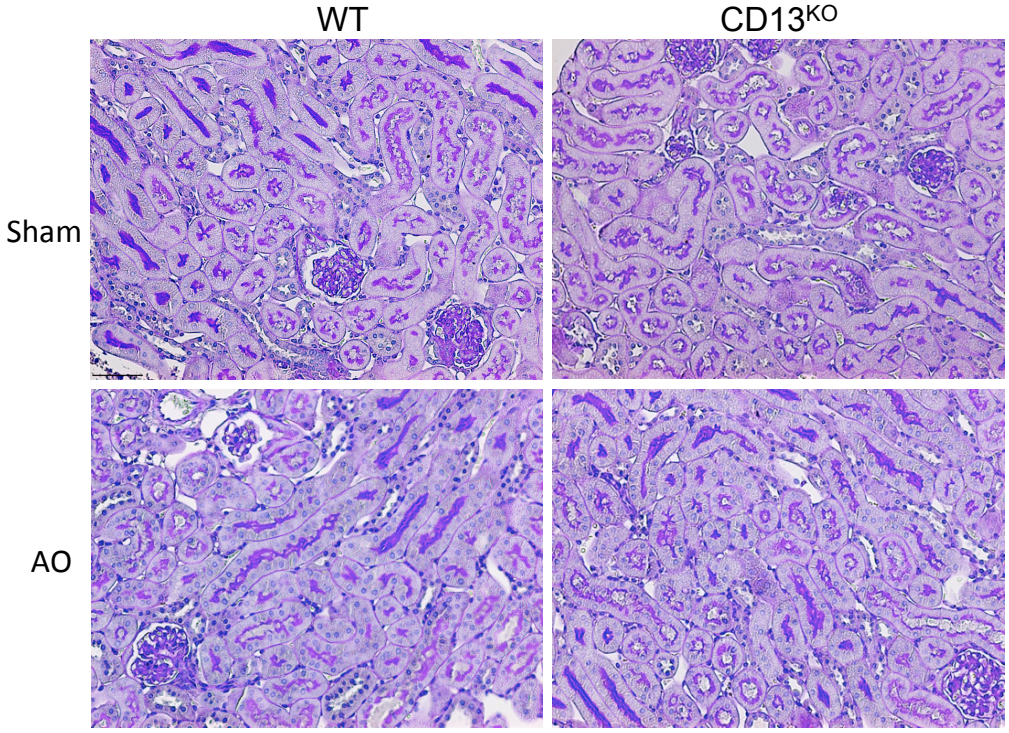

Figure 3.20 – Histology of kidney in sham and AO treated mice.
PAS stain of formalin-fixed paraffin embedded kidneys. These are representative images of kidneys of WT and $CD13^{KO}$ kidneys 9 days after AO or sham treatment. The scale bar represents 50 μm.

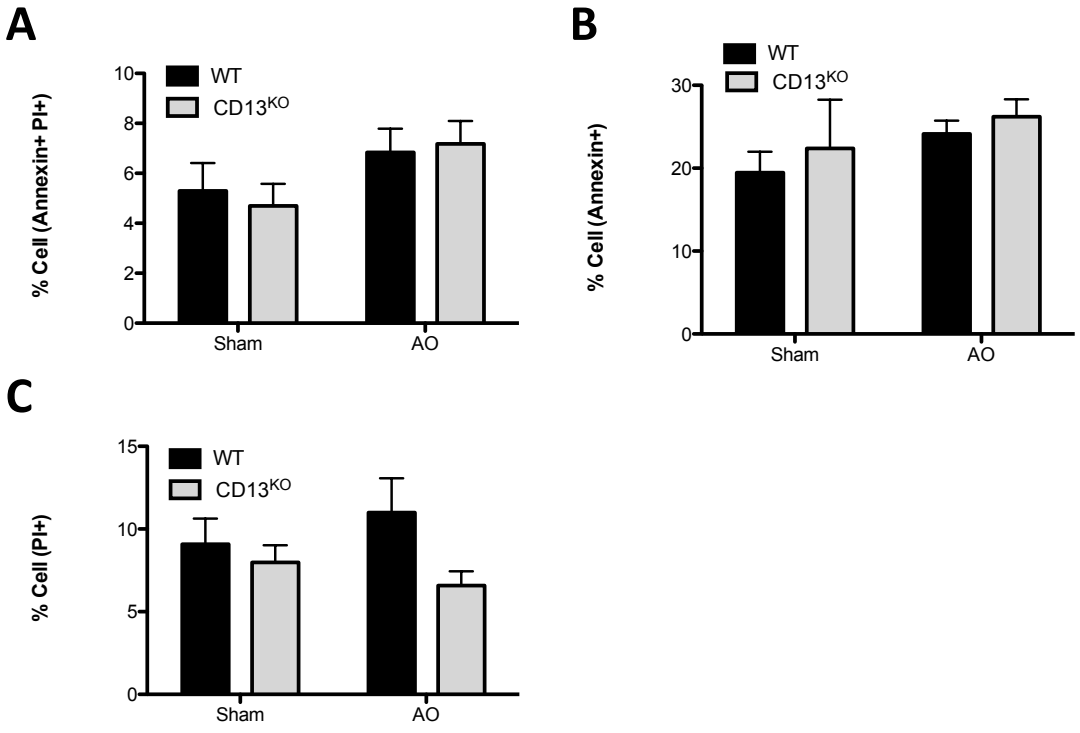

Figure 3.21 – Analysis of apoptosis and necrosis after AO in proximal tubules. WT and CD13^{KO} kidneys were harvested. Total staining was measured by flow cytometry analysis for (A) annexin+ PI+ cells, (B) annexin+ cells and (C) PI+ cells. Data represents mean ± SEM; n = 3 sham, n = 9 AO.

Chapter 4

Biomarkers of renal injury in children with congenital urinary anomalies

*Adapted from Journal of Pediatric Urology, Published November 28, 2015 (doi: 10.1016)

Proximal tubule proteins are significantly elevated in bladder urine of patients with ureteropelvic junction obstruction and may represent novel biomarkers: A pilot study

Claire Gerber[1], Miriam Harel[1,2], Miranda L. Lynch[3], Katherine W. Herbst[2], Fernando A. Ferrer[1,2], Linda H. Shapiro[1,2]

[1]Center for Vascular Biology, University of Connecticut Health Center, Farmington, CT, [2]Divison of Urology, Department of Surgery, Connecticut Children's Medical Center, Hartford, CT, [3]Center for Quantitative Medicine and Department of Community Medicine and Health Care, University of Connecticut Health Center, Farmington, CT

4.1 – Summary

"PURPOSE: Ureteropelvic junction obstruction (UPJO) is the major cause of hydronephrosis in children and may lead to renal injury and early renal dysfunction. However, diagnosis of the degree of obstruction and severity of renal injury relies on invasive and often inconclusive renal scans. Biomarkers from voided urine that detect early renal injury are highly desirable due to their noninvasive collection and their potential to assist in earlier and more reliable diagnosis of the severity of obstruction. Early in response to UPJO, increased intrarenal pressure directly

impacts the proximal tubule brush border. We hypothesize that single-pass, apically-expressed proximal tubule brush border proteins will be shed into the urine early and rapidly and will be reliable non-invasive urinary biomarkers, providing the tools for a more reliable stratification of UPJO patients."[124]

"MATERIALS AND METHODS: We performed a prospective cohort study at Connecticut Children's Medical Center. Bladder urine samples from 12 UPJO patients were obtained prior to surgical intervention. Control urine samples were collected from healthy pediatric patients presenting with primary nocturnal enuresis. We determined levels of neutrophil gelatinase-associated lipocalin (NGAL), kidney injury molecule 1 (KIM-1) (previously identified biomarkers), CD10, CD13 and CD26 (potentially novel biomarkers) by ELISA in control and experimental urine samples. Urinary creatinine levels were used to normalize the urinary protein levels measured by ELISA."[124]

"RESULTS: Each of the proximal tubule proteins outperformed the previously published biomarkers. No differences in urinary NGAL and KIM-1 levels were observed between control and obstructed patients ($p = 0.932$ and $p = 0.799$, respectively). However, levels of CD10, CD13 and CD26 were significantly higher in the voided urine of obstructed individuals when compared to controls ($p = 0.002$, $p = 0.024$, and $p = 0.007$, respectively)."[124]

"CONCLUSIONS: Targeted identification of reliable, noninvasive biomarkers of renal injury is critical to aid in diagnosing patients at risk, guiding therapeutic decisions and monitoring treatment efficacy. Proximal tubule brush border proteins are reliably

detected in the urine of obstructed patients and may be more effective at predicting UPJO."[124]

4.2 – Introduction

"Obstructive nephropathy is the underlying cause of ESRD in the majority of pediatric patients. With an estimated prevalence of 1 in 500 births, UPJO is the major cause of hydronephrosis and may lead to renal injury and early renal dysfunction[16]. With the advent of widespread antenatal ultrasonography, many cases of UPJO are identified prenatally in asymptomatic patients. The indications for surgical intervention have become controversial, with some advocating initial observation with serial imaging techniques and surgical intervention reserved for patients with decreasing ipsilateral renal function and/or worsening drainage[125]. While this strategy may minimize overtreatment in children who may prove to have benign, self-limited hydronephrosis, other patients may suffer ongoing renal damage during this period of nonoperative management."[124]

"Mechanisms to assess the severity of damage caused by obstruction are decisively lacking and primarily rely on serum creatinine, which remains unchanged until 50% of nephron volume is lost[17,126]. Alternatively, differential renal function is determined by nuclear scans such as radiolabeled mercapto-acetyl-triglycine (MAG3) that measure the rate of kidney drainage ($t_{1/2}$) and differential function. Generally, the diagnosis of obstruction on MAG3 renography is based on a $t_{1/2}$ greater than 20 minutes or poor differential renal function, while a $t_{1/2}$ under 10 minutes is consistent

with unobstructed drainage. Cases with a $t_{1/2}$ between 10 and 20 minutes are considered equivocal, which may be difficult to interpret clinically [127]. Furthermore, nuclear renography is costly, may require sedation in younger children, and often requires repeat evaluation to assess progression of obstruction or deterioration in renal function."[124]

"Targeted identification of reliable urinary biomarkers would be invaluable for diagnosing patients at risk for renal damage, guiding therapeutic decisions, and potentially monitoring treatment efficacy. Currently, there are no reliable tests of voided urine that can assist in risk stratification and decision-making in patients with UPJO. While a number of promising urinary biomarkers have been proposed, their efficacy varies with the etiology of renal damage, which undermines their utility[126]. NGAL, interleukin-18 (IL-18), KIM-1 and cystatin C are proteins currently advocated as promising biomarkers of acute kidney injury. Tubular synthesis of some of these proteins is induced in response to injury (NGAL, IL-18, KIM-1), with additional contributions from infiltrating inflammatory cells (IL-18, NGAL), while others accumulate in the urine due to impaired reabsorption by damaged tubular epithelium (NGAL, cystatin C) [126]. While some studies have reported increased urinary NGAL levels in children with UPJO and correlation of NGAL levels with differential renal function, other studies have demonstrated that NGAL levels do not improve risk prediction of progressive CKD[128-131]. While urinary KIM-1 levels were increased in children with UPJO, KIM-1 levels were not elevated in adults with acute obstructive nephropathy secondary to nephrolithiasis[130,132], and urinary KIM-1 levels

demonstrated only a weak diagnostic value for the detection of renal injury of various etiologies[133]. Thus, while NGAL and KIM-1 may hold promise in the detection of some forms of renal injury, further studies are necessary to investigate their potential utility and to determine whether more reliable and consistent biomarkers may be identified."[124]

"An early effect of ureteral obstruction is increased pressure in the proximal tubules causing distention, damage and shedding of proteins expressed on the apical surface of the brush border epithelium[19,134]. Hydronephrosis progressively causes cellular damage due to hypoxia, ischemia, stretching, production of reactive oxygen species and fibrosis. Ultimately, this damage results in tubule cell death, tubular atrophy, interstitial inflammation and collagen deposition, impairing the growth and development of the obstructed kidney and causing compensatory enlargement of the unaffected kidney[19,134]."[124]

"Proteins can be secreted or shed into the urine from a number of cellular sources and at various time frames following renal insult. Tissue injury invariably induces the innate immune response and a concomitant increase in the extrarenal secretion of cytokines and other proteins from infiltrating and resident inflammatory cells. Impaired glomerular filtration resulting from tissue damage can allow release of proteins that are normally trapped by the glomeruli into the urine. These high urinary protein concentrations overwhelm the resorption capacity of the proximal tubule

epithelium, further contributing to proteinuria. Finally, the expression of pro-healing proteins is upregulated in response to injury[126]."[124]

"In UPJO, destruction and shedding of the proximal tubule brush border proteins into the urine is an early event[19]. Recent proteomic analyses of brush border lysates from isolated human proximal tubules identified numerous highly abundant proteins[135,136]. Of these, we identified three proximal tubule metallopeptidases (CD10, CD13 and CD26) that are highly to moderately abundant, apically-expressed, and have a single-pass transmembrane domain, reasoning that these will be more readily shed early and rapidly from the proximal tubule epithelium into the urine and may represent useful non-invasive urinary biomarkers."[124]

In this study, we used a unilateral ureteral obstruction (UUO) model to identify the reliability of CD13 as a biomarker in murine renal injury. Further, we sought to evaluate the relative efficacy of the proximal tubule proteins CD10, CD13 and CD26 in predicting UPJO in pediatric patients when compared to the established, potential biomarkers of kidney injury NGAL and KIM-1. We hypothesized that proximal tubule markers will be predictive of identifying renal injuries due to UPJO.[124]

4.3 – Materials and Methods

Animal model - UUO

Six to eight week old C57/Bl6 WT mice were anesthetized with isoflurane gas and shaved. Following a flank incision to expose the ureter, the right ureter was ligated

with 8-0 nylon[22,137]. The side receiving ligation is referred to as the ligated kidney, while the contralateral kidney is referred to as the unligated kidney. Animals' tissue was collected at Day 1, 2, 4, 3, 5, 7 and 10 after ligation. Micturated, unligated urine was collected 20 min prior to harvest, while ligated urine was collected from pooled urine above the ligation that collected in the renal pelvis (Figure 4.1).

Immunohistochemistry

For histological samples, kidneys were collected and fixed in 10% formalin (Fisher Scientific) overnight at 4°C, followed by dehydration in 70% ethanol. Samples were then processed and paraffin embedded at the University of Connecticut Health Center Research Histology Core. Tissues were cut in thickness of 5-8 μm. For hemoatoxylin and eosin stain, samples were rehydrated before staining. For immunofluorescence, antigen retrieval was performed in a pressure cooker in pH 6.0 sodium citrate buffer (Sigma). Tissues were blocked in 5% BSA/PBS for 1 h at room temperature. Sections were incubated with primary antibody at 1:1000 rat anti-CD13 (Shapiro Lab) in 5%BSA/PBS overnight in a humidity chamber. Samples were washed the following day and probed with secondary antibody goat anti-rat in 5% BSA/PBS. Nuclear was counterstained with hard mounting Vectashield containing DAPI (Vector) and cover slipped. Images were taken on Zeiss Axioplan 2 microscope with AxioCam MRc software.

Western blot

Protein was lysed in NP-40 lysis buffer containing a protease inhibitor cocktail, sodium orthovanadate and NaF. Following lysis, sample concentration was measured by BCA assay (ThermoScientific) according to manufacture instruction. Samples were run on 10% SDS-Page gel and transferred onto PVDF membrane. Membranes were blocked in 5% milk/TBST for 30 minutes at room temperature and then incubated with 1:10,000 rat anti-CD13 (Shapiro Lab) primary antibody in 5% milk/TBST overnight at 4°C on a rocker. The following day, the membrane was washed and probed with secondary goat anti-rat HRP. Samples were visualized with chemiluminescence using SuperSignal. Membrane was developed. Afterward the membrane was stripped for 10 minutes and then probed for loading control, β-actin (1:5000 dilution). Westerns were quantified using ImageJ software.

Collection of case and control patients

“After obtaining institutional review board approval, a prospective cohort study was performed in patients with unilateral UPJO treated with open or robotic dismembered pyeloplasty at Connecticut Children’s Medical Center between 2012 and 2014. Surgical intervention was recommended based on MAG3 renography demonstrating obstructed drainage or equivocal drainage time with decreased ipsilateral renal function. Urine samples were obtained intraoperatively from the bladder by cystoscopy or urethral catheterization.”[124]

Collection and processing of urine samples

"Control urine samples were collected via clean catch from otherwise healthy children presenting for primary nocturnal enuresis without any complicating urologic or nephrologic anomalies. Patient demographics, radiographic imaging and operative details were obtained from medical records. Written informed consent was obtained from all patients."[124]

"Urine samples were collected and stored at 4°C and aliquoted and stored within 24 h of collection at -80°C until urinalysis. Urinary creatinine was measured on the day of urine collection at Connecticut Children's Medical Center. Quantitative urine analysis was performed using commercially available human NGAL, KIM-1, CD10, CD13 and CD26 sandwich ELISA kits (R&D Systems). Each specimen was analyzed in duplicate, and the concentration of the patient samples was determined by using standard curve analysis upon generating a four parameter logistic curve-fit. Urinary creatinine levels were used to normalize the urinary protein levels measured by ELISA."[124]

Statistical analysis

"Statistical analysis of biomarker performance proceeded along two tracks. First, hypothesis tests were used to compare whether there were different levels of biomarker between UPJO cases and controls. Second, we used logistic regression models for the binary outcome of case status, where the predictor variable in the model was the level of biomarker. For the hypothesis testing, Mann-Whitney U tests

were used as a nonparametric robust alternative to t-tests; all tests were two-sided with α = 0.05. In the logistic regression analyses, each biomarker was examined in a univariate model as predictor for outcome. Significance of regression coefficients was assessed at the 0.05 level. All analyses were performed in the statistical software R[138]."[124]

4.4 – Results

After ureteral ligation, damage to the kidney is visible in the cortical proximal tubules[30]. Increased pressure within the kidney causes progressive loss of the brush border in the proximal tubule. Further as injury length increases, there is extended dilation and thinning of the epithelial cells lining the proximal tubules (Figure 4.2 A). Interestingly, CD13 expression progressively decreases in the cortex of kidneys as damage from UUO increases and accumulates in the lumen (Figure 4.2 B,C).

The progression of UUO leads to the shedding of CD13 from the proximal tubules into the urine. CD13 levels were prominently increased in the urine of obstructed kidney compared to contralateral kidney urine at earliest time points following ureteral ligation. The increase of CD13 seen in urine samples was suspected to come from the brush border of proximal tubules found in the kidney. Indeed, upon further evaluation, CD13 levels diminished in ligated kidneys compared to unligated kidneys, suggesting that CD13 is being shed readily into the urine (Figure 4.3). Remarkably, CD13 is being detected in very early stages of renal injury and may be a predictive biomarker of obstructive renal injury.

“The UPJO patient cohort consisted of 12 patients (8 males, 4 females) with a median age of 42 months (range 4 – 240). All patients underwent successful unilateral dismembered pyeloplasty, with bladder urine collected at the time of surgery. Patient demographics and clinical parameters are displayed in Table 4.1. The control group included 12 patients with primary nocturnal enuresis (5 males, 7 females) with a median age of 96 months (range 48 – 186). There was no significant difference in age or gender between the two cohorts.”[124]

“Overall, no statistical differences were observed in the levels of the published candidate biomarkers, KIM-1 and NGAL, between control and experimental groups (Table 4.2, Figure 4.4). However, the urinary concentrations of CD10, CD13 and CD26 were readily detected and significantly higher in samples from UPJO patients when compared to control patient samples ($p = 0.002$, $p = 0.024$ and $p = 0.007$, respectively, Table 4.2, Figure 4.5). In the logistic regression models, a positive regression coefficient would indicate increasing levels of biomarker being associated with higher probability of being a case compared to control. In our analyses, results demonstrated that all three proximal tubule markers had positive coefficients (indicating that increased levels of biomarker predict higher probability of UPJO), with CD10 and CD26 achieving marginal and full significance ($p = 0.086$ and 0.050, respectively). Neither NGAL nor KIM-1 were significantly associated with probability of predicting obstruction, and KIM-1 had a negative fitted coefficient value (i.e., higher biomarker levels predicting absence of UPJO).”[124]

"We investigated correlations between urinary protein levels and differential renal function on MAG3 renography. No significant linear correlations were observed for any of the five urinary proteins studied. We observed trends in the data suggestive that increased levels of CD10 and CD26 are associated with decreased differential renal function; however, the presence of some outliers in these small datasets rendered interpretation of correlation values difficult. Based on Spearman rank correlation tests, the correlation values were -0.28, 0.21, -0.07, 0.55, and -0.32 for CD10, CD13, CD26, KIM-1, and NGAL, respectively, with associated p values 0.0408, 0.536, 0.842, 0.081, and 0.339."[124]

4.5 – Discussion

"In our study, bladder urinary levels of the proximal tubule brush border proteins CD10, CD13 and CD26 were significantly higher in patients with UPJO compared to normal controls, while the levels of KIM-1 and NGAL were not significantly different between UPJO patients versus controls. Furthermore, our murine model of UUO validated CD13 as a strong predictor of renal injury. Our preliminary results suggest that these novel proximal tubule proteins may prove to be useful biomarkers that are more predictive of urinary tract obstruction."[124]

"While there are many proteins expressed in the proximal tubules, CD10, CD13 and CD26 are three highly abundant and single transmembrane brush border proteins that have been previously mentioned as potential biomarkers. CD26 was identified in

biochemically-fractionated urine from patients with renal injury, suggesting that it is, indeed, shed into the urine and detectable[139]. Urinary levels of CD13 and CD10 have been implicated as potential indicators of early renal disease. Compared to healthy controls, urinary levels of CD13 were found to be significantly elevated in patients with glomerulonephritis, and elevated levels of urinary CD13 appeared to be an indicator of very early tubular impairment[140]. Additionally, urinary excretion of CD13 was found to be significantly higher in patients with diabetic nephropathy compared to healthy controls[141]. Urinary levels of CD10 were demonstrated to rise significantly after cardiac surgery, suggesting that urinary excretion of CD10 may be an indicator of acute and impending renal damage following cardiac surgery[142]. The precise mechanisms and utility of these proteins as urinary biomarkers have yet to be fully elucidated."[124]

"While other studies investigating potential urinary biomarkers often sample urine from the obstructed renal pelvis, we chose to test bladder urine, because ideal urinary biomarkers should be measurable in bladder urine. The need to obtain urine from an obstructed renal pelvis in order to improve the sensitivity of the biomarker would diminish the feasibility and utility of such biomarkers. While bladder urine is diluted by the contralateral unobstructed kidney in patients with unilateral UPJO, studies have shown that levels of specific proteins in voided urine of children with UPJO can be elevated up to fourfold that in control patients, demonstrating the utility of biomarkers even in bladder urine[143,144]. Furthermore, others have found that the levels of other urinary marker proteins in children with unilateral UPJO were not

significantly different in the voided versus obstructed renal pelvis urine, possibly due to the lower creatinine excretion with reduced glomerular function of the obstructed kidney, thus offsetting the dilution effect of the contralateral kidney in the bladder urine[145]. This provides further support for the feasibility of detecting sensitive biomarkers in bladder urine from patients with UPJO."[124]

"We investigated the correlation between urinary concentrations of these proteins with differential renal function and drainage time on MAG3 renography; however, no significant linear correlations were identified. This is likely due to the small sample size of our study and the presence of outliers in these small datasets, making any potential correlations difficult to demonstrate. However, this also raises the possibility that other potential measures of renal function or obstruction, such as urinary biomarkers, may prove to be more sensitive than nuclear imaging. We are not suggesting that nuclear renography should not be used in the evaluation of congenital urinary tract obstruction, as this is arguably the best indicator of upper urinary tract obstruction currently available. However, we believe that other potential modalities that might be more sensitive and less invasive should be investigated."[124]

"An obvious limitation of this study is the small sample size; however, despite the small number of patients, a statistically significant difference was still observed in the urinary levels of the novel proximal tubule proteins between UPJO patients versus controls. This study is also limited by lack of matching for age and gender in the two cohorts; however, since there was no significant difference in these parameters

between the control and UPJO cohorts, it is unlikely that age or gender had a significant impact on the observed differences in urinary protein levels. Additionally, it would be useful to study urinary levels of these proximal tubule proteins after surgical repair. In this preliminary study, we did not exclude UPJO patients with other urologic comorbidities that may have potential impact on urinary protein levels. However, none of the patients had evidence of coexisting obstructive processes, and the contralateral partial UPJO obstruction in one patient had resolved spontaneously prior to the ipsilateral pyeloplasty. The two patients with a history of vesicoureteral reflux had no evidence of reflux nephropathy."[124]

"Despite these limitations, our results support the notion that these proximal tubule proteins may represent more predictive biomarkers of urinary tract obstruction, and that further study is warranted in patients with UPJO and potentially in other etiologies of renal injury. We continue to enroll patients with UPJO at our institution in order to increase our sample size and will begin collecting postoperative urine to measure renal recovery and assess the viability of our biomarkers. We are also enrolling control patients that are matched by age and gender to the UPJO patients. In addition, we are investigating the correlation of these urinary proteins with renal damage in a murine model of obstruction to further study their potential utility as biomarkers of renal injury."[124]

4.6 – Conclusions

"Targeted identification of reliable, noninvasive biomarkers of renal injury is critical to aid in diagnosing patients at risk, guiding therapeutic decisions and monitoring treatment efficacy. In our study, bladder urinary levels of the proximal tubule brush border proteins CD10, CD13 and CD26 were significantly higher in patients with UPJO compared to normal controls, while the levels of KIM-1 and NGAL were not significantly different between UPJO patients versus controls. These preliminary results suggest that these novel proximal tubule proteins may prove to be useful noninvasive biomarkers that are more predictive of urinary tract obstruction. Further studies are necessary to validate these findings and to determine the correlation of these urinary protein levels with renal damage."[124]

4.7 – Figures and Legends

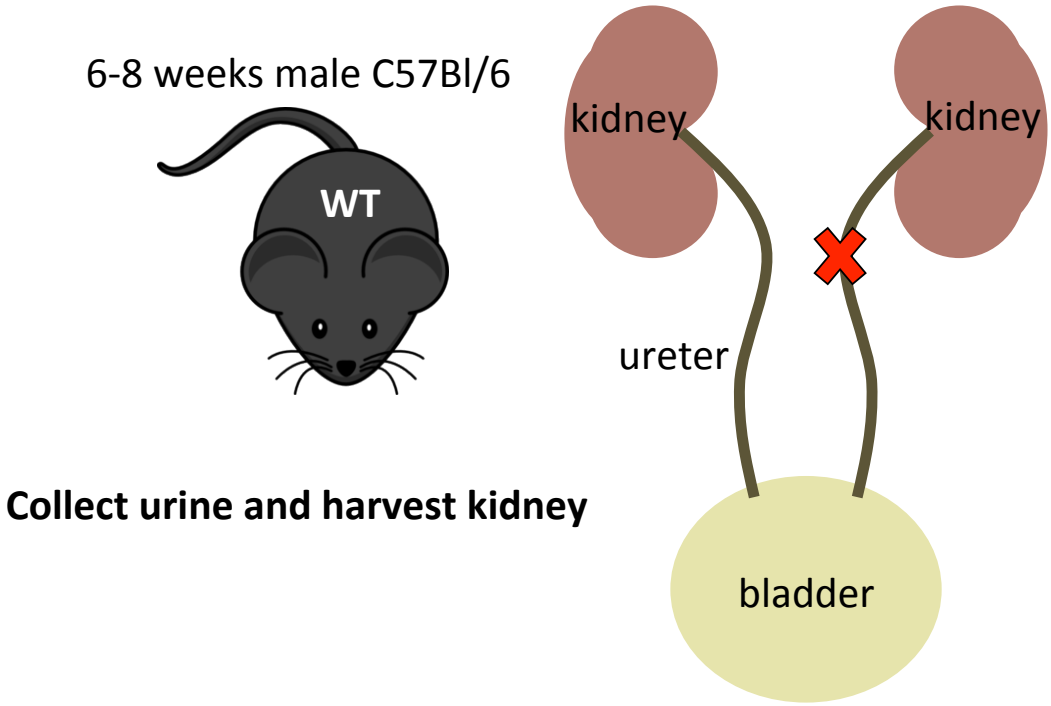

Figure 4.1 – Model of UUO.

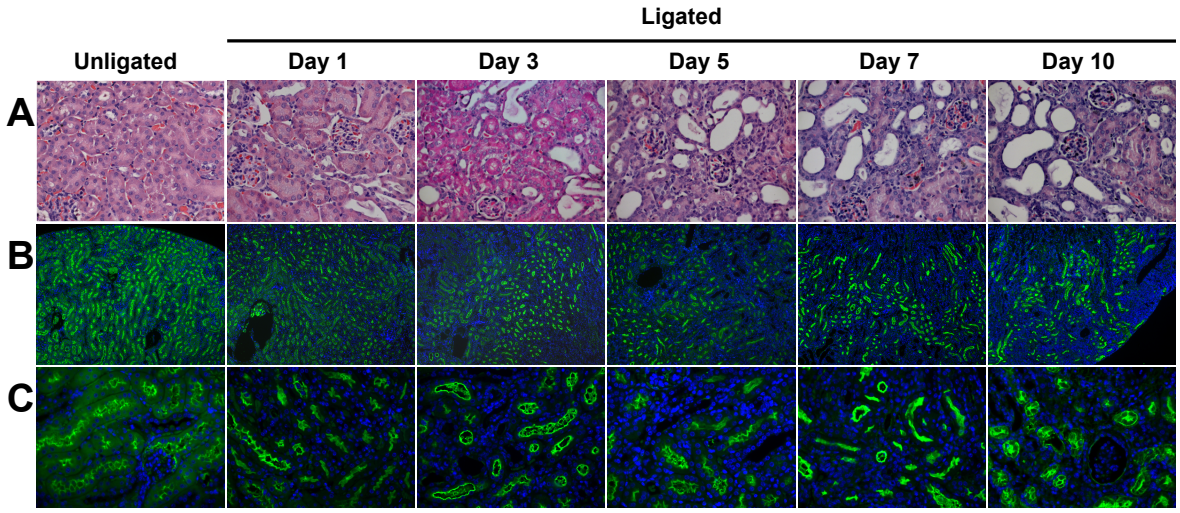

Figure 4.2 – CD13 expression decreases as UUO progresses.
(A) Hematoxylin and eosin stain of obstructed murine kidneys at UUO at 1, 3, 5, 7, and 10 days post ligation show increased tubular damage where proximal tubules lose their shape and become distended as disease progresses. (B) CD13 (green, blue=nuclei) expression in the brush border of the proximal tubules over time, 10x and (C) 40x magnification.

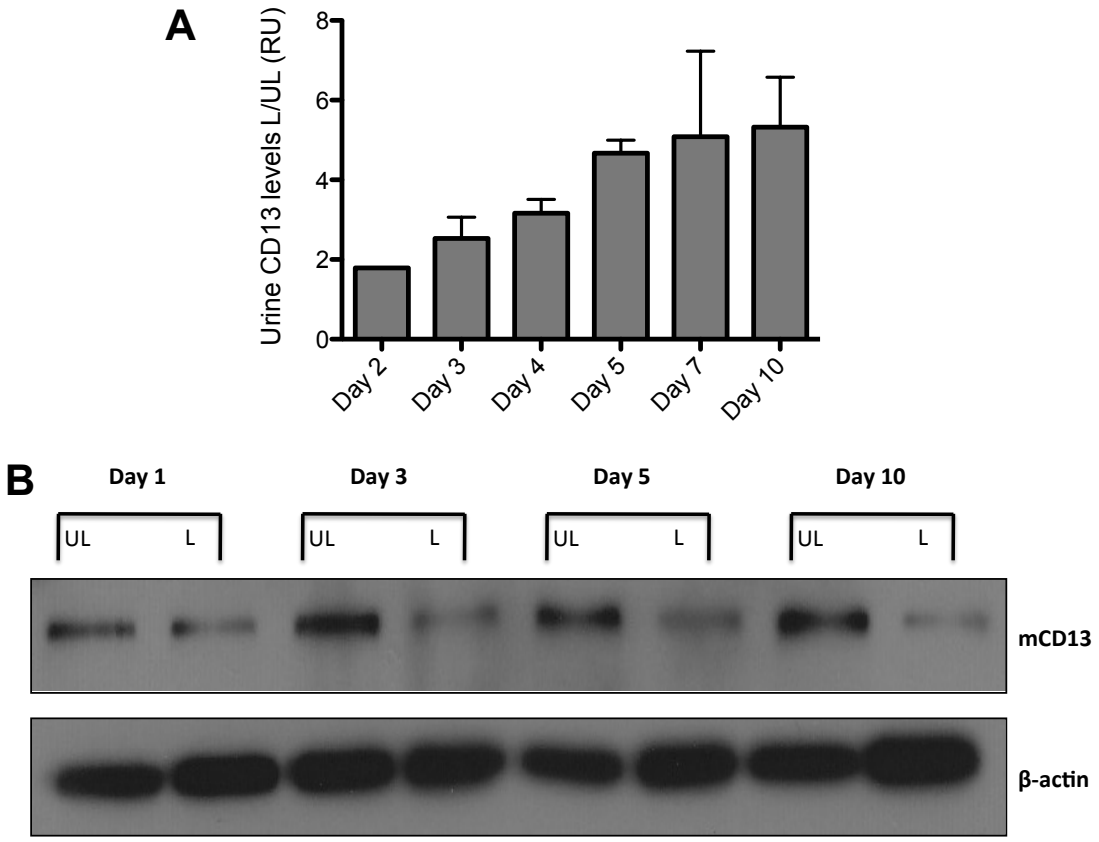

Figure 4.3 – CD13 protein in urine and kidney following UUO.
Digital quantification of western blot of murine urine samples detects CD13 protein at early time points. (A) Normalized urinary CD13 levels (ligated/unligated (L/UL)) increases in obstructed kidneys over time. (B) CD13 levels decreased in ligated (L) as compared to unligated (UL) kidney.

Table 4.1 – UPJO patient demographic characteristics

Case #	Gender	Age at surgery (months)	Presentation	Laterality	MAG3 Data		Other Urologic Comorbidities	Surgical Approach
					$t_{1/2,}$ minutes	Ipsilateral function, %		
1	Female	32	UTI	Right	29	N/A	Solitary right kidney	Robotic
2	Male	4	Prenatal hydronephrosis	Right	*	19.3	None	Open
3	Female	5	Prenatal hydronephrosis	Left	43	25.4	Mild right hydronephrosis	Open
4	Male	4	Prenatal hydronephrosis	Left	329.5	25	None	Open
5	Male	5	Prenatal hydronephrosis	Left	47	52	None	Robotic
6	Female	22	Prenatal hydronephrosis	Right	17	34	None	Robotic
7	Male	32	Prenatal hydronephrosis	Left	*	43	Right partial UPJO, resolved spontaneously	Robotic
8	Male	54	Abdominal pain and vomiting	Left	*	52	Right grade 4 VUR, treated with robotic reimplantation	Robotic
9	Male	76	Postnatal hydronephrosis	Right	22.5	40	Right VUR, resolved spontaneously	Robotic
10	Female	100	UTI	Right	42	39	None	Robotic
11	Male	215	Abdominal pain	Left	*	20	Recurrent UPJO in pelvic kidney after pyeloplasty during infancy	Robotic
12	Male	243	Gross hematuria after renal trauma	Left	45	23	Nephrolithiasis	Robotic

- Unable to calculate due to complete absence of excretion

Table 4.2 – Urinary biomarker values for control and UPJO samples

Case #	Control/ UPJO	Creatinine (mg/dL)	CD10/ Creatinine (RU)	CD13/ Creatinine (RU)	CD26/ Creatinine (RU)	KIM-1/ Creatinine (RU)	NGAL/ Creatinine (RU)
1	UPJO	29	5.77	3.01	181.13	5.47	28.89
2	UPJO	20	20.59	30.50	8188.84	2.30	76.59
3	UPJO	40	9.89	31.14	1398.27	10.50	9587.33
4	UPJO	7	29.05	10.01	290.33	0.84	628.83
5	UPJO	33	14.05	45.51	759.16	8.92	67.69
6	UPJO	31	5.93	2.19	224.47	6.10	32.30
7	UPJO	42	3.46	1.64	113.17	7.53	11.93
8	UPJO	84	3.22	2.42	125.94	3.12	6.15
9	UPJO	51	2.62	1.13	154.19	3.62	263.00
10	UPJO	110	3.19	1.71	198.40	3.90	0.24
11	UPJO	57	3.14	0.25	26.84	0.16	10.63
12	UPJO	40	6.39	0.62	82.04	3.54	118.56
13	Control	72	2.62	1.87	116.94	10.15	55.82
14	Control	54	2.40	1.16	93.87	4.93	19.01
15	Control	79	2.04	1.09	67.93	1.22	29.75
16	Control	103	1.51	0.81	63.03	13.37	27.71
17	Control	128	3.83	2.25	151.36	12.75	191.19
18	Control	99	1.36	1.19	130.33	5.01	14.33
19	Control	278	1.28	0.48	33.44	1.07	77.73
20	Control	128	1.86	0.85	52.86	4.76	16.01
21	Control	73	2.74	1.30	91.58	1.47	100.14
22	Control	71	1.45	0.24	48.32	0.46	154.43
23	Control	31	10.57	1.36	82.00	2.79	37.21
24	Control	110	4.15	1.19	155.08	8.98	74.87

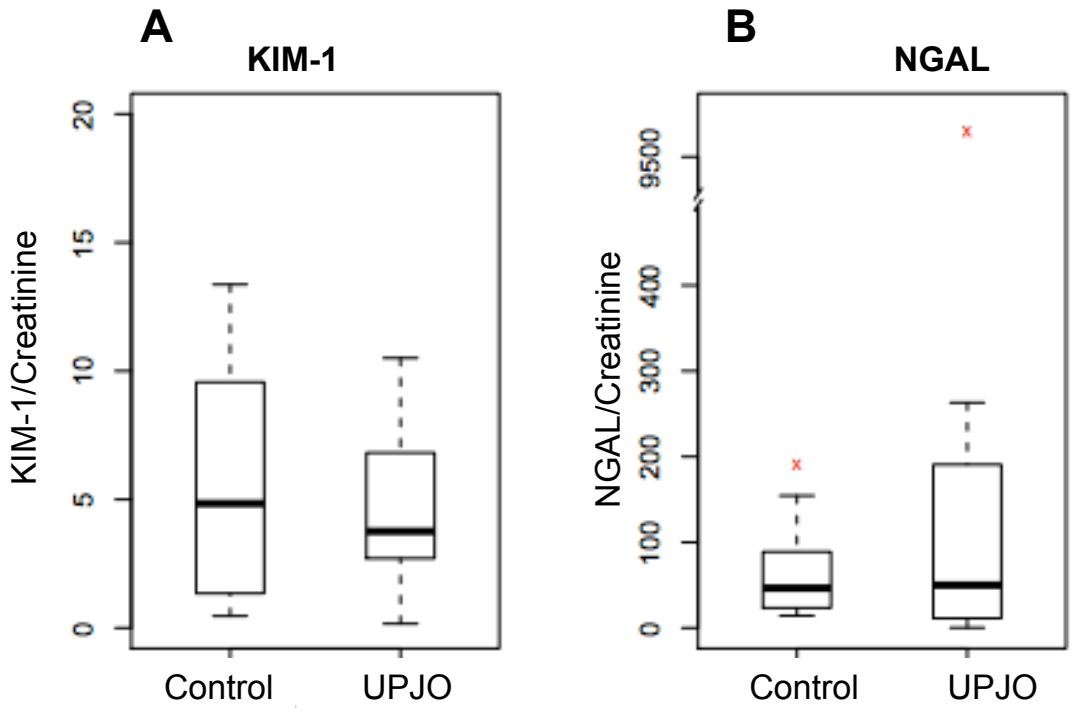

Figure 4.4 – Urinary biomarker levels of known biomarkers.
Box plot of urinary levels of KIM-1 (A) and NGAL (B) normalized to creatinine in control and UPJO patients. Data expressed in relative units.

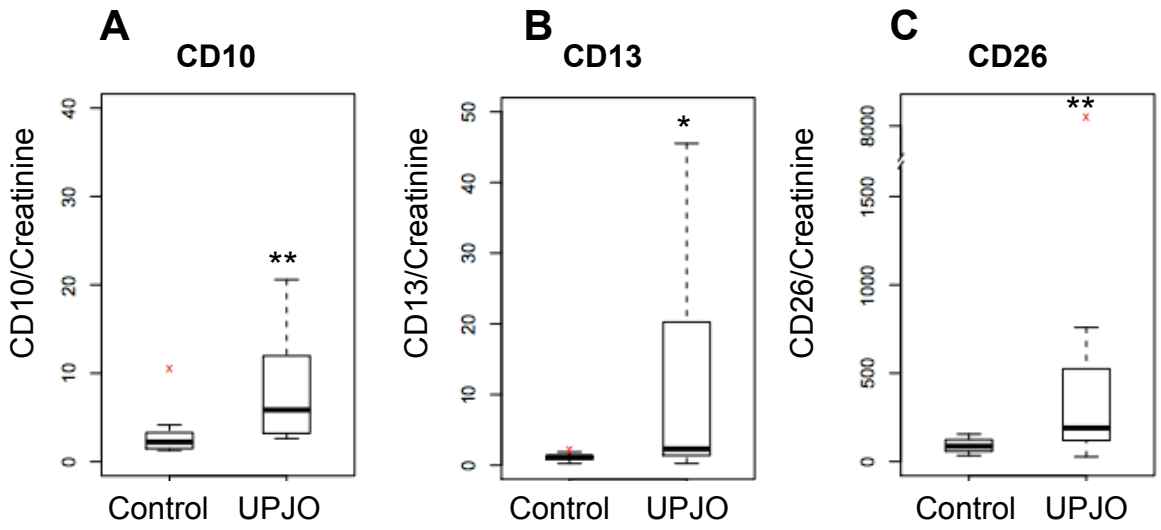

Figure 4.5 – Urinary biomarker levels of novel proximal tubule biomarkers.
Box plot of urinary levels of CD10 (A), CD13 (B) and CD26 (C) normalized to creatinine in control and UPJO patients. Data expressed in relative units. * $p < 0.05$; ** $p < 0.01$

Chapter 5

Concluding Remarks

5.1 – Summary of findings and future directions

CD13 has been identified to regulate various physiological functions including angiogenesis, inflammation and endocytosis[70]. However, the exact mechanisms in which CD13 functions remains unclear. Since CD13 is highly expressed on monocytes and activated endothelial as well as renal proximal tubule cells, this study utilized various models to identify how CD13 regulates inflammation and endocytosis. This thesis focused on (1) identifying domain specific functions of CD13 in regards to inflammation, (2) how CD13 mediated endocytic uptake in response to renal injury and (3) the possibility of CD13 as an early predictor of renal injury in patients with UPJO.

The first investigation of this thesis focused on an in depth evaluation on the structure and functional analysis of CD13 in regards to inflammation. Prior to starting the project, it was known that mice lacking CD13 had altered trafficking of inflammatory cells to the site of injury after hindlimb ischemia and myocardial infarction[86,97]. It was hypothesized that the extracellular domain of CD13 would regulate important homotypic adhesion functions between the activated epithelial layer of injured tissues and circulating monocytes. First, pro-inflammatory subsets of monocytes were higher in WT mice compared to $CD13^{KO}$ mice indicating that CD13 may regulate trafficking of immune cells to the site of injury. In a model of thioglycollate peritonitis peritoneal monocytes, macrophages and DCs were diminished in $CD13^{KO}$ mice. Further, the study used chimeras to identify that homotypic adhesion of CD13 is species specific by using *in vitro* adhesion assays as

well as *in vivo* thioglycollate-induced peritonitis. Blocking CD13 mimicked the results observed in CD13 deficient mice indicating that pro-inflammatory processes can be manipulated with treatment. Finally, it was determined that the C-terminal domain is the specific site for homotypic adhesion. This work established that CD13 regulates inflammatory response by mediating myeloid cell subset trafficking. The *in vitro* analysis indicates that this phenomenon will translate into humans, but finding a blocking agent specific for monocytes remains challenging. Finally, utilizing $CD13^{KO}$ mice can give insight into pro-inflammatory versus anti-inflammatory immune reactions and identifying which inflammatory response aids specific recovery mechanisms beyond peritonitis, hindlimb ischemia and coronary occlusion.

Diabetes mellitus is an intricate disease affecting multiple organs including the pancreas and kidney. ESRD is a common cause of death in patients experiencing diabetic nephropathy. Multiple models of renal injury were utilized to identify the contribution of CD13 to the progression of disease pathology in diabetic nephropathy and to determine the role of CD13 in plasma protein uptake by the proximal tubules. Healthy, renal proximal tubule epithelial cells are equipped with endocytic machinery to efficiently reabsorb glomerular filtrates. However, some diabetics develop nephropathy prompted by hyperglycemia which is the driving component that leads to glomerular damage, gradual nephron deterioration, overload of proximal tubule reabsorption mechanisms and leakage of protein into the urine. Albuminuria is a strong indicator of renal injury, but albuminuria itself may contribute to renal disease progression. $CD13^{KO}$ mice had significantly reduced albuminuria in a model of

diabetic nephropathy as well as AO. CD13 deficient renal proximal tubules were able to take up albumin more efficiently compared to WT proximal tubules. CD13 did not co-localize with the megalin receptor in renal tubules. Interestingly, it did co-localize with the FcRn receptor, which is responsible for the transcytosis of albumin back into the circulation. This study further identified the effects of albuminuria on renal injury. Increased albumin uptake did not lead to more necrosis or apoptosis of renal cells when analyzed by flow analysis. These investigations provide new insight into albuminuria and how it leads to renal injury. It appears to be a combination of increased renal uptake in addition to excess fragmented albumin in the nephron that causes sublethal damage leading to ESRD. Future studies still need to address the precise mechanism in which albuminuria contributes to renal injury by utilizing more models of renal failure. Longer time points after diabetic onset could identify if decreased albuminuria leads to slower progression of renal injury. Further investigations can provide more insight into clinical targets that can reduce nephron loss at earlier time points as clinical interventions today just focus on slowing disease progression.

Congenital anomalies like UPJO often lead to renal injury. Increased intrarenal pressure due to obstruction initiates an injury-signaling cascade resulting in renal dysfunction. Despite growing insight into disease progression, early diagnostic markers that reliably detect renal obstruction are severely lacking. Current diagnostic tests primarily rely on serum creatinine, which remains unchanged until half the nephron volume is lost. Alternative tests include invasive nuclear scans, which also

requires waiting until significant renal functional loss occurs. The third study of this thesis aimed to identify reliable biomarkers that have the potential to diagnose patients at risk, guide therapeutic options and monitor treatment to improve patient care and reduce associated morbidities. It was hypothesized that single-pass, apically expressed proximal tubule brush border proteins including CD13, CD10 and CD26 would shed into the urine early and act as reliable non-invasive urinary biomarkers. A murine model of UUO was initially used to experimentally determine whether renal injury correlated with urinary CD13 levels. CD13 expression decreased in obstructed kidneys and increased in urine. A prospective cohort study was performed at Connecticut Children's Medical Center. Bladder urine samples were collected and analyzed for proximal tubule markers as well as previously published biomarkers, NGAL and KIM1. Proximal tubule brush border proteins are reliably detected in the urine of UPJO patients and outperformed previously established biomarkers in a small sample of patients. This preliminary study identifies new, non-invasive biomarkers that outperform previously published biomarkers. Results from this investigation determined that these biomarkers are elevated in UPJO patients, but it has still to be determined if these biomarkers are capable of distinguishing between UPJO patients and those with suspected hydronephrosis. Patients with suspected hydronephrosis do not require surgical intervention, thus it is imperative that these biomarkers accurately detect obstructive damage. Further investigations need to determine if these biomarkers can eliminate current clinical evaluation tools by correlating biomarker levels with total renal

damage by histological stratification. Perhaps this panel of biomarkers can be utilized to assess other forms of renal injury as well.

5.2 – Clinical Implications

The multifunctional nature of CD13 suggests that CD13 has clinical implications in various settings including in inflammatory responses after injury. The human immune system is highly complex and regulated by various cells and signaling components[146]. Monocytes are recruited to mitigate the effects of viral, bacterial or fungal infections and tissue injuries. These monocytes might contribute to the pathogenesis of inflammatory and degenerative disease. To avoid more injury, the immune system must maintain homeostasis of various pro- and anti-inflammatory signaling[147]. Pro-inflammatory cytokines are released to resolve injury, while anti-inflammatory cytokine inhibitors limit the possibly harmful consequences of sustained or excessive levels of inflammatory reactions[146]. $CD13^{KO}$ mice have abnormal trafficking of monocytes to the site of injury and infection. Abnormal trafficking in response to inflammation can lead to skewed immune responses that lead to improper healing at the site of injury. Recruitment of the appropriate monocytes by the innate immune system to the site of injury is vital for resolution of injury.

While albuminuria is a strong indicator of renal injury, albuminuria may be causal to disease progression. Thus reducing albumin in the urine is a viable therapeutic goal for diabetic patients[148]. A new endocytic regulator that controls physiological

processes in the kidney was discovered. CD13 deficient mice had significantly less albuminuria 20 weeks after the onset of diabetes compared to WT mice. Blocking CD13 in renal proximal tubules could allow for increased uptake of albumin by proximal tubules, which might offer some protection to the nephron in the progression of renal deterioration. New therapies that involve increased albumin uptake in the proximal tubule might halt the progression of ESRD and premature death caused by diabetic nephropathy.

Mechanisms to assess the severity of damage caused by UPJO are decisively lacking and primarily rely on insensitive tests from serum creatinine which remains unchanged until greater than 50% nephron volume is lost. Alternatively, differential renal function is determined by invasive nuclear scans, which requires waiting until significant functional loss occurs[17]. Current treatment for UPJO consists of surgical reconstruction in obvious cases or a watchful waiting approach in asymptomatic patients who have not yet demonstrated loss of differential function on renal nuclear scan, which may be deleterious to young infants where significant renal development occurs both pre- and post-natally. The inability to assess evolving renal damage leaves the physician to base critical decision on inadequate information. Therefore, the discovery and identification of new reliable biomarkers has the potential to diagnose patients at risk, guide therapeutic options and potentially monitor treatment, significantly improving patient care and reducing morbidity. The initial identification of reliable biomarkers might be a useful tool guiding physicians in their treatment strategies.

References

1. Theilig F. Spread of glomerular to tubulointerstitial disease with a focus on proteinuria. Annals of anatomy = Anatomischer Anzeiger : official organ of the Anatomische Gesellschaft 2010;192:125-32.
2. Breyer MD, Bottinger E, Brosius FC, 3rd, et al. Mouse models of diabetic nephropathy. Journal of the American Society of Nephrology : JASN 2005;16:27-45.
3. Oxburgh L, de Caestecker MP. Ischemia-reperfusion injury of the mouse kidney. Methods Mol Biol 2012;886:363-79.
4. Lopez-Novoa JM, Rodriguez-Pena AB, Ortiz A, Martinez-Salgado C, Lopez Hernandez FJ. Etiopathology of chronic tubular, glomerular and renovascular nephropathies: clinical implications. J Transl Med 2011;9:13.
5. Weening JJ, Jennette JC. Historical milestones in renal pathology. Virchows Archiv : an international journal of pathology 2012;461:3-11.
6. Christensen EI, Verroust PJ, Nielsen R. Receptor-mediated endocytosis in renal proximal tubule. Pflugers Arch 2009;458:1039-48.
7. Tan J, Jaung R, Gamble G, Cundy T. Proteinuric renal disease in type 2 diabetes-Is remission of proteinuria associated with improved mortality and morbidity? Diabetes research and clinical practice 2013.
8. Amsellem S, Gburek J, Hamard G, et al. Cubilin is essential for albumin reabsorption in the renal proximal tubule. J Am Soc Nephrol 2010;21:1859-67.
9. Birn H, Christensen EI. Renal albumin absorption in physiology and pathology. Kidney Int 2006;69:440-9.
10. Gorvin CM, Wilmer MJ, Piret SE, et al. Receptor-mediated endocytosis and endosomal acidification is impaired in proximal tubule epithelial cells of Dent disease patients. Proc Natl Acad Sci U S A 2013;110:7014-9.
11. Weyer K, Storm T, Shan J, et al. Mouse model of proximal tubule endocytic dysfunction. Nephrol Dial Transplant 2011;26:3446-51.
12. Vallon V, Thomson SC. Renal function in diabetic disease models: the tubular system in the pathophysiology of the diabetic kidney. Annu Rev Physiol 2012;74:351-75.
13. Brosius FC, 3rd, Alpers CE, Bottinger EP, et al. Mouse models of diabetic nephropathy. Journal of the American Society of Nephrology : JASN 2009;20:2503-12.
14. Vallon V. The proximal tubule in the pathophysiology of the diabetic kidney. Am J Physiol Regul Integr Comp Physiol 2011;300:R1009-22.
15. Kanwar YS, Wada J, Sun L, et al. Diabetic nephropathy: mechanisms of renal disease progression. Exp Biol Med (Maywood) 2008;233:4-11.
16. Madsen MG, Norregaard R, Palmfeldt J, Olsen LH, Frokiaer J, Jorgensen TM. Urinary NGAL, cystatin C, beta2-microglobulin, and osteopontin significance in hydronephrotic children. Pediatr Nephrol 2012;27:2099-106.
17. Mesrobian HG, Mirza SP. Hydronephrosis: a view from the inside. Pediatr Clin North Am 2012;59:839-51.
18. Bartoli F, Penza R, Aceto G, et al. Urinary epidermal growth factor, monocyte chemotactic protein-1, and beta2-microglobulin in children with ureteropelvic junction obstruction. Journal of pediatric surgery 2011;46:530-6.

19. Chevalier RL. Pathogenesis of renal injury in obstructive uropathy. Curr Opin Pediatr 2006;18:153-60.
20. Chevalier RL, Thornhill BA, Forbes MS, Kiley SC. Mechanisms of renal injury and progression of renal disease in congenital obstructive nephropathy. Pediatr Nephrol 2010;25:687-97.
21. Chevalier RL, Thornhill BA, Wolstenholme JT, Kim A. Unilateral ureteral obstruction in early development alters renal growth: dependence on the duration of obstruction. J Urol 1999;161:309-13.
22. Forbes MS, Thornhill BA, Minor JJ, Gordon KA, Galarreta CI, Chevalier RL. Fight-or-flight: murine unilateral ureteral obstruction causes extensive proximal tubular degeneration, collecting duct dilatation, and minimal fibrosis. Am J Physiol Renal Physiol 2012;303:F120-9.
23. Kiley SC, Chevalier RL. Urinary biomarkers: the future looks promising. Kidney Int 2009;76:133-4.
24. Koeppen BM, Stanton BA. Renal Physiology. 5th ed. Philadelphia, PA: Elsevier Mosby; 2013.
25. Costanzo LS. Physiology. 4th ed. Philadelphia, PA: Elsevier Saunders; 2010.
26. Scott RP, Quaggin SE. Review series: The cell biology of renal filtration. J Cell Biol 2015;209:199-210.
27. Saito A, Sato H, Iino N, Takeda T. Molecular mechanisms of receptor-mediated endocytosis in the renal proximal tubular epithelium. J Biomed Biotechnol 2010;2010:403272.
28. Patari A, Forsblom C, Havana M, Taipale H, Groop PH, Holthofer H. Nephrinuria in diabetic nephropathy of type 1 diabetes. Diabetes 2003;52:2969-74.
29. Deb DK, Wang Y, Zhang Z, et al. Molecular mechanism underlying 1,25-dihydroxyvitamin D regulation of nephrin gene expression. J Biol Chem 2011;286:32011-7.
30. Nakhoul N, Batuman V. Role of proximal tubules in the pathogenesis of kidney disease. Contrib Nephrol 2011;169:37-50.
31. Dickson LE, Wagner MC, Sandoval RM, Molitoris BA. The proximal tubule and albuminuria: really! J Am Soc Nephrol 2014;25:443-53.
32. Christensen EI, Birn H. Megalin and cubilin: multifunctional endocytic receptors. Nat Rev Mol Cell Biol 2002;3:256-66.
33. Sleep D, Cameron J, Evans LR. Albumin as a versatile platform for drug half-life extension. Biochim Biophys Acta 2013;1830:5526-34.
34. Gorriz JL, Martinez-Castelao A. Proteinuria: detection and role in native renal disease progression. Transplant Rev (Orlando) 2012;26:3-13.
35. Ware LB, Johnson AC, Zager RA. Renal cortical albumin gene induction and urinary albumin excretion in response to acute kidney injury. Am J Physiol Renal Physiol 2011;300:F628-38.
36. MacIsaac RJ, Ekinci EI, Jerums G. 'Progressive diabetic nephropathy. How useful is microalbuminuria?: contra'. Kidney Int 2014;86:50-7.
37. Caruso-Neves C, Kwon SH, Guggino WB. Albumin endocytosis in proximal tubule cells is modulated by angiotensin II through an AT2 receptor-mediated protein kinase B activation. Proceedings of the National Academy of Sciences of the United States of America 2005;102:17513-8.

38. Eddy AA, Giachelli CM. Renal expression of genes that promote interstitial inflammation and fibrosis in rats with protein-overload proteinuria. Kidney Int 1995;47:1546-57.
39. Eddy AA, Kim H, Lopez-Guisa J, Oda T, Soloway PD. Interstitial fibrosis in mice with overload proteinuria: deficiency of TIMP-1 is not protective. Kidney Int 2000;58:618-28.
40. Ishola DA, Jr., van der Giezen DM, Hahnel B, et al. In mice, proteinuria and renal inflammatory responses to albumin overload are strain-dependent. Nephrol Dial Transplant 2006;21:591-7.
41. Zandi-Nejad K, Eddy AA, Glassock RJ, Brenner BM. Why is proteinuria an ominous biomarker of progressive kidney disease? Kidney Int Suppl 2004:S76-89.
42. Wang Y, Rangan GK, Tay YC, Wang Y, Harris DC. Induction of monocyte chemoattractant protein-1 by albumin is mediated by nuclear factor kappaB in proximal tubule cells. J Am Soc Nephrol 1999;10:1204-13.
43. Reich H, Tritchler D, Herzenberg AM, et al. Albumin activates ERK via EGF receptor in human renal epithelial cells. J Am Soc Nephrol 2005;16:1266-78.
44. Roscioni SS, Lambers Heerspink HJ, de Zeeuw D. Microalbuminuria: target for renoprotective therapy PRO. Kidney Int 2014;86:40-9.
45. Fink SL, Cookson BT. Apoptosis, pyroptosis, and necrosis: mechanistic description of dead and dying eukaryotic cells. Infect Immun 2005;73:1907-16.
46. Erkan E, De Leon M, Devarajan P. Albumin overload induces apoptosis in LLC-PK(1) cells. Am J Physiol Renal Physiol 2001;280:F1107-14.
47. Sanchez-Nino MD, Fernandez-Fernandez B, Perez-Gomez MV, et al. Albumin-induced apoptosis of tubular cells is modulated by BASP1. Cell death & disease 2015;6:e1644.
48. Thomas ME, Brunskill NJ, Harris KP, et al. Proteinuria induces tubular cell turnover: A potential mechanism for tubular atrophy. Kidney Int 1999;55:890-8.
49. Okamura K, Dummer P, Kopp J, et al. Endocytosis of albumin by podocytes elicits an inflammatory response and induces apoptotic cell death. PLoS One 2013;8:e54817.
50. Chang AM, Ohse T, Krofft RD, et al. Albumin-induced apoptosis of glomerular parietal epithelial cells is modulated by extracellular signal-regulated kinase 1/2. Nephrol Dial Transplant 2012;27:1330-43.
51. Sigismund S, Confalonieri S, Ciliberto A, Polo S, Scita G, Di Fiore PP. Endocytosis and signaling: cell logistics shape the eukaryotic cell plan. Physiol Rev 2012;92:273-366.
52. Marsh M, McMahon HT. The structural era of endocytosis. Science 1999;285:215-20.
53. Sorkin A. The endocytosis machinery. J Cell Sci 2000;113 Pt 24:4375-6.
54. McPherson PS, Kay BK, Hussain NK. Signaling on the endocytic pathway. Traffic 2001;2:375-84.
55. Mosesson Y, Mills GB, Yarden Y. Derailed endocytosis: an emerging feature of cancer. Nat Rev Cancer 2008;8:835-50.
56. Zou Z, Chung B, Nguyen T, Mentone S, Thomson B, Biemesderfer D. Linking receptor-mediated endocytosis and cell signaling: evidence for regulated

intramembrane proteolysis of megalin in proximal tubule. J Biol Chem 2004;279:34302-10.
57. Christensen EI, Birn H. Megalin and cubilin: synergistic endocytic receptors in renal proximal tubule. Am J Physiol Renal Physiol 2001;280:F562-73.
58. Christensen EI, Birn H, Storm T, Weyer K, Nielsen R. Endocytic receptors in the renal proximal tubule. Physiology (Bethesda) 2012;27:223-36.
59. Desai KV, Xiao N, Wang W, et al. Initiating oncogenic event determines gene-expression patterns of human breast cancer models. ProcNatlAcadSciUSA 2002;99:6967-72.
60. Sarav M, Wang Y, Hack BK, et al. Renal FcRn reclaims albumin but facilitates elimination of IgG. J Am Soc Nephrol 2009;20:1941-52.
61. Chaudhury C, Mehnaz S, Robinson JM, et al. The major histocompatibility complex-related Fc receptor for IgG (FcRn) binds albumin and prolongs its lifespan. The Journal of experimental medicine 2003;197:315-22.
62. Wada J, Makino H. Innate immunity in diabetes and diabetic nephropathy. Nat Rev Nephrol 2016;12:13-26.
63. Lin M, Yiu WH, Wu HJ, et al. Toll-like receptor 4 promotes tubular inflammation in diabetic nephropathy. J Am Soc Nephrol 2012;23:86-102.
64. Lin M, Tang SC. Toll-like receptors: sensing and reacting to diabetic injury in the kidney. Nephrol Dial Transplant 2014;29:746-54.
65. Dasu MR, Devaraj S, Park S, Jialal I. Increased toll-like receptor (TLR) activation and TLR ligands in recently diagnosed type 2 diabetic subjects. Diabetes care 2010;33:861-8.
66. Jheng HF, Tsai PJ, Chuang YL, et al. Albumin stimulates renal tubular inflammation through an HSP70-TLR4 axis in mice with early diabetic nephropathy. Dis Model Mech 2015;8:1311-21.
67. Li F, Yang N, Zhang L, et al. Increased expression of toll-like receptor 2 in rat diabetic nephropathy. American journal of nephrology 2010;32:179-86.
68. Kuwabara T, Mori K, Mukoyama M, et al. Exacerbation of diabetic nephropathy by hyperlipidaemia is mediated by Toll-like receptor 4 in mice. Diabetologia 2012;55:2256-66.
69. Winnicka B, O'Conor C, Schacke W, et al. CD13 is dispensable for normal hematopoiesis and myeloid cell functions in the mouse. J Leukoc Biol 2010;88:347-59.
70. Mina-Osorio P. The moonlighting enzyme CD13: old and new functions to target. Trends Mol Med 2008;14:361-71.
71. Mina-Osorio P, Winnicka B, O'Conor C, et al. CD13 is a novel mediator of monocytic/endothelial cell adhesion. J Leukoc Biol 2008;84:448-59.
72. Sjostrom H, Noren O, Olsen J. Structure and function of aminopeptidase N [In Process Citation]. AdvExpMedBiol 2000;477:25-34.
73. Wong AH, Zhou D, Rini JM. The X-ray crystal structure of human aminopeptidase N reveals a novel dimer and the basis for peptide processing. J Biol Chem 2012.
74. George AJ, Thomas WG, Hannan RD. The renin-angiotensin system and cancer: old dog, new tricks. Nat Rev Cancer 2010;10:745-59.

75. Roques BP, Fournie-Zaluski MC, Wurm M. Inhibiting the breakdown of endogenous opioids and cannabinoids to alleviate pain. Nat Rev Drug Discov 2012;11:292-310.
76. Proost P, Mortier A, Loos T, et al. Proteolytic processing of CXCL11 by CD13/aminopeptidase N impairs CXCR3 and CXCR7 binding and signaling and reduces lymphocyte and endothelial cell migration. Blood 2007;110:37-44.
77. Ghosh M, McAuliffe B, Subramani J, Basu S, Shapiro LH. CD13 Regulates Dendritic Cell Cross-Presentation and T Cell Responses by Inhibiting Receptor-Mediated Antigen Uptake. J Immunol 2012;188:5489-99.
78. Petrovic N, Schacke W, Gahagan JR, et al. CD13/APN regulates endothelial invasion and filopodia formation. Blood 2007;110:142-50.
79. Delmas B, Gelfi J, L'Haridon R, et al. Aminopeptidase N is a major receptor for the entero-pathogenic coronavirus TGEV. Nature 1992;357:417-20.
80. Yeager CL, Ashmun RA, Williams RK, et al. Human aminopeptidase N is a receptor for human coronavirus 229E. Nature 1992;357:420-2.
81. Vogel LK, Noren O, Sjostrom H. The apical sorting signal on human aminopeptidase N is not located in the stalk but in the catalytic head group. FEBS Lett 1992;308:14-7.
82. Van der Hauwaert C, Savary G, Gnemmi V, et al. Isolation and characterization of a primary proximal tubular epithelial cell model from human kidney by CD10/CD13 double labeling. PloS one 2013;8:e66750.
83. Auffray C, Fogg D, Garfa M, et al. Monitoring of Blood Vessels and Tissues by a Population of Monocytes with Patrolling Behavior. Science 2007;317:666-70.
84. Nahrendorf M, Swirski FK, Aikawa E, et al. The healing myocardium sequentially mobilizes two monocyte subsets with divergent and complementary functions. The Journal of experimental medicine 2007;204:3037-47.
85. Virag JI, Murry CE. Myofibroblast and endothelial cell proliferation during murine myocardial infarct repair. Am J Pathol 2003;163:2433-40.
86. Pereira FE, Cronin C, Ghosh M, et al. CD13 is essential for inflammatory trafficking and infarct healing following permanent coronary artery occlusion in mice. Cardiovasc Res 2013;100:74-83.
87. Rahman MM, Subramani J, Ghosh M, et al. CD13 promotes mesenchymal stem cell-mediated regeneration of ischemic muscle. Front Physiol 2014;4:402.
88. Ghosh M, Gerber C, Rahman MM, et al. Molecular mechanisms regulating CD13-mediated adhesion. Immunology 2014;142:636-47.
89. Nomura R, Kiyota A, Suzaki E, et al. Human coronavirus 229E binds to CD13 in rafts and enters the cell through caveolae. Journal of virology 2004;78:8701-8.
90. Miki T, Takegami Y, Okawa K, Muraguchi T, Noda M, Takahashi C. The reversion-inducing cysteine-rich protein with Kazal motifs (RECK) interacts with membrane type 1 matrix metalloproteinase and CD13/aminopeptidase N and modulates their endocytic pathways. J Biol Chem 2007;282:12341-52.
91. Ghosh M, Subramani J, Rahman MM, Shapiro LH. CD13 Restricts TLR4 Endocytic Signal Transduction in Inflammation. J Immunol 2015;194:4466-76.
92. Kagan JC, Su T, Horng T, Chow A, Akira S, Medzhitov R. TRAM couples endocytosis of Toll-like receptor 4 to the induction of interferon-beta. Nat Immunol 2008;9:361-8.

93. Barton GM, Kagan JC. A cell biological view of Toll-like receptor function: regulation through compartmentalization. Nature reviews Immunology 2009;9:535-42.
94. Vernier KM. CD13 Destabilizes Vasculature in Tumors. Storrs, CT: University of Connecticut; 2013.
95. Ingersoll MA, Platt AM, Potteaux S, Randolph GJ. Monocyte trafficking in acute and chronic inflammation. Trends in Immunology 2011;32:470-7.
96. Subramani J, Ghosh M, Rahman MM, et al. Tyrosine Phosphorylation of CD13 Regulates Inflammatory Cell-Cell Adhesion and Monocyte Trafficking. J Immunol 2013;191:3905-12.
97. Rahman MM, Ghosh M, Subramani J, Fong GH, Carlson ME, Shapiro LH. CD13 regulates anchorage and differentiation of the skeletal muscle satellite stem cell population in ischemic injury. Stem Cells 2014;32:1564-77.
98. Shipp MA, Look AT. Hematopoietic differentiation antigens that are membrane-associated enzymes: cutting is the key! Blood 1993;82:1052-70.
99. Look AT, Ashmun RA, Shapiro LH, Peiper SC. Human myeloid plasma membrane glycoprotein CD13 (gp150) is identical to aminopeptidase N. J Clin Invest 1989;83:1299-307.
100. Noren K, Sjostrom H, Danielsen EM, Cowell GM, Skovbjerg H. Molecular and Cellular Basis of Digestion. Amsterdam: Elsevier; 1986.
101. Matsas R, Stephenson SL, Hryszko J, Kenny AJ, Turner AJ. The metabolism of neuropeptides. Phase separation of synaptic membrane preparations with Triton X-114 reveals the presence of aminopeptidase N. Biochem J 1985;231:445-9.
102. Tresnan DB, Holmes KV. Feline aminopeptidase N is a receptor for all group I coronaviruses. Adv Exp Med Biol 1998;440:69-75.
103. Tresnan DB, Levis R, Holmes KV. Feline aminopeptidase N serves as a receptor for feline, canine, porcine, and human coronaviruses in serogroup I. Journal of virology 1996;70:8669-74.
104. Geissmann F, Gordon S, Hume DA, Mowat AM, Randolph GJ. Unravelling mononuclear phagocyte heterogeneity. Nature reviews Immunology 2010;10:453-60.
105. Sunderkotter C, Nikolic T, Dillon MJ, et al. Subpopulations of Mouse Blood Monocytes Differ in Maturation Stage and Inflammatory Response. J Immunol 2004;172:4410-7.
106. Bonham KS, Kagan JC. Endosomes as platforms for NOD-like receptor signaling. Cell host & microbe 2014;15:523-5.
107. Storm T, Tranebjaerg L, Frykholm C, et al. Renal phenotypic investigations of megalin-deficient patients: novel insights into tubular proteinuria and albumin filtration. Nephrol Dial Transplant 2013;28:585-91.
108. Breyer MD, Bottinger E, Brosius FC, 3rd, et al. Mouse models of diabetic nephropathy. J Am Soc Nephrol 2005;16:27-45.
109. Jais A, Einwallner E, Sharif O, et al. Heme oxygenase-1 drives metaflammation and insulin resistance in mouse and man. Cell 2014;158:25-40.
110. Saito A, Kaseda R, Hosojima M, Sato H. Proximal tubule cell hypothesis for cardiorenal syndrome in diabetes. Int J Nephrol 2010;2011:957164.
111. Dronavalli S, Duka I, Bakris GL. The pathogenesis of diabetic nephropathy. Nature clinical practice Endocrinology & metabolism 2008;4:444-52.

112. Sebekova K, Schinzel R, Ling H, et al. Advanced glycated albumin impairs protein degradation in the kidney proximal tubules cell line LLC-PK1. Cellular and molecular biology 1998;44:1051-60.
113. Verbeke P, Perichon M, Friguet B, Bakala H. Inhibition of nitric oxide synthase activity by early and advanced glycation end products in cultured rabbit proximal tubular epithelial cells. Biochim Biophys Acta 2000;1502:481-94.
114. Gburek J, Birn H, Verroust PJ, et al. Renal uptake of myoglobin is mediated by the endocytic receptors megalin and cubilin. Am J Physiol Renal Physiol 2003;285:F451-8.
115. Sand KM, Bern M, Nilsen J, Noordzij HT, Sandlie I, Andersen JT. Unraveling the Interaction between FcRn and Albumin: Opportunities for Design of Albumin-Based Therapeutics. Front Immunol 2014;5:682.
116. Tenten V, Menzel S, Kunter U, et al. Albumin is recycled from the primary urine by tubular transcytosis. J Am Soc Nephrol 2013;24:1966-80.
117. Wagner MC, Campos-Bilderback SB, Chowdhury M, et al. Proximal Tubules Have the Capacity to Regulate Uptake of Albumin. J Am Soc Nephrol 2016;27:482-94.
118. Mogensen CE. Urinary albumin excretion in diabetes. Lancet 1971;2:601-2.
119. Mogensen CE. Microalbuminuria predicts clinical proteinuria and early mortality in maturity-onset diabetes. N Engl J Med 1984;310:356-60.
120. Nielsen R, Christensen EI. Proteinuria and events beyond the slit. Pediatr Nephrol 2010;25:813-22.
121. Motoyoshi Y, Matsusaka T, Saito A, et al. Megalin contributes to the early injury of proximal tubule cells during nonselective proteinuria. Kidney Int 2008;74:1262-9.
122. Guo JK, Marlier A, Shi H, et al. Increased tubular proliferation as an adaptive response to glomerular albuminuria. J Am Soc Nephrol 2012;23:429-37.
123. Molitch ME, DeFronzo RA, Franz MJ, et al. Nephropathy in diabetes. Diabetes care 2004;27 Suppl 1:S79-83.
124. Gerber C HM, Lynch M, Herbst KW, Ferrer FA, Shapiro LH. Proximal tubule proteins are significantly elevated in bladder urine of patients with ureteropelvic junction obstruction and may represent novel biomarkers: A pilot study. Journal of pediatric urology 2015;in press.
125. Koff SA, Campbell K. Nonoperative management of unilateral neonatal hydronephrosis. J Urol 1992;148:525-31.
126. Martensson J, Martling CR, Bell M. Novel biomarkers of acute kidney injury and failure: clinical applicability. Br J Anaesth 2012;109:843-50.
127. Taylor AT. Radionuclides in nephrourology, Part 2: pitfalls and diagnostic applications. J Nucl Med 2014;55:786-98.
128. Liu KD, Yang W, Anderson AH, et al. Urine neutrophil gelatinase-associated lipocalin levels do not improve risk prediction of progressive chronic kidney disease. Kidney Int 2013;83:909-14.
129. Nielsen SE, Andersen S, Zdunek D, Hess G, Parving HH, Rossing P. Tubular markers do not predict the decline in glomerular filtration rate in type 1 diabetic patients with overt nephropathy. Kidney Int 2011;79:1113-8.

130. Wasilewska A, Taranta-Janusz K, Debek W, Zoch-Zwierz W, Kuroczycka-Saniutycz E. KIM-1 and NGAL: new markers of obstructive nephropathy. Pediatr Nephrol 2011;26:579-86.
131. Cost NG, Noh PH, Devarajan P, et al. Urinary NGAL levels correlate with differential renal function in patients with ureteropelvic junction obstruction undergoing pyeloplasty. J Urol 2013;190:1462-7.
132. Urbschat A, Gauer S, Paulus P, et al. Serum and urinary NGAL but not KIM-1 raises in human postrenal AKI. European journal of clinical investigation 2014;44:652-9.
133. Holzscheiter L, Beck C, Rutz S, et al. NGAL, L-FABP, and KIM-1 in comparison to established markers of renal dysfunction. Clinical chemistry and laboratory medicine : CCLM / FESCC 2014;52:537-46.
134. Klein J, Gonzalez J, Miravete M, et al. Congenital ureteropelvic junction obstruction: human disease and animal models. International journal of experimental pathology 2011;92:168-92.
135. Walmsley SJ, Freund DM, Curthoys NP. Proteomic profiling of the effect of metabolic acidosis on the apical membrane of the proximal convoluted tubule. Am J Physiol Renal Physiol 2012;302:F1465-77.
136. Walmsley SJ, Broeckling C, Hess A, Prenni J, Curthoys NP. Proteomic analysis of brush-border membrane vesicles isolated from purified proximal convoluted tubules. Am J Physiol Renal Physiol 2010;298:F1323-31.
137. Galarreta CI, Thornhill BA, Forbes MS, Simpkins LN, Kim DK, Chevalier RL. Transforming growth factor-beta1 receptor inhibition preserves glomerulotubular integrity during ureteral obstruction in adults but worsens injury in neonatal mice. Am J Physiol Renal Physiol 2013;304:F481-90.
138. R: A Language and Environment for Statistical Computing. R Foundation for Statistical Computing Vienna, 2014. at http://www.R-project.org.)
139. Scherberich JE, Wiemer J, Schoeppe W. Biochemical and immunological properties of urinary angiotensinase A and dipeptidylaminopeptidase IV. Their use as markers in patients with renal cell injury. Eur J Clin Chem Clin Biochem 1992;30:663-8.
140. Holdt-Lehmann B, Lehmann A, Korten G, Nagel H, Nizze H, Schuff-Werner P. Diagnostic value of urinary alanine aminopeptidase and N-acetyl-beta-D-glucosaminidase in comparison to alpha 1-microglobulin as a marker in evaluating tubular dysfunction in glomerulonephritis patients. Clinica chimica acta; international journal of clinical chemistry 2000;297:93-102.
141. Mitic B, Lazarevic G, Vlahovic P, Rajic M, Stefanovic V. Diagnostic value of the aminopeptidase N, N-acetyl-beta-D-glucosaminidase and dipeptidylpeptidase IV in evaluating tubular dysfunction in patients with glomerulopathies. Ren Fail 2008;30:896-903.
142. Blaikley J, Sutton P, Walter M, et al. Tubular proteinuria and enzymuria following open heart surgery. Intensive care medicine 2003;29:1364-7.
143. Taha MA, Shokeir AA, Osman HG, Abd el-Aziz Ael A, Farahat SE. Diagnosis of ureteropelvic junction obstruction in children: role of endothelin-1 in voided urine. Urology 2007;69:560-4; discussion 4-5.

144. Furness PD, 3rd, Maizels M, Han SW, Cohn RA, Cheng EY. Elevated bladder urine concentration of transforming growth factor-beta1 correlates with upper urinary tract obstruction in children. J Urol 1999;162:1033-6.
145. Taranta-Janusz K, Wasilewska A, Debek W, Waszkiewicz-Stojda M. Urinary cytokine profiles in unilateral congenital hydronephrosis. Pediatr Nephrol 2012;27:2107-13.
146. Opal SM, DePalo VA. Anti-inflammatory cytokines. Chest 2000;117:1162-72.
147. Shi C, Pamer EG. Monocyte recruitment during infection and inflammation. Nature reviews Immunology 2011;11:762-74.
148. de Zeeuw D, Remuzzi G, Parving HH, et al. Proteinuria, a target for renoprotection in patients with type 2 diabetic nephropathy: lessons from RENAAL. Kidney Int 2004;65:2309-20.